ABSTRACT

A NUMERICAL METHOD FOR THE SOLUTION OF PROBLEMS IN THREE DIMENSIONAL ELASTICITY

by Hotten A. Elleby

A numerical method was developed based on expanded finite differences of the displacements of the nodal points for use in the solution of problems involving solid bodies. The method presented was derived using the equilibrium of the region around a nodal point of the finite difference grid as the basis of solution rather than the classical approach which uses the equilibrium of the nodal point as the basis for solution.

To investigate this method, the solutions using this method were found for a concentrated line load acting on the surface of a cube, a concentrated load acting on the cube, a distributed load acting on the cube, an eccentric load acting on a beam column, and a beam column under constant applied moment. These solutions were also studied with respect to variations in Poisson's ratio.

The solution of these problems was determined without the use of external fictitious nodal points to satisfy the boundary stress conditions, and also without the use of superposition of solutions when the problems contained singularities.

The solutions of these problems converged very rapidly with respect to decreasing grid spacing, except in the proximity of singularities.

The equations became very unstable as Poisson's ratio
approached one-half. This is the case of zero dilatancy of the
material which means the average stress at a point is independent
of the strains at that point. However, within the usual range of
Poisson's ratio, the solutions appear to have an accuracy of at least
three percent when not in close proximity to points of singularity
and with a reasonable choice of grid size.

A NUMERICAL METHOD FOR THE SOLUTION OF PROBLEMS IN THREE DIMENSIONAL ELASTICITY

By
Hotten A. Elleby

A THESIS

Submitted to
Michigan State University
in partial fulfillment of the requirements
for the degree of

DOCTOR OF PHILOSOPHY

Department of Civil and Sanitary Engineering

ACKNOWLEDGEMENTS

The author wishes to express his sincere appreciation and thanks to his major professor, Dr. Charles E. Cutts, for his generous help and encouragement which made this thesis possible.

The author would also like to thank Dr. William A. Bradley for his invaluable help and also Dr. Robert K. Wen and Dr. Edward A. Nordhaus for their guidance.

Acknowledgement is made to the Computer Laboratory for their services in the use of the Control Data Corporation 3600 computer.

TABLE OF CONTENTS

		Page
I.	INTRODUCTION	1
II.	THEORETICAL DEVELOPMENT OF THE	
	METHOD OF EXPANDED DIFFERENCES	4
III.	METHOD OF SOLUTION	31
IV.	EXAMPLE PROBLEMS	37
	Example Problem One	4 5
	Example Problem Two and Three	63
	Example Problem Four	76
	Example Problem Five	88
v.	SUMMARY AND CONCLUSIONS	91
VI.	APPENDIX	96
/II.	BIBLIOGRAPHY	108

LIST OF TABLES

Γable		Page
1	Vector components used for the determination of	
	an octant	15
2	Values of r used to determine the location of the	
	centroid of a stress on an octant	27
3	Values of $\sigma_{\mathbf{z}}$ for the two solutions with various	
	grid spacings	5 4

LIST OF FIGURES

Figure		Page
1	Isometric view of basic model octants	
	surrounding the reference nodal point, and also	
	the rectangular parallelepipeds of which they are	
	a part	10
2	Position of stresses as used in Equations 9 for the	
	classical finite difference solution of the three	
	dimensional equilibrium equations	11
3	Position of the centroidal stresses on the first	
	octant, l, of the model, and also the nodal points	
	which determine the internal displacement func-	
	tions within this octant	12
4	Isometric view of cube with line load for Example	
	Problem One	40
5	Isometric view of a cube showing concentrated	
	load on the Z-Axis for Example Problem Two	41
6	Isometric view of a cube showing concentric	
	distributed load over small portion of the top	
	surface for Example Problem Three	42
7	Isometric view of a beam column showing the	
	location of the eccentric load for Example Prob-	
	lem Four	43

Figure		Page			
8	Isometric view of a beam column showing the				
	surface stress distribution for the applied moment				
	for Example Problem Five	44			
9	Outline of a thin plate with the concentrated loads				
	and the associated boundary phi functions for the				
	biharmonic solution for Example Problem One	50			
10	Values of $\sigma_{\mathbf{z}}$ for the two solutions plotted with				
	respect to the inverse of the mesh size	55			
11	Values of $\sigma_{\mathbf{z}}$ on the centroidal Z-Axis for various				
	values of z plotted with respect to Poisson's ratio.	56			
12	Values of $\sigma_{\mathbf{x}}$ on the centroidal Z-Axis for various				
	values of z plotted with respect to Poisson's ratio.	57			
13	Values of $\sigma_{\mathbf{z}}$ on the centroidal Z-Axis for				
	z = 15B/16 plotted with respect to Poisson's ratio.	58			
14	$\sigma_{\mathbf{x}}$ and $\sigma_{\mathbf{y}}$ on the centroidal Z-Axis for $\mathbf{v} = 0.3$	59			
15	Lines of constant $\sigma_{\mathbf{x}}$ on the Y-Z plane with $\mathbf{x} = 0$				
	for Poisson's ratio of 0.3	60			
16	Lines of constant σ on the Y-Z plane with $x = 0$				
	for Poisson's ratio of 0.3	61			
17	Lines of constant σ_z on the Y-Z plane with $x = 0$				
	for Poisson's ratio of 0.3	62			

Figure		Page
18	Distributed load for Problem Two with a grid	
	spacing of B/8 (a) and for Problem Three with	
	a grid spacing of B/16 (b)	65
19	Values of $\sigma_{\mathbf{z}}$ on the centroidal Z-Axis for various	
	values of z plotted with respect to Poisson's ratio.	68
20	Values of $\sigma_{\mathbf{z}}$ on the centroidal Z-Axis for	
	z = 15 B/16 plotted with respect to Poisson's ratio.	69
21	Values of $\sigma_{\mathbf{x}}$ and $\sigma_{\mathbf{y}}$ on the centroidal Z-Axis for	
	various values of $\sigma_{\mathbf{z}}$ plotted with respect to	
	Poisson's ratio	70
22	Values of $\sigma_{\mathbf{x}}$ and $\sigma_{\mathbf{y}}$ on the centroidal Z-Axis for	
	z = B plotted with respect to Poisson's ratio	71
23	Lines of constant σ_{x} on the Y-Z plane with $x = 0$	
	for Poisson's ratio of 0. Problem Two	72
24	Lines of constant σ_z on the Y-Z plane with $x = 0$	
	for Poisson's ratio of 0. Problem Two	73
25	Lines of constant $\sigma_{\mathbf{x}}$ on the Y-Z plane with $\mathbf{x} = 0$	
	for Poisson's ratio of 0. Problem Three	74
26	Lines of constant σ_z on the Y-Z plane with $x = 0$	
	for Poisson's ratio of 0. Problem Three	75
27	Load distribution areas for Problem Four	77

Figure		Page
28	$\sigma_{\mathbf{z}}$ stress distribution on the centroidal X-Axis	
	with z = 0 for various values of Poisson's ratio.	
	Part One	81
29	$\sigma_{\mathbf{z}}$ stress distribution on the centroidal X-Axis	
	with z = 0 for various values of Poisson's ratio.	
	Part Two	82
30	$\sigma_{\mathbf{z}}$ stress distribution parallel to the X-Axis with	
	y = 0 and for various values of z and with Poisson's	
	ratio of 0.2. Part One	83
31	$\sigma_{\mathbf{z}}$ stress distribution parallel to the X-Axis with	
	y = 0 and for various values of z and with	
	Poisson's ratio of 0.2. Part Two	84
32	Lines of constant $\sigma_{\mathbf{z}}$ for the X-Z centroidal plane	
	with Poisson's ratio of 0.2. Part One	85
33	Lines of constant $\sigma_{\mathbf{z}}$ for the X-Z centroidal plane	
	with Poisson's ratio of 0.2. Part Two	86
34	Lines of constant $\sigma_{\mathbf{x}}$ for the X-Z centroidal plane	
	with Poisson's ratio of 0.2. Part Two	87
35	Assumed stress distribution acting on beam (a),	
	nodal forces as determined by contributing areas,	
	(b), for grid spacing of $B/4$, and nodal forces as	
	determined by contributing areas, (c), for grid	
	spacing of B/8	89

Figure		Page
36	Extreme fiber stress at $x = B/2$, $y = 0$, and	
	z = 0 for grid spacings of B/4 and B/8 for various	
	values of Poisson's ratio	90

CHAPTER I

INTRODUCTION

Advances in computer technology in the past few years have made possible the development of high speed, large storage digital computers. Problems which formerly required many hours of computation, or were limited by the available storage capacity, can now be solved with much less difficulty. Therefore, it is now possible to work problems, involving a great amount of calculation and a large amount of storage capacity, that would previously have been avoided because of the impracticability of solution.

The study of three dimensional solids is an area that for this very reason has only recently been given attention outside of those problems which can be solved in closed form, or those problems which can be reduced to a less complicated level, i.e., one or two degrees of freedom instead of three, such as, problems in plane stress, plane strain, torsion, etc.

This dissertation will investigate the stress distribution in three dimensional elastic solids using a special numerical method developed by the author. This dissertation will be limited to solid rectangular parallelepipeds which have at least two planes of symmetry at their centroid. This dissertation will also investigate the effect of Poisson's ratio on the stress distribution within the solid.

The solution of problems in three dimensional solids has been considered by many authors. One proposed method of solution has been the application of a frame-work or a lattice type analogy as suggested by Hrennikoff (2), D'appolonia and Newmark (1) as well as McHenry (7). Another method has been to use a direct stiffness matrix for various basic solid shapes as suggested by Melosh (8).

The method which will be presented in this dissertation will also be an analogous method based on a three dimensional grid-work system, except that this method will be concerned with the equilibrium of a region around a nodal point of the grid, as opposed to the classical approach which satisfies equilibrium based on the derivatives of the stresses at the nodal point and which is also based on the assumption that the stress condition at the point is the average representation of the region around the point. In essence, the method to be presented uses a solid model to represent the solid region around the point, and will be concerned with the equilibrium of this solid model.

The solution of the three dimensional equilibrium equations is found by applying Lagrangian linear interpolation formulas. The resulting equations will be in the finite difference form, except they will be representative of the solid instead of the nodal point and thus be appropriately called "Expanded Differences."

Chapter II will discuss the development of the theory used in the proposed method, and will compare this method to the classical approach when such a comparison will be helpful to the general understanding of the method. The technique of applying this method for the general solution of a problem will be developed in Chapter III. Chapter IV is devoted to the application of the method to a few selected example problems. These include, concentrated loads (concentric and eccentric), a distributed concentric load, and also the solution using this method for a beam-column with an applied moment and zero end shear. Chapter V summarizes the use of the proposed method. Appendix A indicates the programming in Fortran language for one of the example problems.

CHAPTER II

THEORETICAL DEVELOPMENT OF THE METHOD OF EXPANDED DIFFERENCES

The three dimensional relationships between stress and strain have been known for many years. These relationships have been presented in detail by many authors (6), (9), (10), (13), (14) and (15). In the derivations which follow, it will be assumed that the material is isotropic, homogeneous and can be considered to be a continuum. Also, that Hooke's Law is an adequate representation of the relationship between stress and strain. It will also be assumed that the functions which will be used to represent the stresses and deformations within the body will possess piecewise continuity across the grid lines in the body.

The three principal axes will be called X, Y and Z and the displacements of a point within the body will be called u, v and w in the X, Y and Z directions respectively.

The equations which relate stress to strain for three dimensions in elastic solids are:

$$\sigma_{\mathbf{x}} = \lambda \mathbf{e} + 2G \frac{\partial \mathbf{u}}{\partial \mathbf{x}} \qquad \tau_{\mathbf{x}\mathbf{y}} = G \left(\frac{\partial \mathbf{u}}{\partial \mathbf{y}} + \frac{\partial \mathbf{v}}{\partial \mathbf{x}} \right)$$

$$\sigma_{\mathbf{y}} = \lambda \mathbf{e} + 2G \frac{\partial \mathbf{v}}{\partial \mathbf{y}} \qquad \tau_{\mathbf{x}\mathbf{z}} = G \left(\frac{\partial \mathbf{u}}{\partial \mathbf{z}} + \frac{\partial \mathbf{w}}{\partial \mathbf{x}} \right) \qquad (1)$$

$$\sigma_{\mathbf{z}} = \lambda \mathbf{e} + 2G \frac{\partial \mathbf{w}}{\partial \mathbf{z}} \qquad \tau_{\mathbf{y}\mathbf{z}} = G \left(\frac{\partial \mathbf{v}}{\partial \mathbf{z}} + \frac{\partial \mathbf{w}}{\partial \mathbf{y}} \right)$$

In the previous equations E is Young's modulus, ν is Poisson's ratio, and G is the shearing modulus where,

$$G = \frac{E}{2(1+\nu)} \tag{2}$$

λ is Lamé's constant,

$$\lambda = \frac{\nu \mathbf{E}}{(1+\nu)(1-2\nu)} \tag{3}$$

and e is the dilatation per unit volume of a point,

$$e = \frac{\partial u}{\partial x} + \frac{\partial v}{\partial y} + \frac{\partial w}{\partial z}$$
 (4)

Equations 1 can be written in a somewhat more usable form for computation purposes when the following terms are defined,

$$E' = \frac{E}{2(1+\nu)(1-2\nu)} \tag{5}$$

and,

$$a = 1 - 2\nu \tag{6}$$

Using these constants, equations 1 become,

$$\sigma_{x} = E' \left[(1+a) \frac{\partial u}{\partial x} + (1-a) \left(\frac{\partial v}{\partial y} + \frac{\partial w}{\partial z} \right) \right]$$

$$\sigma_{y} = E' \left[(1+a) \frac{\partial v}{\partial y} + (1-a) \left(\frac{\partial u}{\partial x} + \frac{\partial w}{\partial z} \right) \right]$$

$$\sigma_{z} = E' \left[(1+a) \frac{\partial w}{\partial z} + (1-a) \left(\frac{\partial u}{\partial x} + \frac{\partial v}{\partial y} \right) \right]$$

$$\tau_{xy} = E' a \left(\frac{\partial u}{\partial y} + \frac{\partial v}{\partial x} \right)$$

$$\tau_{xz} = E' a \left(\frac{\partial u}{\partial z} + \frac{\partial w}{\partial x} \right)$$

$$\tau_{yz} = E' a \left(\frac{\partial v}{\partial z} + \frac{\partial w}{\partial y} \right)$$

These equations relate the stress at a point to the displacement derivatives at the point. The exact displacement functions u(x, y, z), v(x, y, z) and w(x, y, z) are usually not available as continuous functions throughout the whole body except for a very few special cases, and thus, various numerical methods must be developed to attain approximate solutions. There are also series solutions available using the Neuber-Papkovitch equations, (9) and (11).

The displacement functions are derived (or approximated) by simultaneously satisfying internal equilibrium and compatibility of the body along with the external boundary conditions either in terms of stress or displacement.

The equations of equilibrium are:

$$\Sigma F_{x} = 0$$

$$\Sigma F_{y} = 0$$

$$\Sigma F_{z} = 0$$
(8)

If we assume that u, v and w are continuous functions we can derive the following equilibrium equations of an infinitely small element (dx, dy, dz) as follows for zero body forces.

$$\frac{\partial \sigma}{\partial x} + \frac{\partial \tau}{\partial y} + \frac{\partial \tau}{\partial z} = 0$$

$$\frac{\partial \sigma}{\partial y} + \frac{\partial \tau}{\partial x} + \frac{\partial \tau}{\partial z} = 0$$

$$\frac{\partial \sigma}{\partial z} + \frac{\partial \tau}{\partial y} + \frac{\partial \tau}{\partial x} = 0$$

$$(9)$$

Substituting Equations 7 into these Equations 9, the equilibrium equations can be written in terms of the displacements which means that compatibility of displacement will be automatically satisfied.

These equations are:

$$E' \frac{\partial \mathbf{e}}{\partial \mathbf{x}} + E' \mathbf{a} \nabla^{2} \mathbf{u} = 0$$

$$E' \frac{\partial \mathbf{e}}{\partial \mathbf{y}} + E' \mathbf{a} \nabla^{2} \mathbf{v} = 0$$

$$E' \frac{\partial \mathbf{e}}{\partial \mathbf{z}} + E' \mathbf{a} \nabla^{2} \mathbf{w} = 0$$
(10)

where,

$$\nabla^2 = \frac{\partial^2}{\partial x^2} + \frac{\partial^2}{\partial y^2} + \frac{\partial^2}{\partial z^2} \tag{11}$$

These equations are generally known as the Navier-Stokes equations of equilibrium. These equations satisfy equilibrium at a point within the body and everywhere within the body, providing u, v and w are continuous functions in x, y and z. If u, v and w are not continuous functions throughout the entire body, such as in the case when the displacements in the body are specified only at points, as for example in a grid work of nodal points, then equilibrium is only satisfied at the nodal points where the derivatives of these discontinuous functions are obtained. These derivatives will only be accurate to the order of the equation assumed passing through the nodal points, and the equilibrium equations will be only accurate to the degree in which these derivatives represent the true average

conditions around the point. The accuracy of the final solution will then be dependent upon the accuracy of the displacement functions and the size of grid employed. The classical method of solving the equilibrium equations in terms of the grid work, is to substitute into the equilibrium Equations 10 the normal second order finite difference approximations for the needed derivatives (4) and then write the finite difference equations for every nodal point of the grid work in the solid. This will lead to a set of linear simultaneous algebraic equations which can then be solved by various methods (12). The existence and uniqueness to solutions of the partial differential Equations 10 has been shown by Korn (3) and Lichtenstein (5), for first and second boundary value problems under general conditions.

The method as outlined above is the classical method of solving three-dimensional problems based on the Navier-Stokes equilibrium equations. As mentioned previously, these equations only satisfy, in general, the equilibrium of a nodal point in the grid work of the body. It would seem that a solution that converges faster (with respect to the size of the grid) could be obtained by satisfying equilibrium within a region around the nodal point instead of simply at the nodal point alone.

The basic philosophy of the method to be described stems from the fundamental viewpoint that the prime interest is in satisfying equilibrium throughout the entire body. It would seem then that since a grid work is being used to represent the solid body, the equilibrium equations can be written in terms of the forces in the body as represented by the grid system, rather than using the derivatives of the stresses at each nodal point in the grid system, as is presented in Equations 9.

The stresses at any point within the body are given in terms of the first derivatives of the displacement functions. Assuming straight line variation of displacement between nodal points, the first derivative of one of these functions along a grid line and in the direction of the grid line between two nodal points will be a constant. Therefore, the point where this derivative can be best represented is at the center of the particular grid line segment. This idea can then be extended to all three coordinate axes which leads to the concept that the equilibrium equations can be formed by using the summation of forces on the planes passing through the center of the grid lines and perpendicular to them as shown in Figure 1. When there are no body forces, the sum of the forces acting on the planes surrounding a nodal point can then be set equal to zero for equilibrium. In the classical approach it can be shown that the equilibrium equations can be formed by representing the average stress on these planes as the stresses which exist at the intersection of the coordinate axes with these planes (Figure 2). In the method to be developed, the average stress will be computed from the expanded derivative in each

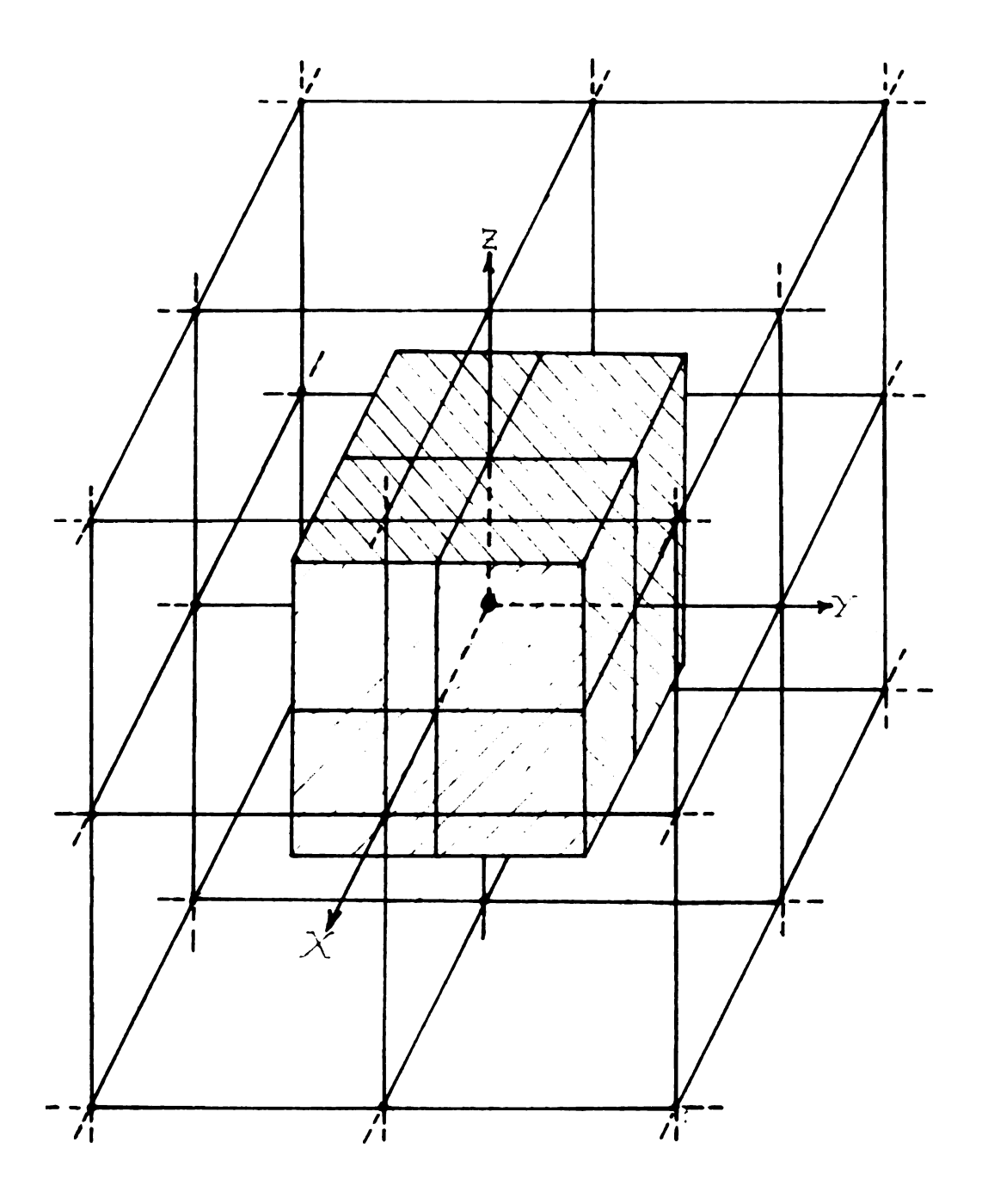


Figure 1. Isometric view of basic model octants surrounding the reference nodal point, and also the rectangular parallelepipeds of which they are a part.

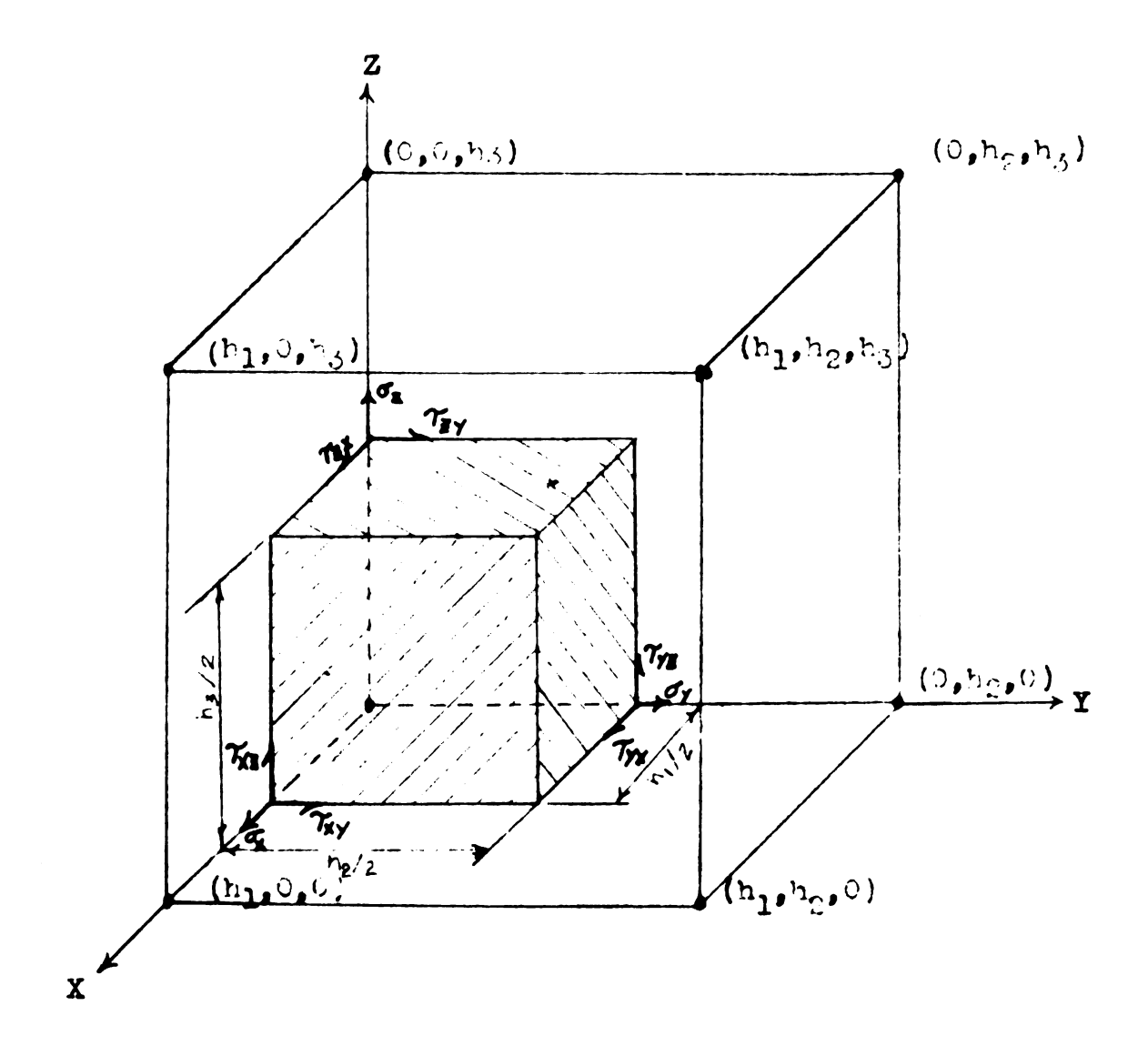


Figure 2. Position of stresses as used in Equations 9 for the classical finite difference solution of the three dimensional equilibrium equations.

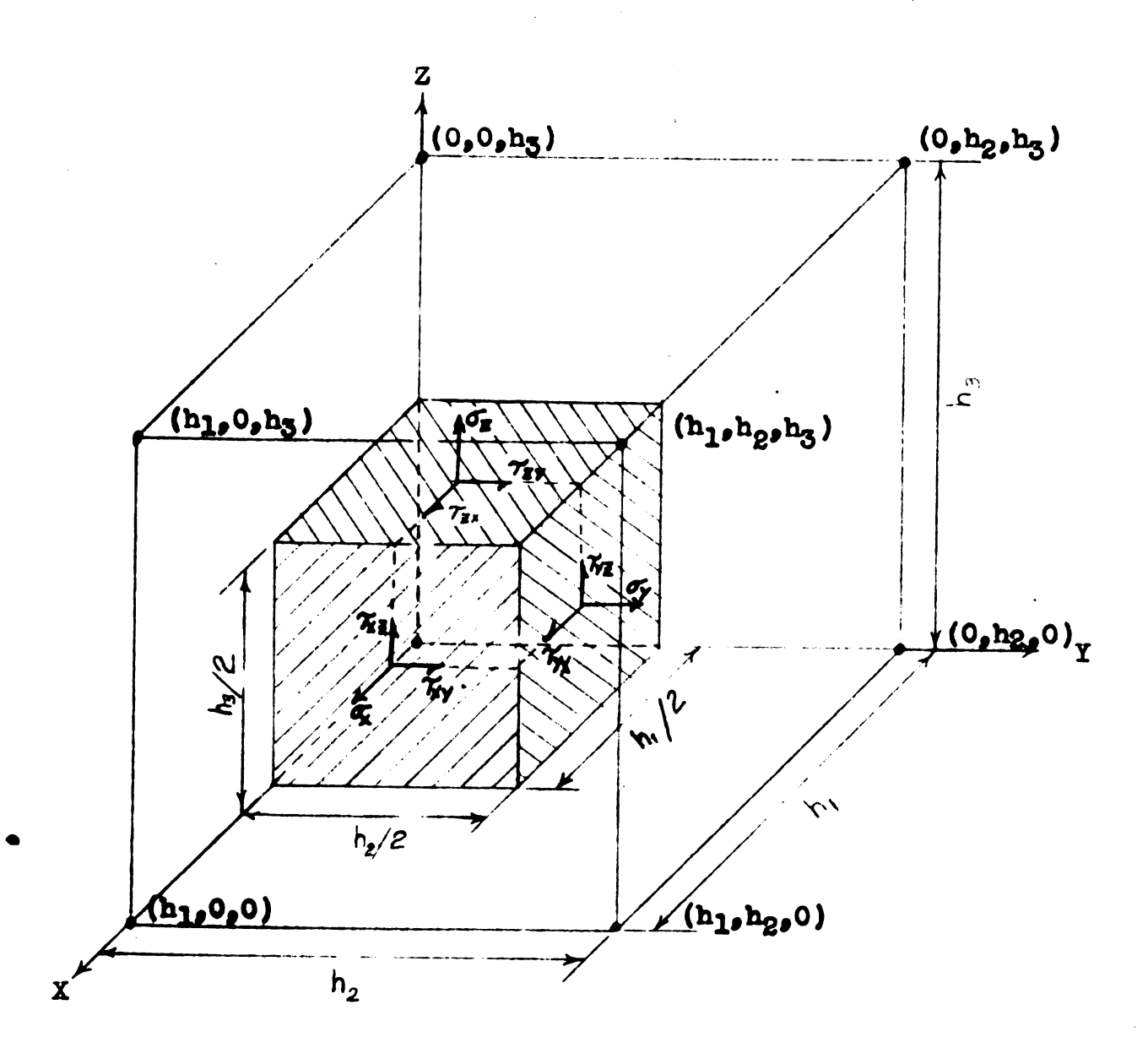


Figure 3. Position of the centroidal stresses on the first octant, 1, of the model, and also the nodal points which determine the internal displacement functions within this octant.

quadrant of the plane, and the equilibrium equations will then be determined from these stresses (Figure 3). With linearity assumed in both cases, the total sum of the forces acting on any plane through the body will be the same, but the forces when resolved to the nodal point will be different, depending on the curvature of the stress pattern. The efficiency of the method will become apparent when comparing the relative convergence of the two solutions.

This method can be described by comparing the volume enclosed by the planes which pass through the center of the grid line segments around a nodal point to a solid model. The displacement functions for an octant of the model will be determined by the parallelepiped of nodal points of which that octant is a part (Figure 1). Linearity will be assumed between the nodal points of this rectangular parallelepiped and will be used in determining the displacement functions. The displacement functions will be continuous within the parallelepiped, but they will be only piecewise continuous across the grid line boundaries. The model to be used in deriving the equilibrium equations will be, in general, composed of the eight smaller octants which surround the nodal point and each of which is one octant of the parallelepiped of nodal points which is used to determine the displacement functions. The dimensions of one of these smaller octants will be one-half of the dimensions of the parallelepiped used in determining the displacement functions. The equations of stress within an

octant of the model will be determined from the first derivatives of the displacement functions within the octant. The resulting stress equations will be, in general discontinuous across the boundaries between the octants of the model because the displacement functions are, in general, only piecewise continuous across these boundaries. The eight octants which surround a nodal point will have forces acting on their faces (Figure 3) as determined by the displacements of the nodal points of which that octant is a part. These forces can then be used to determine the equations of equilibrium.

The displacement functions within a particular octant will be derived by using an extension of the Lagrange interpolation formula within the boundaries of the eight nodal points needed for linearly describing the stresses and displacements between nodal points.

Before the equations of displacements are determined for each octant, it will be convenient for future developments to define the method to be used in identifying the relative position of the nodal points surrounding the reference nodal point from which equilibrium equations will be formed, and also in identifying the eight separate octants surrounding the reference nodal point. The position of a functional value with reference to the centroidal nodal point of the model can be indicated by showing the function to be dependent on three arguments I, J and K which will be the vector components of the point in the x, y and z directions respectively from the reference

nodal point. These three arguments will uniquely describe this point. For example, u(I,J,K) would be a typical use of these arguments. This quantity would signify the u displacement of the point at $\vec{I} + \vec{J} + \vec{K}$ with respect to the reference nodal point. A particular octant of the solid model can be identified by a set of vectors \vec{I} , \vec{J} and \vec{K} which are set equal to the vector components of the grid lines coinciding with the internal edges of that particular octant. There are then eight sets of identification vectors, one for each possible octant. If we number the octants (n) one through eight, and express the grid spacings h_1 , h_2 , and h_3 in the x, y and z directions respectively, a table of the eight sets of identification vectors for the octants can be formed as follows:

TABLE I

OCTANT IDENTIFICATION V			ECTORS
n	Ī	Ĵ	\vec{K}
1	h ₁	h ₂	h ₃
2	h	h ₂	-h ₃
3	h ₁	-h ₂	h ₃
4	h ₁	-h ₂	-h ₃
5	-h ₁	h ₂	h ₃
6	-h ₁	h ₂	-h ₃
7	-h ₁	-h ₂	h ₃
8	-h ₁	-h ₂	-h ₃

These sets of identification vectors can be made into sets of unit vectors by dividing them by their respective grid spacings and thus,

$$\vec{B}_{1n} = \vec{I}_{n} / h_{1}$$

$$\vec{B}_{2n} = \vec{J}_{n} / h_{2}$$

$$\vec{B}_{3n} = \vec{K}_{n} / h_{3}$$
(12)

The x, y and z coordinates of a point within an octant can then be expressed in the following form:

$$x_{n} = r_{1n} B_{1n} h_{1}$$

$$y_{n} = r_{2n} B_{2n} h_{2} \qquad 0 \le r \le 1$$

$$z_{n} = r_{3n} B_{3n} h_{3}$$
(13)

The x, y and z coordinates of nodal points governing an octant can be expressed in somewhat the same form by setting the value of r_1 , r_2 and r_3 to be equal to zero or one. The constants m_1 , m_2 and m_3 can be used to represent these values of r where,

$$m_1 = 0, 1$$
 $m_2 = 0, 1$
 $m_3 = 0, 1$
(14)

The x, y and z coordinates of a nodal point for a particular octant can then be expressed as follows and omitting the vector notation for convenience,

$$x_{nm_1} = m_1 B_{1n} h_1$$
 $y_{nm_2} = m_2 B_{2n} h_2$
 $z_{nm_3} = m_3 B_{3n} h_3$
(15)

The interpolation equations for the displacement functions between the nodal points will be found by using an extension of the Lagrange interpolation formula for equal intervals as found in Kunz (4). The development of the equation for a single dependent variable and only one argument x is as follows.

Suppose, $f(x_0)$, $f(x_1)$,...., $f(x_n)$ are the functional values for arguments x_0 , x_1 ,..., x_n where the interval between the x's is a constant h and,

$$\mathbf{x}_{m} = \mathbf{x}_{0} + mh \qquad (0 \le m \le n)$$

$$\mathbf{x} = \mathbf{x}_{0} + rh \qquad (16)$$

In finding an n^{th} -degree polynomial P(x) passing through the n+1 points $(x_0, f(x_0)), (x_1, f(x_1)), \ldots, (x_n, f(x_n)), let <math>a_m(r)$ be an n^{th} -degree polynomial that is zero (possesses roots) for all the tabulated arguments except x_m , and for this argument it is equal to one, i.e.,

$$a_{m}(r_{k}) = \begin{cases} 0 & \text{for } k \neq m \\ 1 & \text{for } k = m \end{cases}$$
 (17)

From these equations it follows, $a_m(r)$ has n zeros 0, 1, ..., m-1, m+1, ..., n and that $a_m(r_m) = 1$. It is found from satisfying these conditions that,

$$a_{m}(r) = \frac{r(r-1)(r-2)...(r-m+1)(r-m-1)..(r-n)}{m(m-1)(m-2)...(+1)(-1)..(m-n)}$$

$$= \frac{(-1)^{n-m} r^{[n+1]}}{m! (n-m)! (r-m)}$$
(18)

The equation for the interpolating polynomial P(x) that passes through all points becomes,

$$P(x) = \sum_{m=0}^{n} \frac{(-1)^{n-m} r^{[n+1]}}{m! (n-m)! (r-m)} f(x_m)$$
 (19)

or,

$$P(x) = \sum_{m=0}^{n} a_m(r) f(x_m)$$
 (20)

also,

$$P(x_k) = a_k(r_k)f(x_k) = f(x_k)$$
 (21)

The same development can be used to find the interpolation equation for a dependent variable which is a function of two arguments x and y. Suppose that $f(x_0, y_0), \ldots, f(x_0, y_n), \ldots, f(x_n, y_0), \ldots, f(x_{n_1}, y_{n_2})$ are functional values for arguments $x_0, y_0; \ldots; x_{n_1}, y_{n_1}$ where the interval between the x's is a constant h_1 and between the y's is a constant h_2 and,

$$x_{m_{1}} = x_{0} + m_{1}h_{1} \qquad (0 \le m_{1} \le n_{1})$$

$$y_{m_{2}} = y_{0} + m_{2}h_{2} \qquad (0 \le m_{2} \le n_{2})$$

$$x = x_{0} + r_{1}h_{1}$$

$$y = y_{0} + r_{2}h_{2}$$
(22)

To find polynomial P(x, y), a function of two arguments, x and y which passes through all of the points one may proceed as follows.

Let $a_{m_1m_2}(r_1, r_2)$ be the polynomial that is zero (possesses roots) for all the tabulated arguments except x_{m_1}, y_{m_2} , and for this argument it is equal to one, i.e.,

$$a_{m_{1}m_{2}}(r_{1}, r_{2}) = \begin{cases} 0 & \text{for } k_{1} \neq m_{1} \\ 0 & \text{for } k_{2} \neq m_{2} \\ 1 & \text{for } k_{1} = m_{1}, k_{2} = m_{2} \end{cases}$$
 (23)

In order to determine the two variable polynomial which will satisfy the above conditions, consider,

$$a_{m_{1}}(r_{1}) = \begin{cases} 0 & \text{for } k_{1} \neq m_{1} \\ 1 & \text{for } k_{1} = m_{1}^{r} \end{cases}$$
 (24)

$$a_{m_{2}(r_{2})} = \begin{cases} 0 & \text{for } k_{2} \neq m_{2} \\ 1 & \text{for } k_{2} = m_{2} \end{cases}$$
 (25)

It follows that if there is a polynomial that satisfies Equation 24 and another polynomial that satisfies Equation 25, then,

$$a_{m_1}(r_1) \cdot a_{m_2}(r_2) \equiv a_{m_1m_2}(r_1, r_2)$$
 (26)

Equation 26 must be an identity because Equation 24 satisfies Equation 23 for the zeros in the x direction and Equation 25 satisfies Equation 23 for the zeros in the y direction and therefore the two multiplied together must satisfy the combined conditions of Equation 23. The

form of the polynomials for Equations 24 and 25 has already been determined in Equation 18. The polynomial $a_{m_1 m_2}$ (r_1 , r_2) becomes,

$$a_{m_1m_2}(r_1, r_2) = \frac{(-1)^{(n_1-m_1)(n_2-m_2)}r_1^{[n_1+1]}r_2^{[n_2+1]}}{m_1! m_2! (n_1-m_1)! (n_2-m_2)! (r_1-m_1)(r_2-m_2)}$$
(27)

The equation of the interpolating polynomial P(x, y) that passes through all of the functional values becomes, P(x, y)

$$P(x,y) = \sum_{m_1=0}^{n_1} \sum_{m_2=0}^{n_2} \frac{(-1)^{(n_1+n_2-m_1-m_2)} r_1^{[n_1+1]} r_2^{[n_2+2]}}{m_1! m_2! (n_1-m_1)! (n_2-m_2)! (r_1-m_1) (r_2-m_2)} f(x_{m_1}, y_{m_2}) \quad (28)$$

or,
$$P(x,y) = \sum_{m=0}^{n_1} \sum_{m=0}^{n_2} a_{m_1 m_2}(r_1, r_2) f(x_{m_1}, y_{m_2})$$
 (29)

also,
$$P(x_{k_{1}}, y_{k_{2}})$$

$$= a_{k_{1}k_{2}}(r_{1_{k_{1}}}, r_{2_{k_{2}}}) f(x_{k_{1}}, y_{k_{2}}) = f(x_{k_{1}}, y_{k_{2}})$$
(30)

If the dependent variable is a function of three arguments x, y and z, the polynomial that passes through all points can be determined in the same manner as in the last two cases. The subscript 3 will be used to refer to those variables in the z direction. The polynomial which possesses zeros at all of the tabulated arguments except for the unique set of arguments x_{m_1} , y_{m_2} , x_{m_3} becomes,

$$a_{m_1 m_2 m_3} (r_1, r_2, r_3) = a_{m_1} (r_1) \cdot a_{m_2} (r_2) \cdot a_{m_3} (r_3)$$
 (31)

or,

$$=\frac{\left(-1\right)^{\left(n_{1}^{+}n_{2}^{+}n_{3}^{-}m_{1}^{-}m_{2}^{-}m_{3}^{-}\right)}r_{1}^{\left[n_{1}^{+}1\right]}r_{2}^{\left[n_{2}^{+}1\right]}r_{3}^{\left[n_{3}^{+}1\right]}}{r_{1}^{\left[n_{2}^{+}m_{3}^{+}\right]\left(n_{1}^{-}m_{1}^{+}\right)!\left(n_{2}^{-}m_{2}^{-}\right)!\left(n_{3}^{-}m_{3}^{-}\right)!\left(r_{1}^{-}m_{1}^{+}\right)\left(r_{2}^{-}m_{2}^{-}\right)\left(r_{3}^{-}m_{3}^{-}\right)}}$$

$$(32)$$

The equation of the interpolating polynomial P(x, y, z) which passes through all of the functional values becomes,

P(x, y, z)

$$= \sum_{m_1=0}^{n_1} \sum_{m_2=0}^{n_2} \sum_{m_3=0}^{n_3} a_{m_1 m_2 m_3} (r_1, r_2, r_3) f(x_{m_1}, y_{m_2}, z_{m_3})$$
(33)

In order to apply this polynomial to the particular problem at hand, there must be included the position of the octant, and the displacement function that is being determined. This can be done in the following manner.

Because of linearity in x, y and z,

$$n_1 = n_2 = n_3 = 1$$

n = the octant identification number

i = the displacement function number

then,

$$u_{n}(x, y, z) = f_{1n}(x, y, z)$$

 $v_{n}(x, y, z) = f_{2n}(x, y, z)$
 $w_{n}(x, y, z) = f_{3n}(x, y, z)$
(34)

The general polynomial $P_{in}(x, y, z)$ that passes through all of the tabulated displacements for one of the above equations becomes,

$$P_{in}(x, y, z) = \frac{\sum_{m_1=0}^{1} \sum_{m_2=0}^{2} \sum_{m_3=0}^{2} \frac{(-1)^{(3-m_1-m_2-m_3)} r_1(r_1-1) r_2(r_2-1)}{(r_1-m_1)(r_2-m_2)} \cdot \frac{r_3(r_3-1)}{(r_3-m_3)} f_i(x_{nm_1}, y_{nm_2}, z_{nm_3})$$
(35)

The derivative of this function with respect to x, y or z can be performed in the usual manner. For example, the derivative of this function with respect to x would be the following:

$$\frac{\partial P_{ln}}{\partial x} = \frac{\sum_{m_1=0}^{1} \sum_{m_2=0}^{\Sigma} \sum_{m_3=0}^{\Sigma} \frac{(-1)^{(3-m_1-m_2-m_3)} (r_1^2 - 2m_1r_1 + m_1)}{(r_1-m_1)^2 (r_2-m_2) (r_3-m_3)} \cdot \frac{r_2 r_3 (r_2-1) (r_3-1)}{h_1} \frac{B_{ln}}{h_1} f_1 (x_{n_1 m_1}, y_{n_1 m_2}, z_{n_1 m_3})$$
(36)

but,

$$m_1 = m_1^2$$

therefore,

$$\frac{\partial P_{1n}}{\partial x} = \frac{1}{m_1} = 0 \quad \frac{1}{m_2} = 0 \quad \frac{1}{m_3} = 0 \qquad \frac{(-1)^{(3-m_1-m_2-m_3)} r_2 r_3 (r_2-1) (r_3-1)}{(r_2-m_2) (r_3-m_3)}$$

$$\cdot \frac{B_{\ln}}{h_1} f_1(x_{n m_1}, y_{n m_2}, z_{n m_3})$$
 (37)

The derivatives of Equation 35, as can be seen from the example derivative in Equation 37, are functions of only two of the three arguments, and being that they are linear equations, they form warped plane surfaces with respect to these two arguments.

If it is desired, the previous equations can also be shown in matrix form. As an example, Equation 35 is shown in matrix form on page 25. When Equation 35 is expanded, for a particular variable displacement function, as for example u, it will appear in the following form, where r_1 , r_2 and r_3 and also I, J and K are the variable quantities for a particular octant from Table I, and with the subscript n omitted from these variables for convenience,

$$u(r_{1}, r_{2}, r_{3}) = u(0, 0, 0) + r_{1}[u(I, 0, 0) - u(0, 0, 0)]$$

$$+ r_{2}[u(0, J, 0) - u(0, 0, 0)]$$

$$+ r_{3}[u(0, 0, K) - u(0, 0, 0)]$$

$$+ r_{1}r_{2}[u(I, J, 0) - u(0, J, 0) - u(I, 0, 0) + u(0, 0, 0)]$$

$$+ r_{2}r_{3}[u(0, J, K) - u(0, J, 0) - u(0, 0, K) + u(0, 0, 0)]$$

$$+ r_{1}r_{3}[u(I, 0, K) - u(I, 0, 0) - u(0, 0, K) + u(0, 0, 0)]$$

$$+ r_{1}r_{2}r_{3}[u(I, J, K) - u(I, J, 0) - u(0, J, K) - u(I, 0, K)$$

$$+ u(I, 0, 0) + u(0, J, 0) + u(0, 0, K) - u(0, 0, 0)]$$

When Equation 37 is expanded in the same manner as in the above equation, it will appear as follows:

$$\frac{\partial u(\mathbf{r}_{1}, \mathbf{r}_{2}, \mathbf{r}_{3})}{\partial x} = \frac{B_{\ln}}{h_{1}} [u(I, 0, 0) - u(0, 0, 0)]$$

$$+ \frac{B_{\ln}^{r} 2}{h_{1}} [u(I, J, 0) - u(0, J, 0) - u(I, 0, 0) + u(0, 0, 0)]$$

$$+ \frac{B_{\ln}^{r} 3}{h_{1}} [u(I, 0, K) - u(0, 0, K) - u(I, 0, 0) + u(0, 0, 0)]$$

$$+ \frac{B_{\ln}^{r} 2^{r} 3}{h_{1}} [u(I, J, K) - u(0, J, K) - u(I, J, 0) + u(0, J, 0)$$

$$- u(I, 0, K) + u(0, 0, K) + u(I, 0, 0) - u(I, 0, 0)]$$
(39)

Equation 35, which represents the general equation for the u, v and w displacement function within a particular octant, can also be transformed to the following form for a more general view of the type of equation involved,

$$u = A_0 + A_1x + A_2y + A_3z + A_4xy + A_5xz + A_6yz + A_7xyz$$

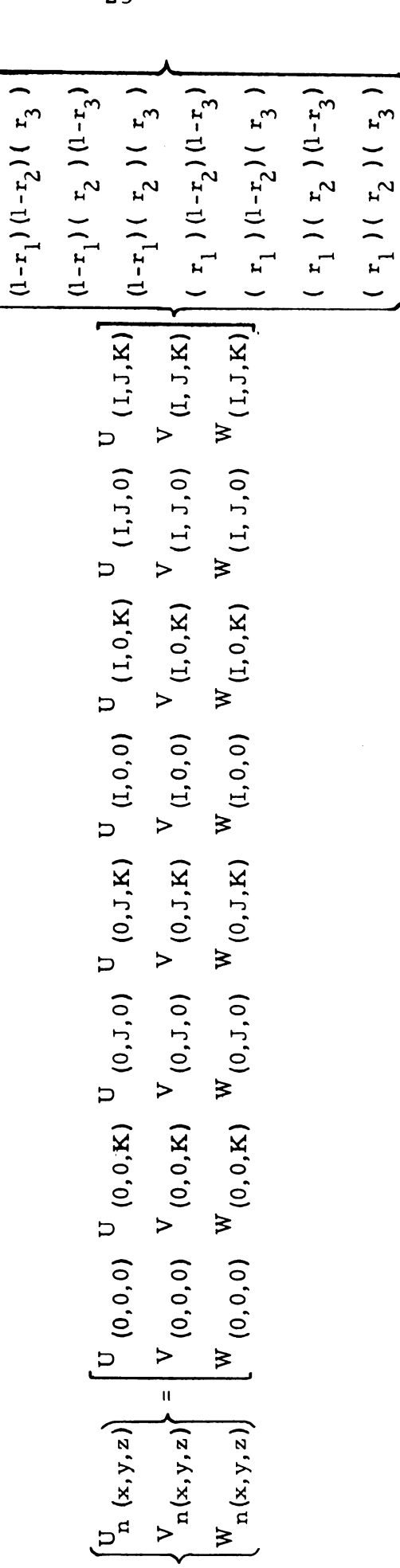
$$v = B_0 + B_1x + B_2y + B_3z + B_4xy + B_5xz + B_6yz + B_7xyz$$

$$w = C_0 + C_1x + C_2y + C_3z + C_4xy + C_5xz + C_6yz + C_7xyz$$
(40)

If these equations are substituted into the equations of compatibility, which are given by various authors (6), (10), (13) and (15), it will be found that compatibility of displacement is satisfied. If these equations are substituted into the equations of equilibrium in terms of displacement, Equation 10, it will be found that these equations are not identically satisfied. However, when the solution for the displacements at the nodal points has been determined, the equations

 $(1-r_1)(1-r_2)(1-r_3)$

Equation 41
DISPLACEMENT EQUATIONS IN MATRIX FORM



I, J, K are the identification vectors for the nth octant.

of equilibrium will be satisfied for the region of the nodal point.

The conclusion can also be reached that since the body is being represented as a mesh work of nodal points with linearity assumed between the nodal points, the accuracy of the solution will be dependent on the size of the mesh chosen, since the linear lines will then be able to represent the true configuration of the displacement functions with less error.

As was stated previously, the determination of the equations of equilibrium is to be developed on the basis of the integration of the forces acting on the surfaces of the octants which are formed by passing planes through the mid-point of the mesh lines (Figure 3). The average stress on any octant's surface will be the stress that occurs at the centroid of the octant's surface. This is due to the fact that the stress surface is a warped plane, and the average elevation of a warped plane surface occurs at the centroid of the area covered. The appropriate values of r for the centroid of the stresses on the surfaces of an octant are shown in Table II. To find the stress at one of these points, substitute the appropriate derivatives, as illustrated in Equation 39, into the stress function, Equations 7, and introduce the required values of the variables for that particular octant and then substitute in the values of r taken from Table II.

TABLE II

STRESS	$^{\mathbf{r}}$ ln	r _{2n}	r _{3n}
σ xn	1/2	1/4	1/4
σ yn	1/4	1/2	1/4
σ zn	1/4	1/4	1/2
τ xyn	1/2	1/4	1/4
τ xzn	1/2	1/4	1/4
τ yxn	1/4	1/2	1/4
τ yzn	1/4	1/2	1/4
τ zxn	1/4	1/4	1/2
τzyn	1/4	1/4	1/2

The positive direction of the total force on an octant should be made consistent with the major coordinate axes. The stresses are considered positive according to the usual conventions. Therefore, the vector direction of the stress must be determined, by multiplying the stresses by the appropriate B coefficient for the octant on which the stress appears. Thus,

$$\overrightarrow{\sigma}_{xn} = \overrightarrow{B}_{1n} \overrightarrow{\sigma}_{xn}$$

$$\overrightarrow{\sigma}_{yn} = \overrightarrow{B}_{2n} \overrightarrow{\sigma}_{yn}$$

$$\overrightarrow{\sigma}_{zn} = \overrightarrow{B}_{3n} \overrightarrow{\sigma}_{zn}$$

$$\overrightarrow{\tau}_{xyn} = \overrightarrow{B}_{1n} \overrightarrow{\tau}_{xyn}$$

$$\overrightarrow{\tau}_{xzn} = \overrightarrow{B}_{1n} \overrightarrow{\tau}_{xzn}$$

$$\overrightarrow{\tau}_{yzn} = \overrightarrow{B}_{2n} \overrightarrow{\tau}_{yzn}$$

$$\overrightarrow{\tau}_{yxn} = \overrightarrow{B}_{2n} \overrightarrow{\tau}_{yxn}$$

$$\overrightarrow{\tau}_{zxn} = \overrightarrow{B}_{3n} \overrightarrow{\tau}_{zxn}$$

$$\overrightarrow{\tau}_{zyn} = \overrightarrow{B}_{3n} \overrightarrow{\tau}_{zyn}$$

The total vector force acting on an octant can then be determined by summing the individual average vector stresses by the area over which they act. This produces three total vector forces for any octant $(\overrightarrow{F}_x, \overrightarrow{F}_y)$ and (\overrightarrow{F}_z) . If the grid divisions are all the same, a, then,

$$h_1 = h_2 = h_3 = a$$
 (43)

and the forces acting on an octant can be developed as follows:

$$\frac{F}{xn} = \frac{1}{\sigma_{Xn}} + \frac{1}{\sigma_{yxn}} + \frac{1}{\sigma_{zxn}}$$

$$\frac{F}{xn} = E' \frac{1}{16a} \left[(1+\alpha) \left[-9u(0,0,0) - 3u(0,0,K) - 3u(0,J,0) - u(0,J,K) + 9u(I,0,0) + 3u(I,0,K) + 3u(I,J,0) + u(I,J,K) \right] \right]$$

$$+ (1-\alpha) \cdot 2B_{ln}B_{2n} \left[-3v(0,0,0) - 3v(I,0,0) - v(0,0,K) - v(I,0,K) + 3v(I,J,0) + v(0,J,K) + v(I,J,K) \right]$$

$$+ (I-\alpha) \cdot 2B_{ln}B_{3n} \left[-3w(0,0,0) - 3w(I,0,0) - w(0,J,0) - w(I,J,0) + 3w(I,0,K) + w(0,J,K) + w(I,J,K) \right]$$

$$+\alpha E' \frac{1}{16a} \left[-9u(0,0,0) - 3u(0,0,K) - 3u(I,0,0) - u(I,0,K) + 9u(0,J,K) + 3u(I,J,0) + u(I,J,K) + 2B_{1}B_{2} \left[-3v(0,0,0) - 3v(0,J,0) - v(0,0,K) - v(0,J,K) + 3v(I,0,0) + 3v(I,0,0) + 3v(I,J,0) + v(I,J,K) \right] - 9u(0,0,0)$$

$$-3u(I,0,0) - 3u(0,J,0) - u(I,J,0) + 9u(0,0,K) + 3u(I,0,K) + 3u(I,0,K) + 3u(I,J,K) + 2B_{1n}B_{3n} \left[-3w(0,0,0) - 3w(0,0,K) + 3u(I,0,K) + 3u(I,J,K) + 2B_{1n}B_{3n} \left[-3w(0,0,0) - 3w(0,0,K) + 3u(I,0,K) + 3u(I,J,K) + 2B_{1n}B_{3n} \left[-3w(0,0,0) - 3w(0,0,K) + 3u(I,0,K) + 3u(I,J,K) + 2B_{1n}B_{3n} \left[-3w(0,0,0) - 3w(0,0,K) + 3u(I,0,K) + 3u(I,J,K) + 2B_{1n}B_{3n} \left[-3w(0,0,0) - 3w(0,0,K) + 3w(0,0,K) + 3u(I,0,K) + 3u(I,J,K) + 2B_{1n}B_{3n} \left[-3w(0,0,0) - 3w(0,0,K) + 3w(0,0,K) + 3u(I,0,K) + 3u(I,J,K) + 2B_{1n}B_{3n} \left[-3w(0,0,0) - 3w(0,0,K) + 3w(0,0,K) + 3u(I,0,K) + 3u(I,J,K) + 2B_{1n}B_{3n} \left[-3w(0,0,0) - 3w(0,0,K) + 3w(0,0,K) + 3u(I,J,K) + 2B_{1n}B_{3n} \left[-3w(0,0,0) - 3w(0,0,K) + 3w(0,0,K) +$$

-w(0, J, 0) -w(0, J, K) +3w(I, 0, 0) +3w(I, 0, K)+w(I, J, 0)

+w(I, J, K)]

or,

$$\frac{F_{xn}}{a^2} = \frac{E'}{16a} \left[-(9+27a)u(0,0,0) + (-3+3a)[u(0,0,K) + u(0,J,0)] + (-1+5a)u(0,J,K) + (9+3a)u(I,0,0) + (3+5a)[u(I,J,0) + u(I,0,K)] + (1+3a)u(I,J,K) + 2 \cdot B_{ln}B_{2n}[-3v(0,0,0) + (3-6a)v(0,J,0) - v(0,0,K) + (1-2a)v(0,J,K) + (-3+6a)v(I,0,0) + 3v(I,J,0) + (-1+2a)v(I,0,K) + v(I,J,K)] + 2 \cdot B_{ln}B_{3n}[-3w(0,0,0) + (3-6a)w(0,0,K) - w(0,J,0) + (1-2a)w(0,J,K) + (-3+6a)w(I,0,0) + 3w(I,0,K) + (-1+2a)w(I,J,0) + (-$$

Similarly,

$$\frac{F}{yn} = \frac{E'}{16a} \left[-(9+27a)v(0,0,0) + (-3+3a)[v(0,0,K)+v(I,0,0)] + (-1+5a)v(I,0,K) + (9+3a)v(0,J,0) + (3+5a)[v(I,J,0)+v(0,J,K)] + (1+3a)v(I,J,K) + 2 \cdot B_{ln}B_{2n}[-3u(0,0,0) + (3-6a)u(I,0,0) - u(0,0,K) + (1-2a)u(I,0,K) + (-3+6a)u(0,J,0) + 3u(I,J,0) + (-1+2a)u(0,J,K) + (1-1+2a)u(0,J,K) + (1-1+2a)u(0,J,K) + (1-1+2a)u(0,J,K) + (1-1+2a)u(1,0,K) + (1-1+2a)u(1,0,K) + (1-1+2a)u(1,0,K) + (1-1+2a)u(1,0,K) + (1-1+2a)u(1,0,K) + (1-1+2a)u(1,J,K) \right]$$

and,

$$\frac{F}{2n} = \frac{E^{1}}{16a} \left[-(9+27a)w(0,0,0) + (-3+3a)[w(I,0,0)+w(0,J,0)] + (-1+5a)w(I,J,0) + (9+3a)w(0,0,K) + (3+5a)[w(0,J,K)+w(I,0,K)] + (1+3a)w(I,J,K) + (2 \cdot B_{2n}B_{3n}[-3v(0,0,0) + (3-6a)v(0,J,0) - v(I,0,0) + (1-2a)v(I,J,0) + (-3+6a)v(0,0,K) + 3v(0,J,K) + (-1+2a)v(I,0,K) + v(I,J,K)] + 2 \cdot B_{1n}B_{3n}[-3u(0,0,0) + (3-6a)u(I,0,0) - u(0,J,0) + (1-2a)u(I,J,0) + (-3+6a)u(0,0,K) + 3u(I,0,K) + (-1+2a)u(0,J,K) + (-1+2a)u(0,J,K) + (u(I,J,K)] \right]$$

These three equations represent the three principal vector forces acting on each octant. The general total force acting on an octant would then be the sum of these three vectors. The total force acting on the planes surrounding a nodal point would then be the sum of the forces on the individual octants. If the octants used are to be actually part of the physical solid body, then the number of octants surrounding a nodal point can vary from one octant for a corner, two octants for an edge, four octants for a surface to eight octants for an interior nodal point.

The method for combining these forces into the proper equilibrium equations will be discussed in the following chapter.

CHAPTER III

METHOD OF SOLUTION

The general solution of solid problems using the octant force equations developed in the last chapter is obtained by simultaneously solving a set of equilibrium equations formed from the nodal points of the whole body.

Each nodal point in the body, in general, has three degrees of freedom of displacement. There is available an equation of equilibrium in the direction of each unknown displacement component.

Therefore, there is one equation for each unknown displacement throughout the whole body, forming a complete and solvable set of equations with no ambiguity.

In the interior of the body, the equilibrium equations are formed by summing the vector forces on all eight octants to zero in each of the principal directions. The equilibrium equations formed on the boundary, however, require fairly close attention, especially in those regions where the curvature of the displacements along the boundary is comparatively large. In the interior of the body the equilibrium equations are formed by essentially taking the difference of two first order equations, thus, forming a second order difference. On the boundary, there are two alternatives to the solution. The first method would be to eliminate the octants that are not actually

part of the body and use the boundary forces as part of the equilibrium equations for the affected nodal points. This will then lead to a first order solution in the neighborhood of the boundary, which will lead to small error, for small curvatures of the boundary displacements. The second method would be to create external fictitious nodal points one grid spacing removed from the boundary. These fictitious nodal points can be determined by substituting the boundary stress conditions for their finite difference equivalents in terms of these fictitious points. The stresses on the boundary will be correct and the equilibrium equations will be of the second order throughout the body. The first method will be applied to the solution of the example problems in the following chapter because of their relative simplicity.

Using the first method, the general equation for the equilibrium of a nodal point can be shown as follows:

$$F_{x} = 0 = \sum_{n=1}^{8} T_{n} F_{xn} + \sum_{n=1}^{8} X_{n}$$

$$F_{y} = 0 = \sum_{n=1}^{\infty} T_{n} F_{yn} + \sum_{n=1}^{\infty} Y_{n}$$
 (48)

$$F_{z} = 0 = \sum_{n=1}^{\infty} T_{n} F_{zn} + \sum_{n=1}^{\infty} Z_{n}$$

If there are no body forces and the nth octant exists, $T_n = 1$ and $X_n = Y_n = Z_n = 0$. If the nth octant does not exist and there are no

body forces, then $T_n = 0$ and X_n , Y_n and Z_n are the appropriate boundary forces in terms of the boundary normal force and shearing forces. The identification subscripts which occur in the equations for the forces on the octants, Equations 45 to 47, are at this point only identified with respect to the reference nodal point where the equilibrium equation is being formed. For a complete set of equations, the reference nodal point for the equilibrium equation must be referenced to the main centroidal axis system of the whole body. This can be accomplished if we define the distance to the nodal point in the following manner,

$$x_L = La$$
 $L = 0, 1, 2, 3,$ $y_M = Ma$ $M = 0, 1, 2, 3,$ $z_N = Na$ $N = 0, 1, 2, 3,$

Therefore, the identification of the position of a nodal point for a particular displacement function can be indicated as follows:

$$u(I, J, K)_{L, M, N} = u(La+I, Ma+J, Na+K)$$

$$v(I, J, K)_{L, M, N} = v(La+I, Ma+J, Na+K)$$

$$w(I, J, K)_{L, M, N} = w(La+I, Ma+J, Na+K)$$
(50)

The general equations of equilibrium of a nodal point with respect to the main centroidal axis system then become:

In general, the system of equations produced for a given body with even a fairly small number of grid spacings, would yield a tremendous number of equations to be solved simultaneously. This would then eliminate as a possible method of solution the methods using the inverse of the coefficient matrix. The remaining choices are those which use relaxation and iteration. These methods are comparatively simple for the types of equations being used for solution, because there are only 57 basic types of equations. The only variables of this system of equations will then be the location of the reference nodal point (L, M and N), the type of equation to be used (one of the 57 basic types) and the boundary forces, if present at that particular nodal point. The equations can, therefore, be written with these variables built into them. In order to converge to a solution by iterating on the equations thus formed, a relaxation or even an over relaxation procedure can be adopted. If this is done, the relaxation of the equations can proceed until the change in the values of the displacements between iterations is a small acceptable value.

This value represents the convergence error of the iteration solution.

When this method of iteration is applied to the previous general equations of equilibrium, the equations can be represented in the following form,

$$R_{x}(L, M, N) = \sum_{n=1}^{8} T_{n} + \sum_{n=1}^{8} X_{n} + \sum_{n=1}^{8} X_{n} + \sum_{n=1}^{8} T_{n} + \sum_{n=1}^{8} T_{n} + \sum_{n=1}^{8} T_{n} + \sum_{n=1}^{8} X_{n} + \sum_{n=1}$$

$$u(L, M, N)_{new} = u(L, M, N)_{old} + C_{r}R_{x}(L, M, N)$$
 (53)

$$R_{y}(L, M, N) = \sum_{n=1}^{8} T_{n} F_{yn} + \sum_{n=1}^{8} Y_{n} L, M, N$$

$$\frac{*}{*} \sum_{n=1}^{8} T_{n} (9 + 27a)$$

$$(54)$$

$$v(L, M, N)_{new} = v(L, M, N)_{old} + C_r R_y(L, M, N)$$
 (55)

$$R_{z}(L, M, N) = \sum_{n=1}^{8} T_{n} F_{zn} + \sum_{n=1}^{8} Z_{n} L, M, N + \sum_{n=1}^{8} Z_{n} L, M, N$$

$$\vdots \sum_{n=1}^{8} T_{n} (9+27a)$$
(56)

$$w(L, M, N)_{new} = w(L, M, N)_{old} + C_r R_z(L, M, N)$$
 (57)

Where, the acceptable error

=
$$e \ge R_x(L, M, N) \ge R_v(L, M, N) \ge R_z(L, M, N)$$
 (58)

and, C_r is the over relaxation constant that can be used when desired.

When the error in the displacements has converged to the small error, e, the stresses at the nodal points can be determined using Equations 7. These stresses can then be used for the usual purposes and applications.

CHAPTER IV

EXAMPLE PROBLEMS

The example problems that will be shown in this chapter are for the purpose of demonstrating the application of the method and the behavior of the equations involved under different types of loading conditions.

The first is an example problem which will be used to compare the stress distribution in a solid cube supported on a plane surface under the loading of a line load acting perpendicular to the top surface along the centroidal X-Axis (Figure 4) when computed with the proposed method and Poisson's ratio equal to zero, to the stress distribution computed using the plane stress and plane strain classical solution of a thin plate, with a concentrated load acting at the center of one edge. The classical solution will be solved using the Airy's stress function (15) and finite difference methods. The stress distribution for various other values of Poisson's ratio will also be shown using the proposed method. The stress distribution, for Poisson's ratio equal to zero, is unique because the normal stress is dependent only on the normal derivative. Thus, when the boundary conditions are constant in the direction of one of the principal axes, the stress distribution on any plane perpendicular to that axis is a constant. When Poisson's ratio is not zero, the normal stresses are

dependent on all three normal derivatives and the stress distribution will vary along this axis.

The second problem will consider the stress distribution in a solid cube due to the application of a concentrated load acting in the direction of the Z-Axis at the intersection of the centroidal Z-Axis and the surface of the cube (Figure 5). The effect of Poisson's ratio on the stress distribution will also be investigated.

The third problem will find the stress distribution in a solid cube due to a distributed load over a small concentric area on the surface of the cube (Figure 6). This stress distribution will be compared to the solution determined in problem two. This problem will also demonstrate whether some of the effects of the changing of Poisson's ratio are due to the nature of the concentrated load, or due to the behavior of the equations when the ratio approaches a value of one-half. When Poisson's ratio is one-half, the dilatation of the material is zero, and in such a case, the average stress for a point in the body is indeterminate, and only the differences between the average stress and normal stresses are determinate. Therefore, a solution of problems using the displacements of the body is impossible.

The fourth problem will show the stress distribution in a beamcolumn due to the action of an eccentric load (Figure 7). This will
correspond to the case of a post-tensioned member, or a column with
an eccentric load.

The fifth problem will find the stress distribution in a beamcolumn subjected to the theoretical stress distribution of a beam under
constant moment (Figure 8). Since the solution of this problem is
already known, the problem will demonstrate the relative error
associated with the use of this method's first order equilibrium
equations at the boundary surfaces in conjunction with a variable
Poisson's ratio.

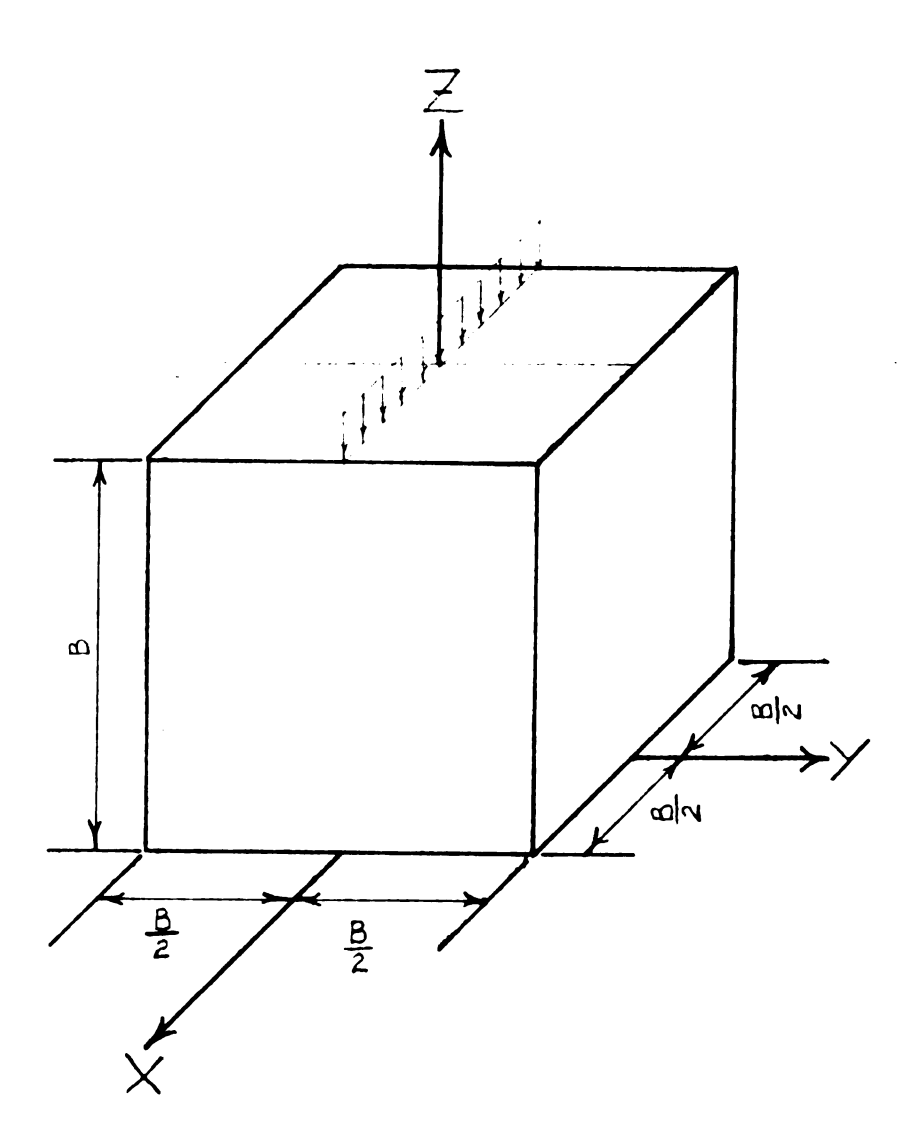


Figure 4. Isometric view of cube with line load for Example Problem One.

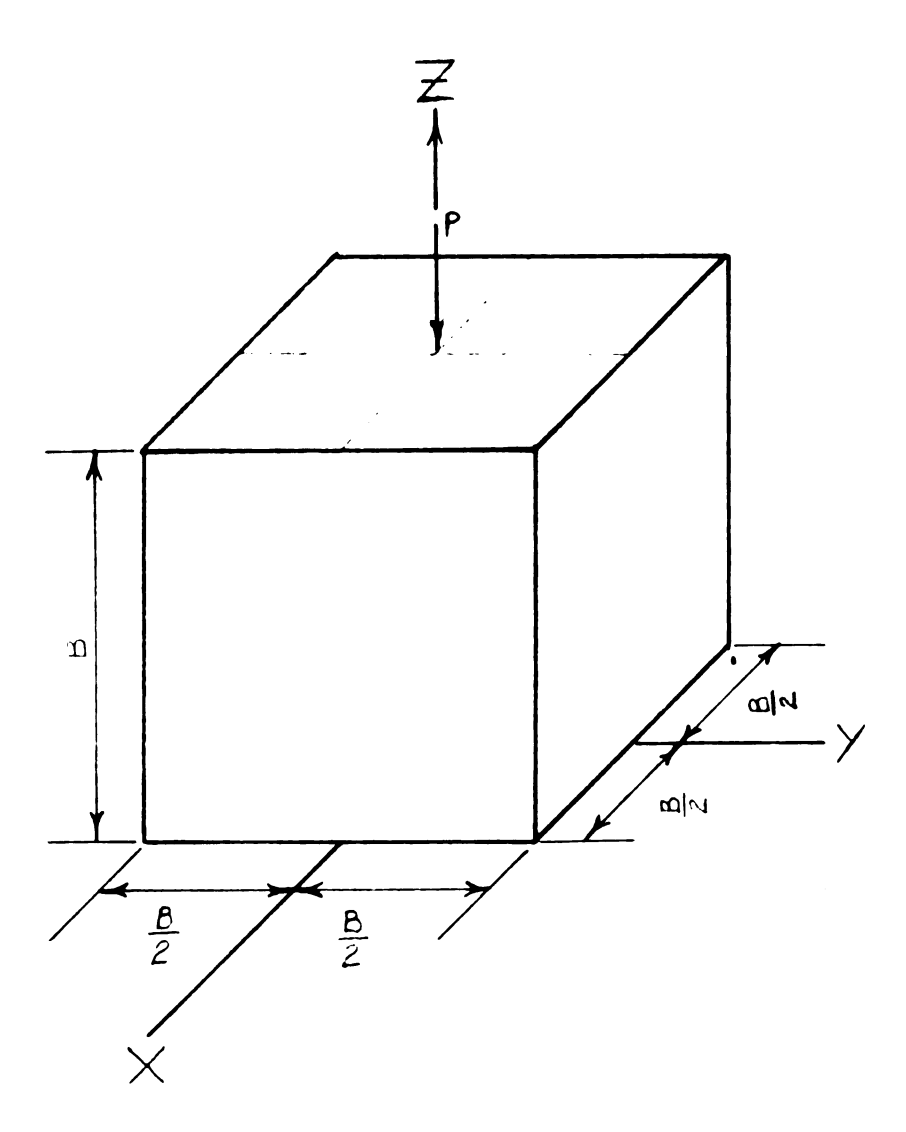


Figure 5. Isometric view of cube showing concentrated load on the Z-Axis for Example Problem Two.

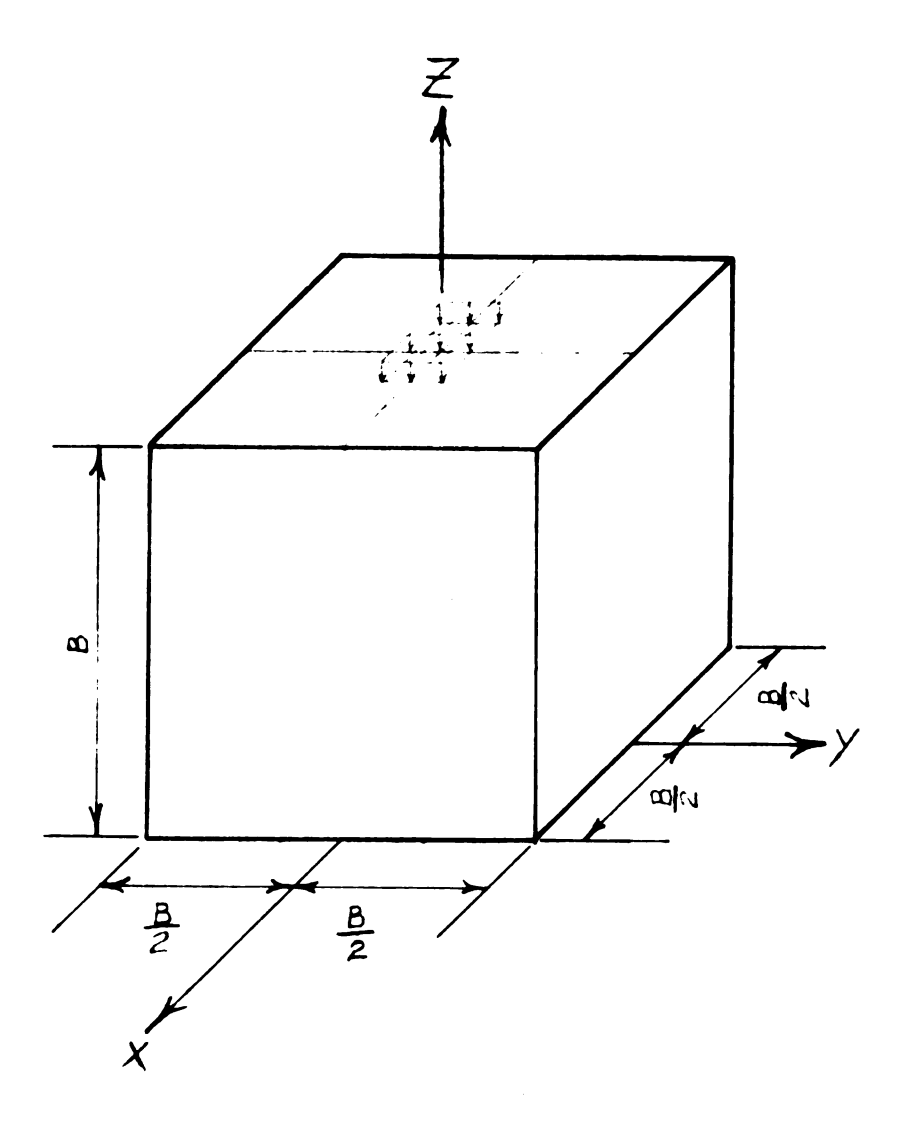


Figure 6. Isometric view of cube showing concentric distributed load over small portion of the top surface for Example Problem Three.

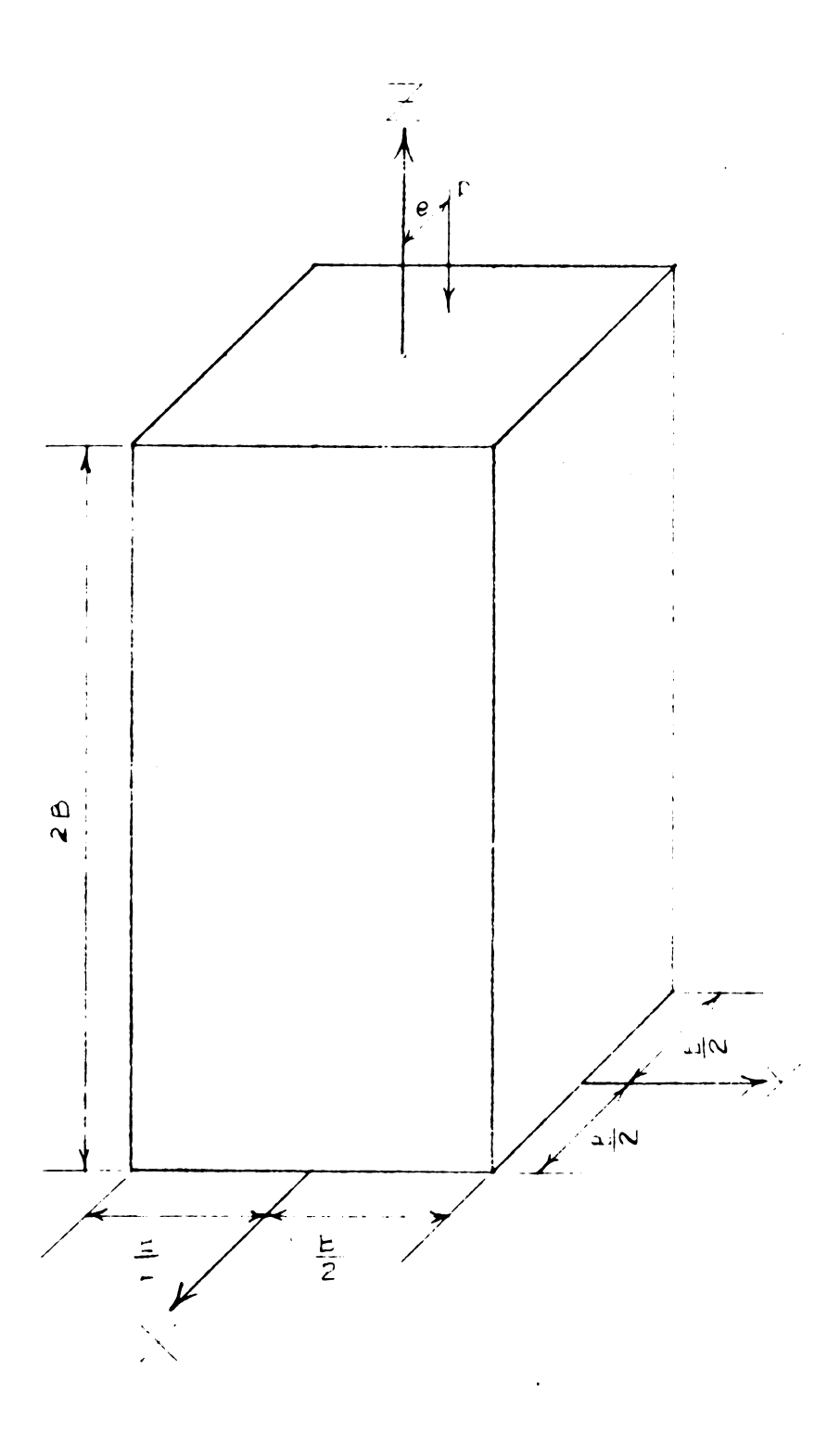


Figure 7. Isometric view of a beam-column showing the location of the eccentric load for Example Problem Four.

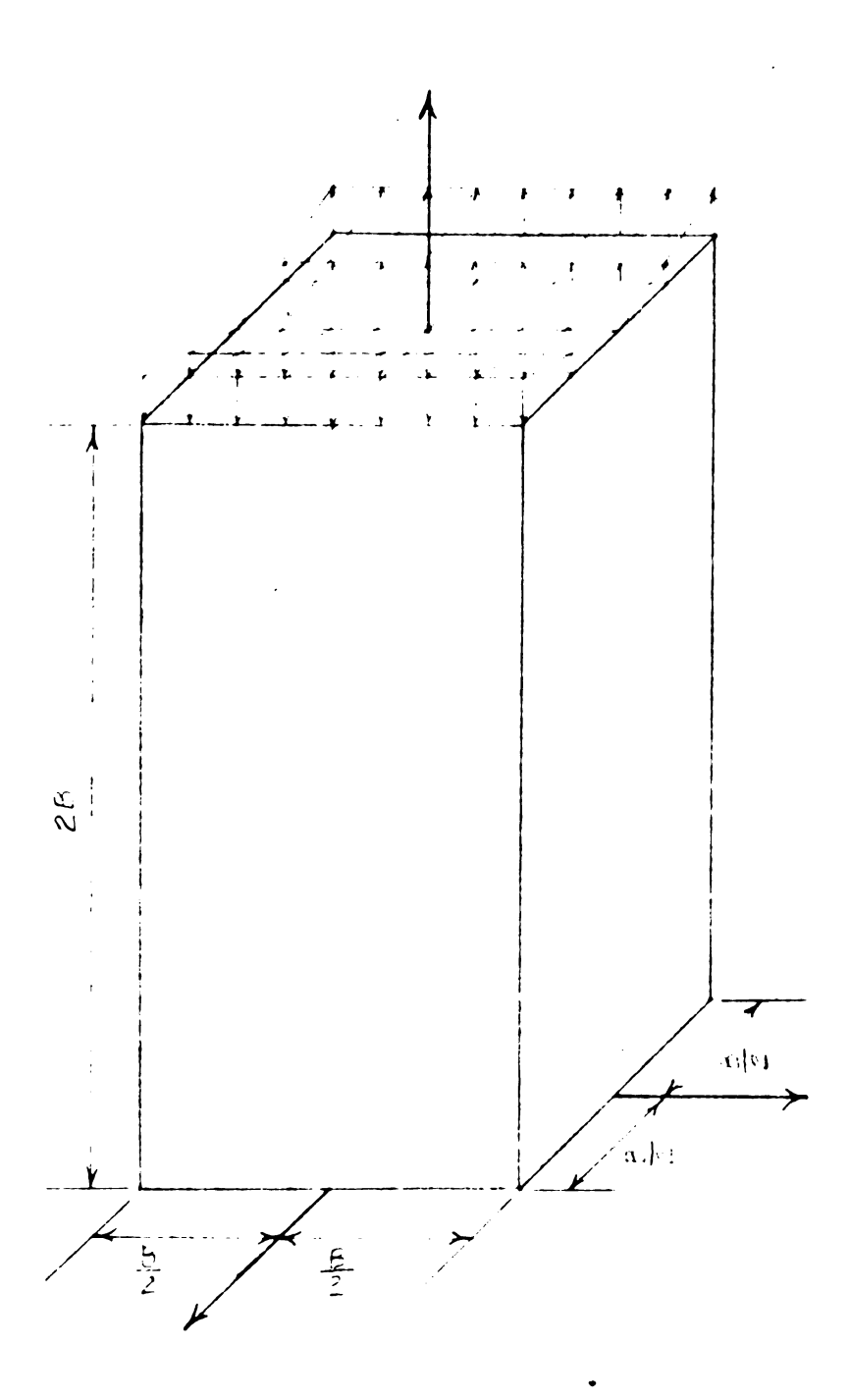


Figure 8. Isometric view of a beam-column showing the surface stress distribution for the applied moment for Example Problem Five.

EXAMPLE PROBLEM NUMBER ONE

In this first problem, we will find the stress distribution in a cube due to a line load acting along the X-Axis on the surface of the cube as is shown in Figure 4. The solution will be found for three different grid spacings. The grid spacing in any particular solution will be the same in all three principal directions. Each solution using the proposed method, with Poisson's ratio equal to zero, will also have a parallel solution computed using the classical biharmonic approach using finite differences. For the first grid, we will use a grid spacing of B/4, for the second grid, we will use a grid spacing of B/8 and for the third grid, we will use a grid spacing of B/16. For purposes of comparison between the various solutions, we will specify that the average stress on any X-Y plane be unity. Therefore, the computed stresses will be stress concentration factors for the assumed unit average stress. If we consider the line load to be distributed over a one-half grid spacing on either side of the loaded line, then we can develop the following relationship between the specified unit stress on the cross section, the stress on the distributed line load, and the size of the grid spacing.

a = grid spacing

B = dimension of cube

N = number of segments in B length

Therefore.

B = Na

Q = stress on loaded area

then.

$$QaB = 1B^2$$

or,

$$Q = 1 \frac{B}{a} = 1 \cdot N$$

By inspection, the w displacements will be symmetrical with respect to the centroidal Y-Z and X-Z planes on any X-Y plane, and the u and v displacements will be anti-symmetrical with respect to these same planes.

The numerical solution is, therefore, required in only one quadrant of any X-Y plane. All boundary forces can be set equal to zero except for those nodal points which lie along the loaded area. In the equations of equilibrium, for the nodal points, the boundary forces can be expressed in the equation in terms of the boundary stresses because the grid spacing is a constant. Therefore, the equations can be divided by the area over which the stresses act.

It will be convenient for programing purposes to write the equations such that the boundary forces can be included in the equations. This can be done by entering the equation with the proper nodal displacement incremented by some value and when leaving the equation subtracting this incremental value, leaving the nodal displacement at the correct value. This technique and the method

of determining stresses can be demonstrated as follows: As an example, part of the equation of equilibrium for a quadrant on the Z surface (Equations 47 and 48) can be written in the following form,

$$\frac{E'}{16a}$$
 [-(9+27a)w(0,0,0)+ etc...] + $K\sigma_z^{boundary} = 0$ where

K is an arbitrary constant for the boundary stresses. Defining,

$$w' = \frac{E'(9+27a)}{16a} w$$

$$v' = \frac{E'(9+27a)}{16a} v$$

$$u' = \frac{E'(9+27a)}{16a}u$$

the equation can be written in the following form,

$$[-(9+27a)w'(0,0,0)+... \text{ etc.}]/(9+27a)]+K_z^{\text{boundary}}=0$$

Setting

$$w'(0,0,0) = w'(0,0,0) = w'(0,0,0) - C$$

then

$$C = K\sigma_z^{boundary}$$

as a correct substitution. When the equation has been relaxed (Equations 56 and 57), C can be eliminated as part of the w displacement,

$$w(0,0,0) = (w(0,0,0)-C) + C$$

This is a very simple means of expressing the boundary forces, since C can be chosen as any convenient constant consistent with the boundary stress distribution.

When the stresses are determined from the primed values of the displacements, the equations must be corrected for the value of K and for the elastic constants. As an example of the procedure, the σ_z stress at a nodal point L, M, N would be determined in the following manner:

$$\sigma_{z}(L, M, N) = E' \left[(1 + a) \frac{\partial w}{\partial z} + (1 - a) \frac{\partial u}{\partial x} + \frac{\partial v}{\partial y} \right]$$

$$= \frac{E'}{K} \frac{16a}{E'(9+27a)} \left[(1+a) \frac{\partial w'}{\partial z} + (1-a) \frac{\partial u'}{\partial x} + \frac{\partial v'}{\partial y} \right]$$

The normal finite difference equations for these derivatives, Kunz (4), would be substituted giving the correct stresses for the given loading condition.

The solution to the problem as a plane strain problem for Poisson's ratio equal to zero, was found by applying the familiar biharmonic solution as explained by S. Timoshenko and J. N.

Goodier (15),

$$\sigma_{y} = \frac{\partial^{2} \phi}{\partial z^{2}}$$
 $\sigma_{z} = \frac{\partial^{2} \phi}{\partial y^{2}}$
 $\tau_{zy} = -\frac{\partial^{2} \phi}{\partial y \partial z}$

which satisfies equilibrium for zero body forces.

Then, $\nabla^4 \phi = 0$ for compatibility.

For the boundaries,

$$-\frac{\partial \phi}{\partial y} = \int \bar{Z} \, ds \qquad \frac{\partial \phi}{\partial z} = \int \bar{Y} ds$$

or,

$$\phi_s = y \frac{\partial \phi}{\partial y} + z \frac{\partial \phi}{\partial z} - \int (z \frac{\partial^2 \phi}{\partial s \partial z} + y \frac{\partial^2 \phi}{\partial s \partial y}) ds$$

The solution of the values for phi and its normal derivative on the boundary is shown in Figure 9. An approximate solution of the stress distribution within the boundaries is found by dividing the plate into the same grid sizes as used in the other method, computing the phi values on the boundary, determining the fictitious phi values once removed from the boundaries by using the known value of the slope of the phi function normal to the boundary, and then writing the biharmonic operator in terms of phi for all points with an unknown phi value. This will lead to a set of linear algebraic equations which can be solved by the same methods applied to the three-dimensional equations. The stress distribution for the plate can be determined by using the known relationships between the stresses and phi. A typical comparison between the three-dimensional solution and the biharmonic solution can be seen in Table 3. In this table, the magnitude of the stress at various elevations on the Z-Axis is tabulated for the three grid sizes and these values are compared as a percentage to the extrapolated value of the function assuming an error of the second order. A graphical representation of this table is shown in Figure 10 for elevations z = 0, z = B/2, and z = 15B/16. Similar tables and graphs would show approximately the same trends for the two methods.

The values of σ_z and σ_x on the Z-Axis are shown in Figures 11 and 12 respectively for z = 0, z = B/2 and z = 7B/8 for varying

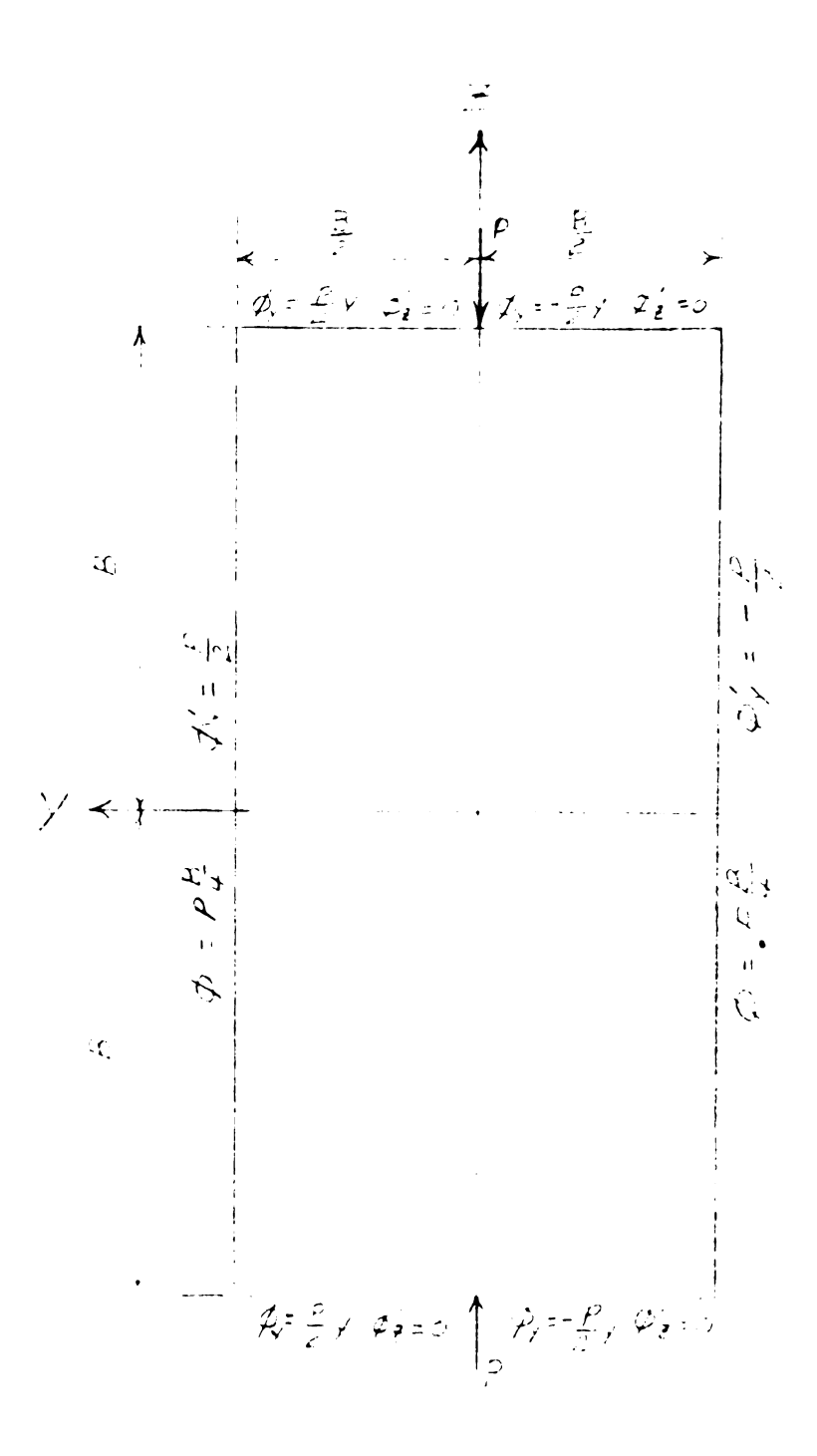


Figure 9. Outline of a thin plate with a concentrated load and the associated boundary phi functions for the biharmonic solution for Example Problem One.

Poisson's ratio and for the grid spacings of B/8 and B/16. The values of σ_z at z = 15 B/16 for the same parameters are shown in Figure 13. From these figures, it can be seen that as Poisson's ratio approaches one-half, the divergence between the solutions of the two grids greatly increases even when comparatively far from the loading surface. This would seem to indicate that the convergence of the equations to the true solution with increasing Poisson's ratio is not dependable for large grid spacings. It will also be noted, that within the usual range of Poisson's ratio for structural materials, 0.1 to 1/3, that the discrepancies between the solutions for the two grid sizes are small when comparatively far from the loaded surface where the singularity exists. For solutions of the stress distribution near the singularity, increasingly small grid spacings would be necessary. This is clearly evident in Figure 13 which shows the σ_{α} stress at z = 15B/16 for various Poisson's ratios and the two smaller grid sizes. The values for the larger of the two grid spacings were computed on the basis of straight line interpolation between z = 7B/8and the assumed distributed stress on the top surface. The lower line represents an assumed stress over one grid spacing of B/8 or a stress of 8 at the top surface and the upper line for the smaller grid length of B/16 or a stress of 16 on the top surface. The Flamant (15) solution for a concentrated load for z = 15B/16 and z = 7B/8 also is indicated in Figures 11 and 13 for Poisson's ratio of zero. The

agreement between the Flamant solution and the numerical method solution seem to indicate that as far as the vertical stress distribution is concerned, the solution in the neighborhood of the concentrated load is the Flamant solution. However, this will not be true for the σ and σ stress distributions. The σ stress does not exist as part of the Flamant solution because the problem is assumed to be that of the solution of a flat plate in plane strain or plane stress. In the Flamant solution, the $\sigma_{_{_{\mathbf{V}}}}$ stress is always of the same sign. In the real problem under investigation, we are not dealing with the semiinfinite plane and it is required in this problem that the sum of the normal stresses on any vertical section be zero, and therefore, the $\sigma_{\mathbf{v}}$ stress will be of varying sign so as to satisfy this condition. The Flamant solution for σ on the Z-Axis is zero and the σ stress on the Z-Axis would be the σ_z stress multiplied by Poisson's ratio (assuming the plane strain solution). Figure 14 shows the $\sigma_{\mathbf{x}}$ and $\sigma_{\mathbf{v}}$ stress on the Z-Axis for a Poisson's ratio of 0.3 and a grid spacing of B/16.

The Flamant solution can be used in the neighborhood of the concentrated load for the vertical stresses because the boundary conditions on the surface where the load is applied agree in both cases. The Flamant solution can not be used for the horizontal stresses because the boundary conditions on the vertical planes do not agree. The relative importance of this consideration would be

unimportant for design purposes in materials which are equally as strong in tension as in compression. However, in materials which are not equally as strong in tension as in compression, such as concrete, the presence of tension in the material could be of concern. The presence of these tension stresses will be even more marked in the example problem to follow which is the case of the concentric concentrated load.

As an example of the general distribution of the stresses throughout the block, lines of constant stress for σ_x , σ_y and σ_z on the Y-Z plane with x = 0 are shown in Figures 15, 16 and 17 respectively for the grid spacing of B/16 and with Poisson's ratio of 0.3.

VALUES OF $\sigma_{\mathbf{z}}$ WITH VARIOUS MESH SIZES FOR THE TWO SOLUTIONS TABLE III

t	Solution				Mesh Size			σ Extr	$\sigma_{\mathbf{z}}$ Extrapolated
٦	Method	B/4	$\sigma_{\mathbf{z}}/\sigma_{\mathbf{z}}$ Extr. %	B/8	$\sigma_{\mathbf{z}}/\sigma_{\mathbf{z}}$ Extr. %	B/16	$\sigma_{\mathbf{z}}/\sigma_{\mathbf{z}}$ Extr. %	1, 2, 4	2, 4
0	4 ∇ ф 3-D	1.123	105.7	1.077	101.3	1.066	100.3	1.062	1.062
B/2	2 ⁴ ♦ 3-D	1.554	106.0	1.504	102.6	1.477	100.6	1.467	1.468 1.473
B.4	4 ∇ ф 3-D	2.590	90.9	2.781	105.0	2.693	101.7	2.648	2.664
8 B	4 ∇ ⁴ 3-D	*3.205 *3.295	56.3 60.9	4.655 4.999	81.8	5.403 5.246	94.9 97.2	5.687	5.652
15 B	⁴ φ 3-D	*3.603 *3.648	**35.2 **33.0	*6.328 *6.500	**61.8 **58.7	9.247	**90.3 **89.7	10.419	10.220

* From straight line interpolation between points

^{**} Computed from extrapolation 2, 4

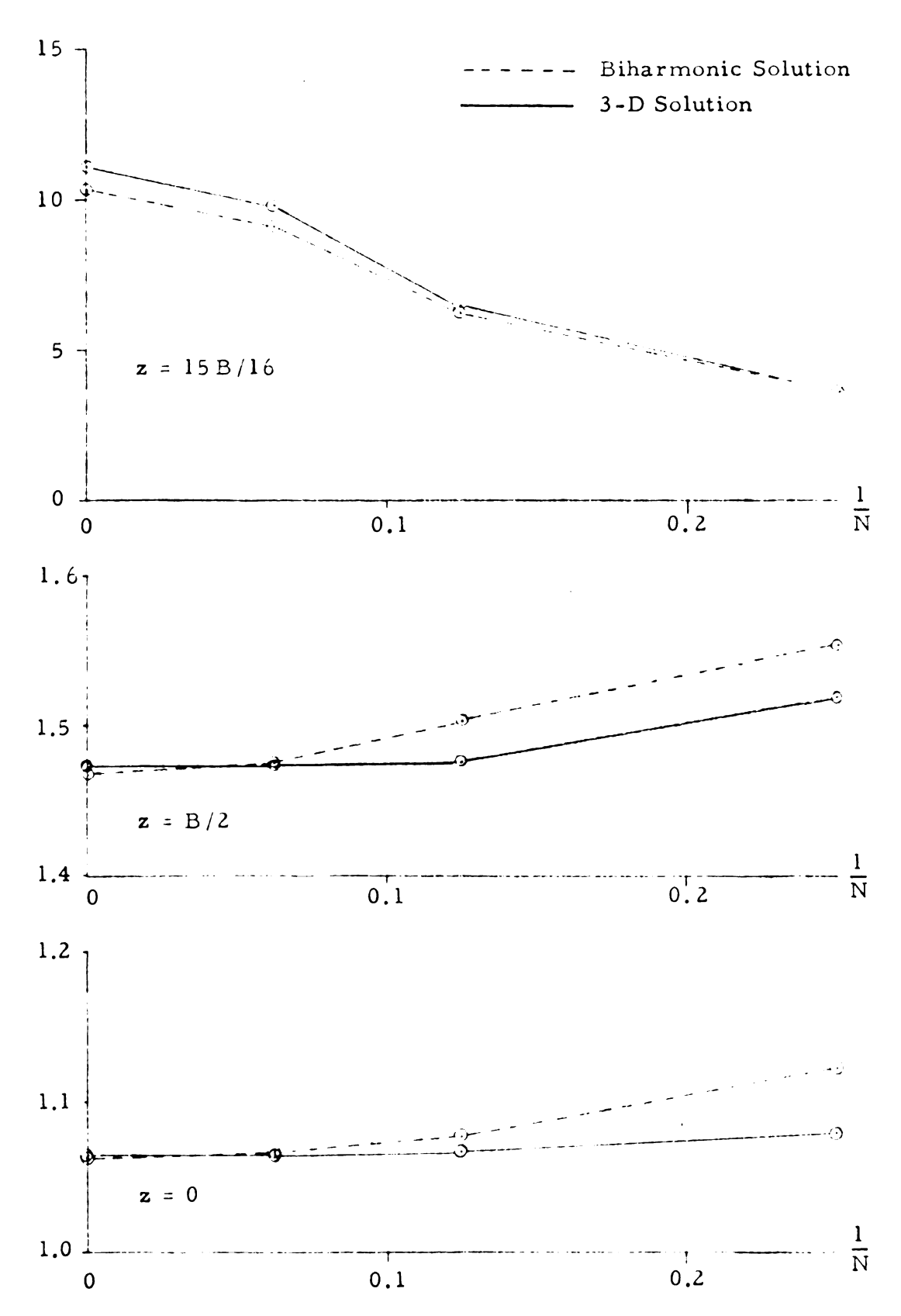


Figure 10. Values of σ for the two solutions plotted with respect to the inverse of the mesh size.



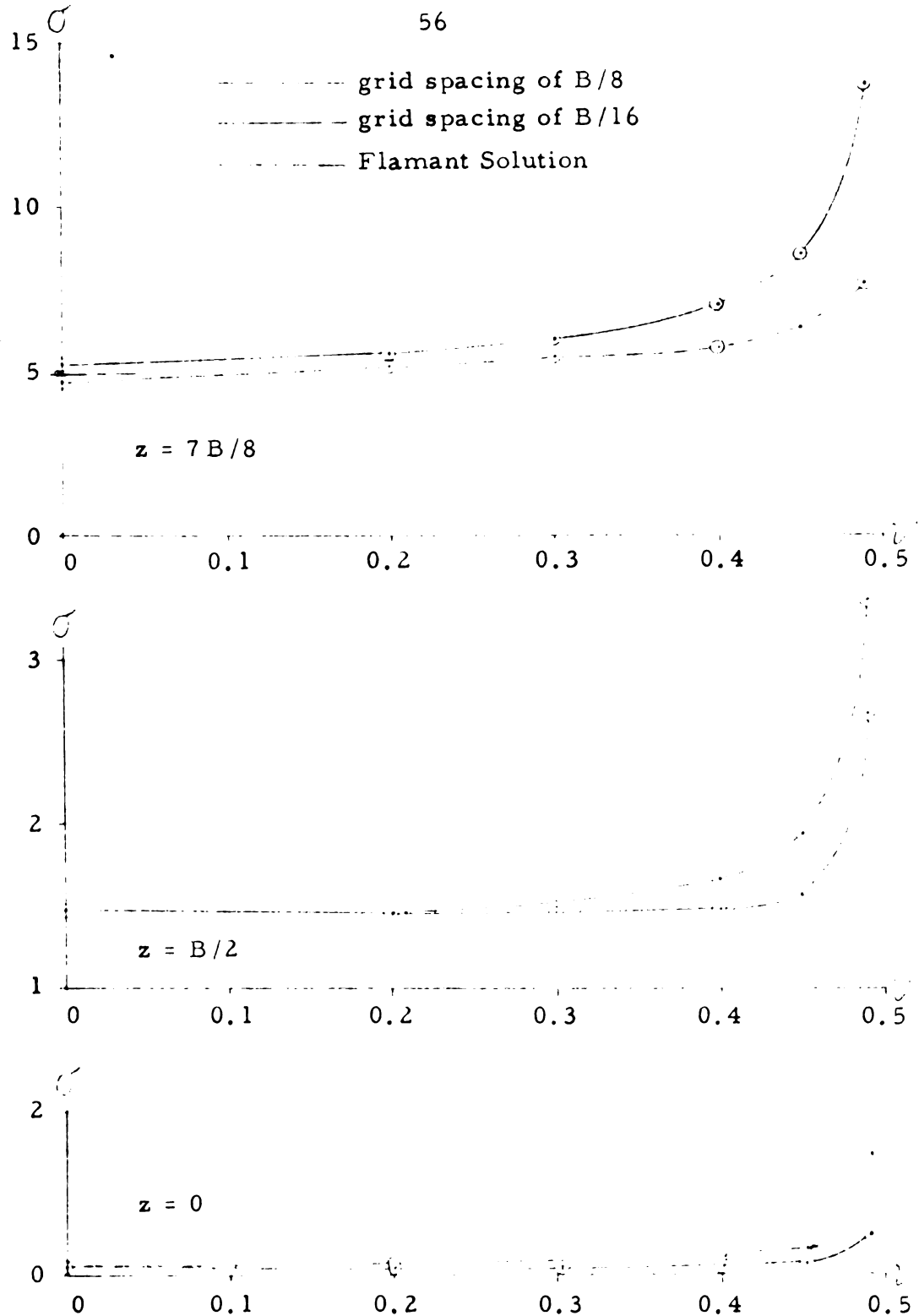


Figure 11. Values of $\sigma_{\boldsymbol{z}}$ on the centroidal Z-Axis for various values of z plotted with respect to Poisson's ratio.

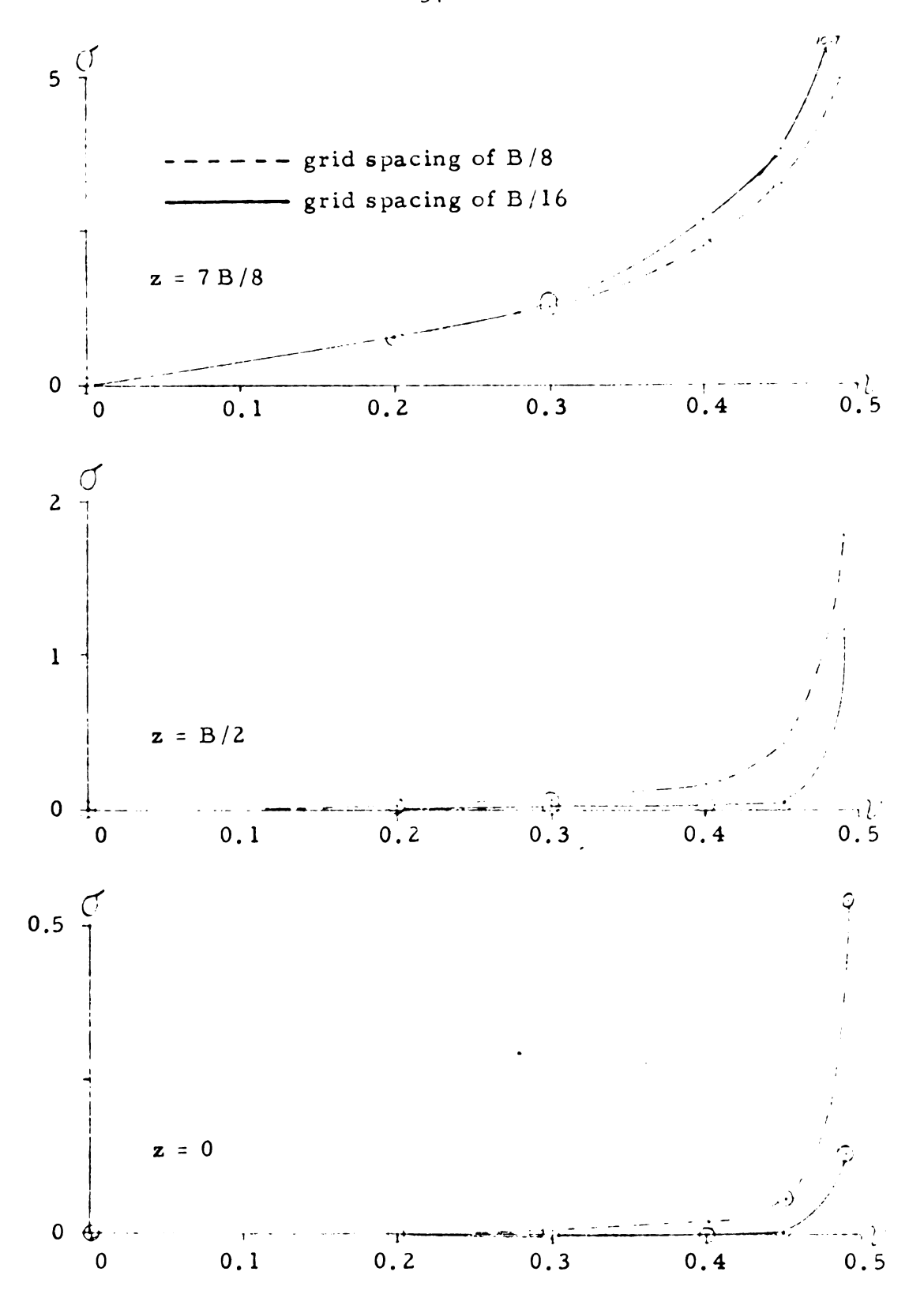


Figure 12. Values of $\sigma_{\mathbf{x}}$ on the centroidal Z-Axis for various values of z plotted with respect to Poisson's ratio.

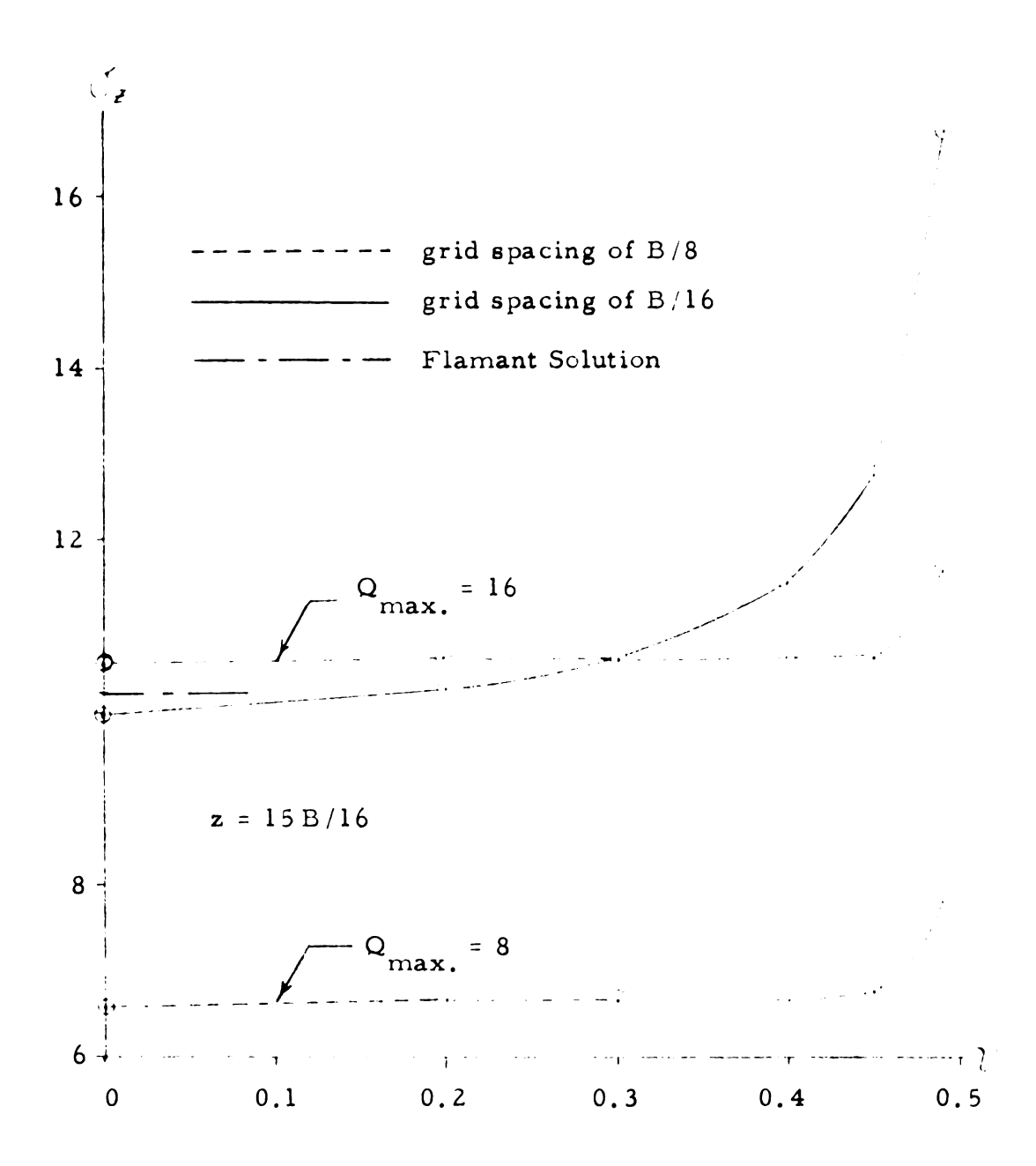


Figure 13. Values of σ_z on the centroidal Z-Axis for z=15B/16 plotted with respect to Poisson's ratio.

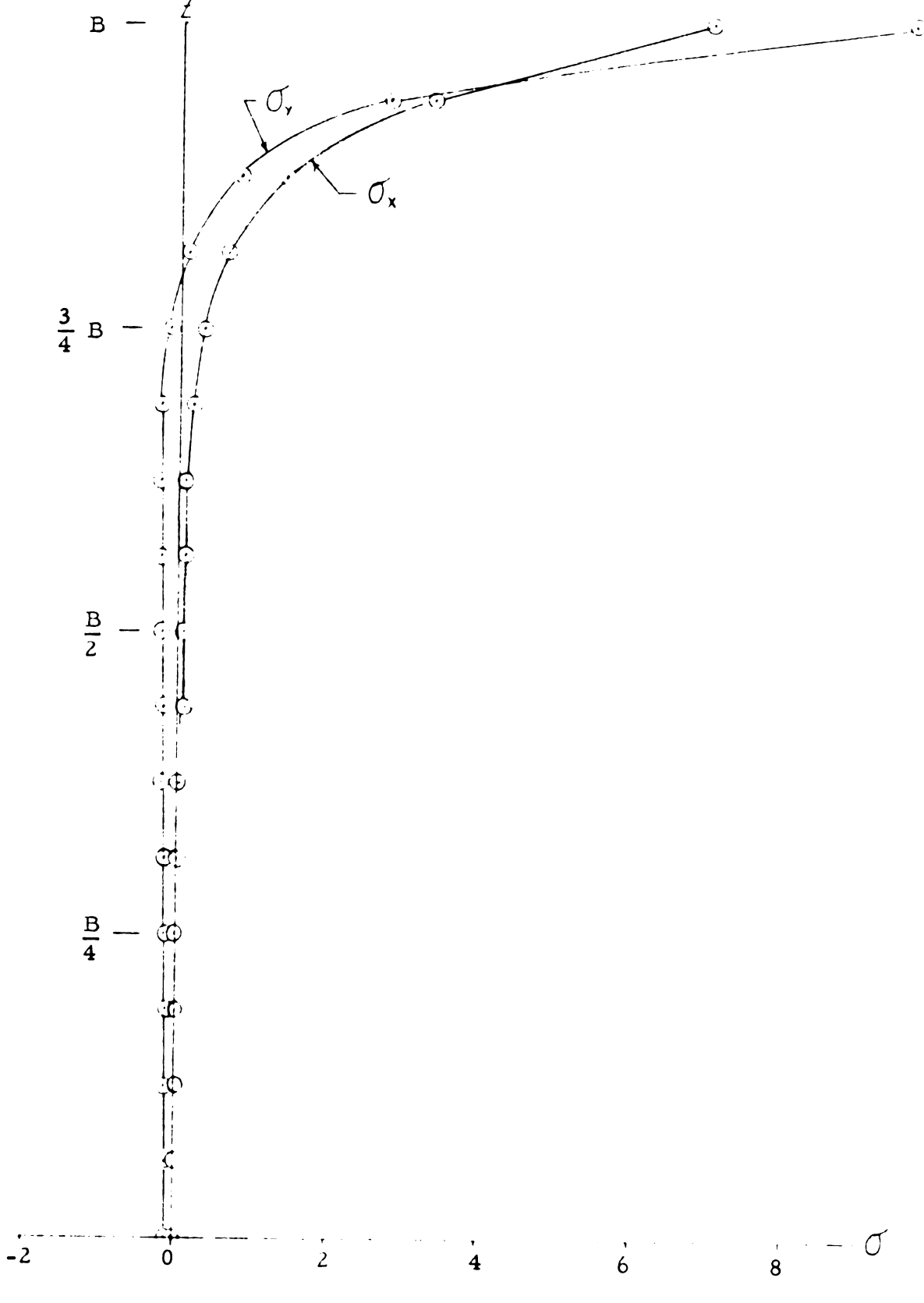


Figure 14. σ_x and σ_y on the centroidal Z-Axis for ν = 0.3.

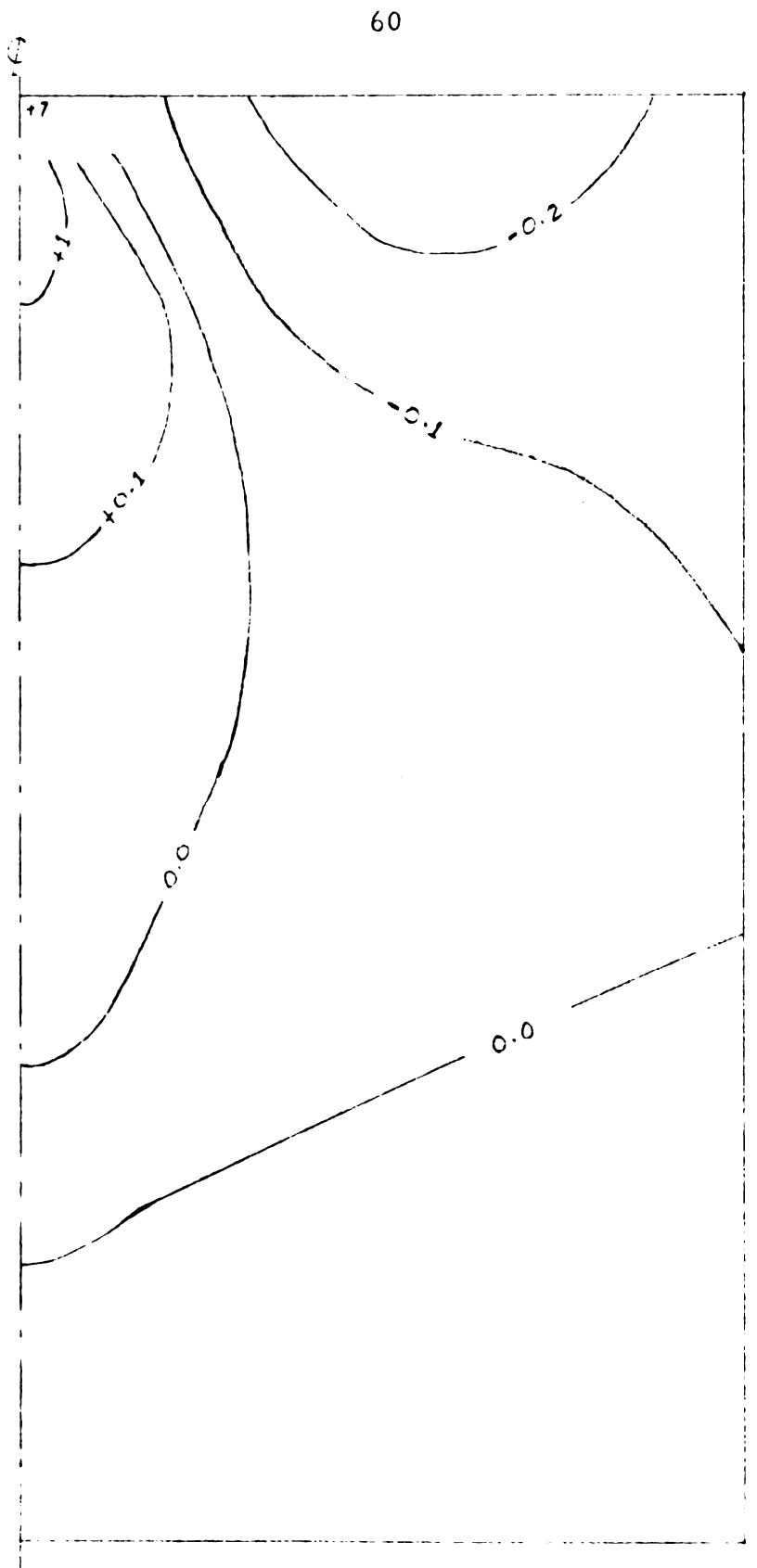


Figure 15. Lines of constant σ_{x} on the Y-Z plane with x = 0 for Poisson's ratio of 0.3 (+ = comp.).

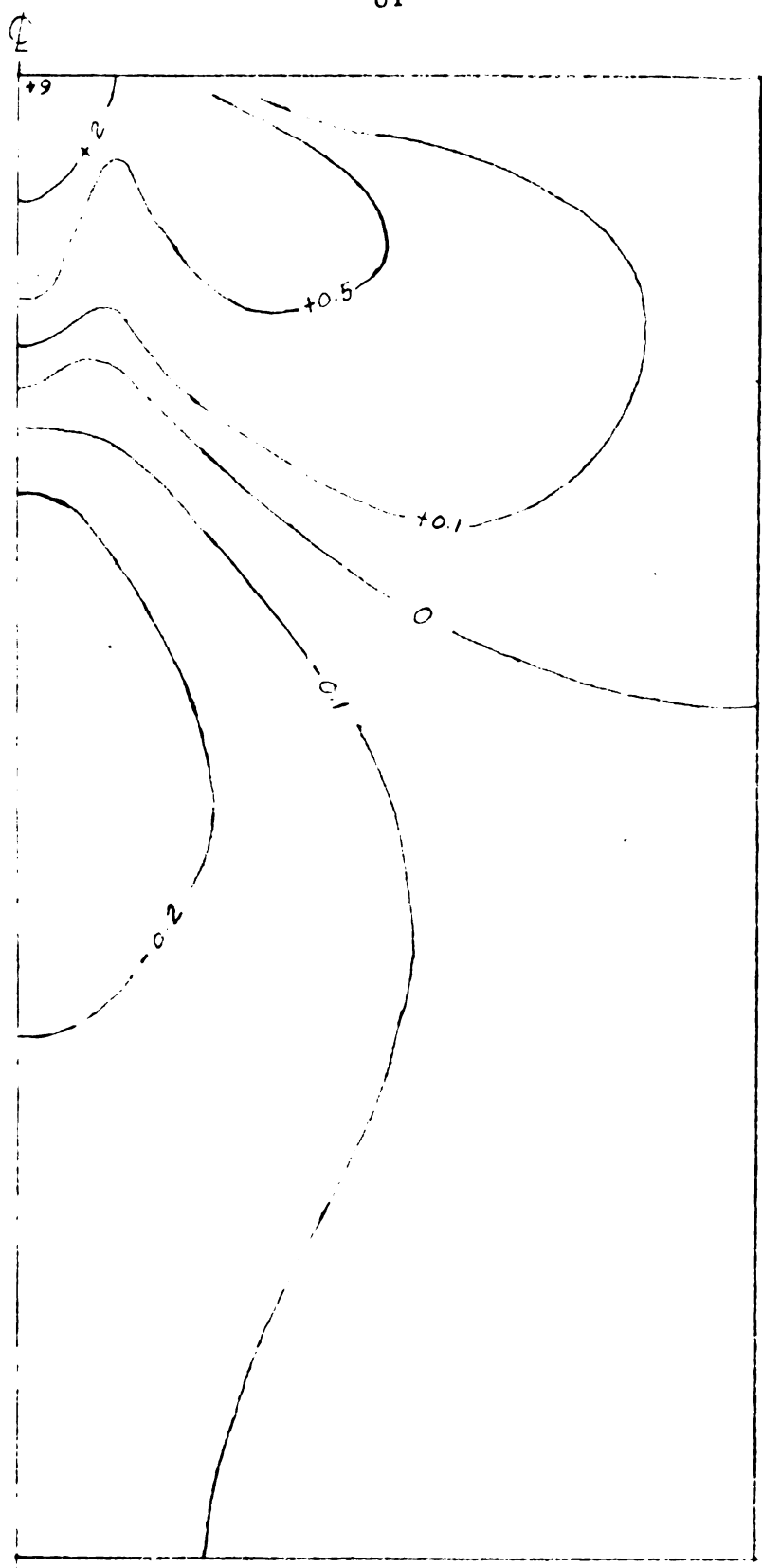


Figure 16. Lines of constant σ_y on the Y-Z plane with x = 0 for Poisson's ratio of 0.3 (+ = comp.).

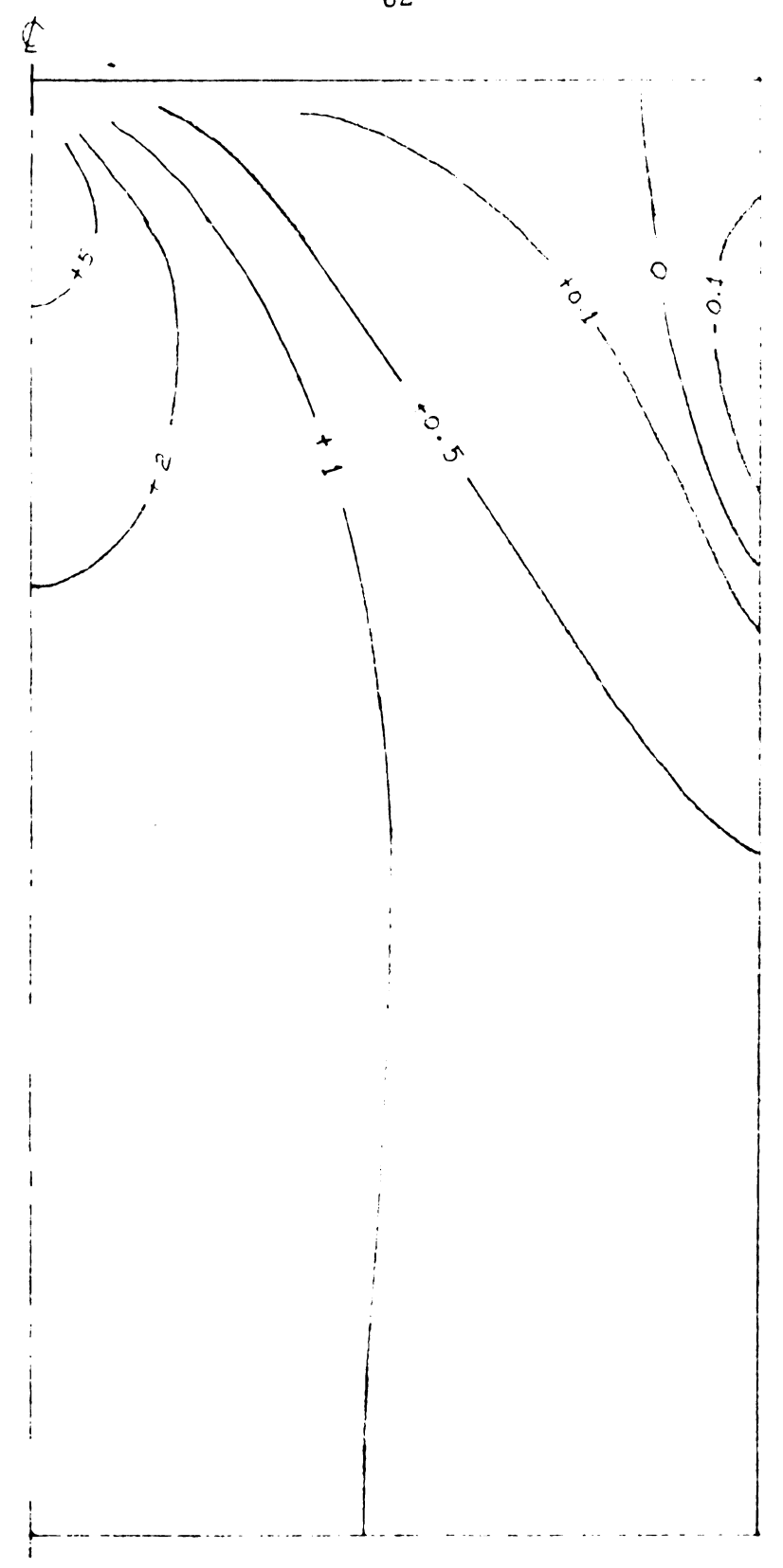


Figure 17. Lines of constant σ_z on the Y-Z plane with x = 0 for Poisson's ratio of 0.3 (+ = comp.).

EXAMPLE PROBLEMS TWO AND THREE

Problems two and three will be treated together because of the similarity between them (see Figures 5 and 6). In problem two, the load will be assumed to be distributed over an area enclosed by lines one-half of the grid spacing in each direction. Two grid sizes will be used, B/8 and B/16. In problem three, the load will be distributed in such a manner using a grid spacing of B/16 such that the stress distribution on the surface closely approximates that of the stress distribution for problem two with the grid spacing of B/8. Comparisons can then be made between all three solutions at the same time. In order to achieve an exact duplication of the stress distribution for the grid spacing of B/8 in problem two with the next possible finer grid, the grid spacing would have actually had to have been divided by three. This would have meant many more equations to solve and of course the solution time would have been much longer. The grid spacing of B/16 was, therefore, chosen to accomplish this purpose as reasonably as possible.

As in problem one, problem two and three possess the same type of symmetry which will require only one quadrant solution on the X-Y plane for a solution of the whole. In problem two, the magnitude of the distributed stress for the concentrated load for a unit average stress on the X-Y plane will be N², where N is the number of grid spacings in width B. In problem three, the total load acting on each

nodal point must be such that it agrees with the nodal loads caused by the stress distribution of problem two with a grid spacing of B/8. The resulting stress distributions are shown in Figure 18. The method of setting up the boundary equations and computing the stresses from the displacements will be the same as in problem one.

The solution for the stress distribution in the neighborhood of the concentrated load in problem two should approach the theoretical solution of a concentrated load on a semi-infinite body, or that of a concentrated distributed load on a semi-infinite body. These solutions will be computed and compared with the numerical solution when possible. The theoretical solution for the distributed load will be computed on the assumption that the load is distributed over a circular area whose radius is one-half of the grid spacing.

Figures 19 and 20 show the σ_z stress at various elevations on the Z-Axis. The theoretical solutions are shown for those elevations of z equal to or greater than 7B/8. As in problem one, it can be seen that the convergence of the two grid spacings becomes poor as Poisson's ratio approaches one-half. From the results of these two problems, the explanation of the poor convergence lies entirely in the size of grid chosen to represent the body. This is quite evident when the solution for the larger grid size of problem two is compared to the solution of the smaller grid size in problems two and three. When z is not in close proximity to the loaded area, the solutions for

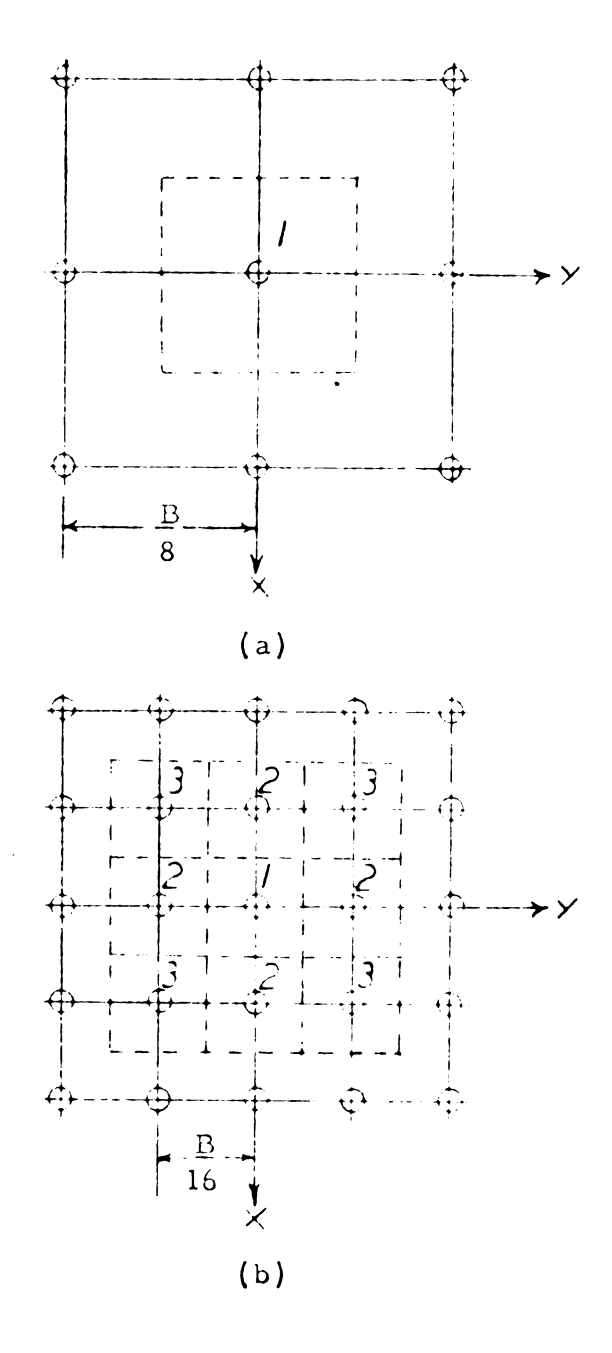


Figure 18. Distributed load for Problem Two with a grid spacing of B/8 (a) and for Problem Three with a grid spacing of B/16 (b).

the two small grid sizes agree with small error even though the stress distribution of the concentrated load is different. However, as Poisson's ratio approaches one-half, the solution of the larger grid size diverges sharply from the two smaller grid size solutions. This definitely means that the equations are unstable when Poisson's ratio approaches one-half and the effect of this instability is greater on the overall solution as the grid size becomes larger. It will be noted, however, that within the usual range of Poisson's ratio the solutions are in close agreement.

Figures 21 and 22 show the σ_x and σ_y stress for various elevations on the Z-Axis. The theoretical solution for a concentrated distributed load is shown for z = 7 B/8 and z = B.

As in problem one, there is a great discrepancy between the theoretical and numerical solution for these horizontal stresses. This is again attributed to the lack of agreement of the boundary conditions on the vertical faces. Some of the discrepancy can also be attributed to the largeness of the grid with respect to the area which is loaded.

Figures 23 and 24 show the constant stress lines of problem two on the Y-Z plane for $\sigma_{\mathbf{x}}$ and $\sigma_{\mathbf{z}}$ respectively with Poisson's ratio of zero and for a grid spacing of B/16. Figures 25 and 26 show the constant stress lines on the Y-Z plane of problem three for $\sigma_{\mathbf{x}}$ and $\sigma_{\mathbf{z}}$ respectively for the same parameters. These figures are again

as in problem one only examples of the types of stress diagrams that could be constructed for different planes in the body.

It will be noticed in comparing Figures 23 and 24 to Figures 25 and 26, that the difference between the two solutions is minimal except in the region of the concentrated load.

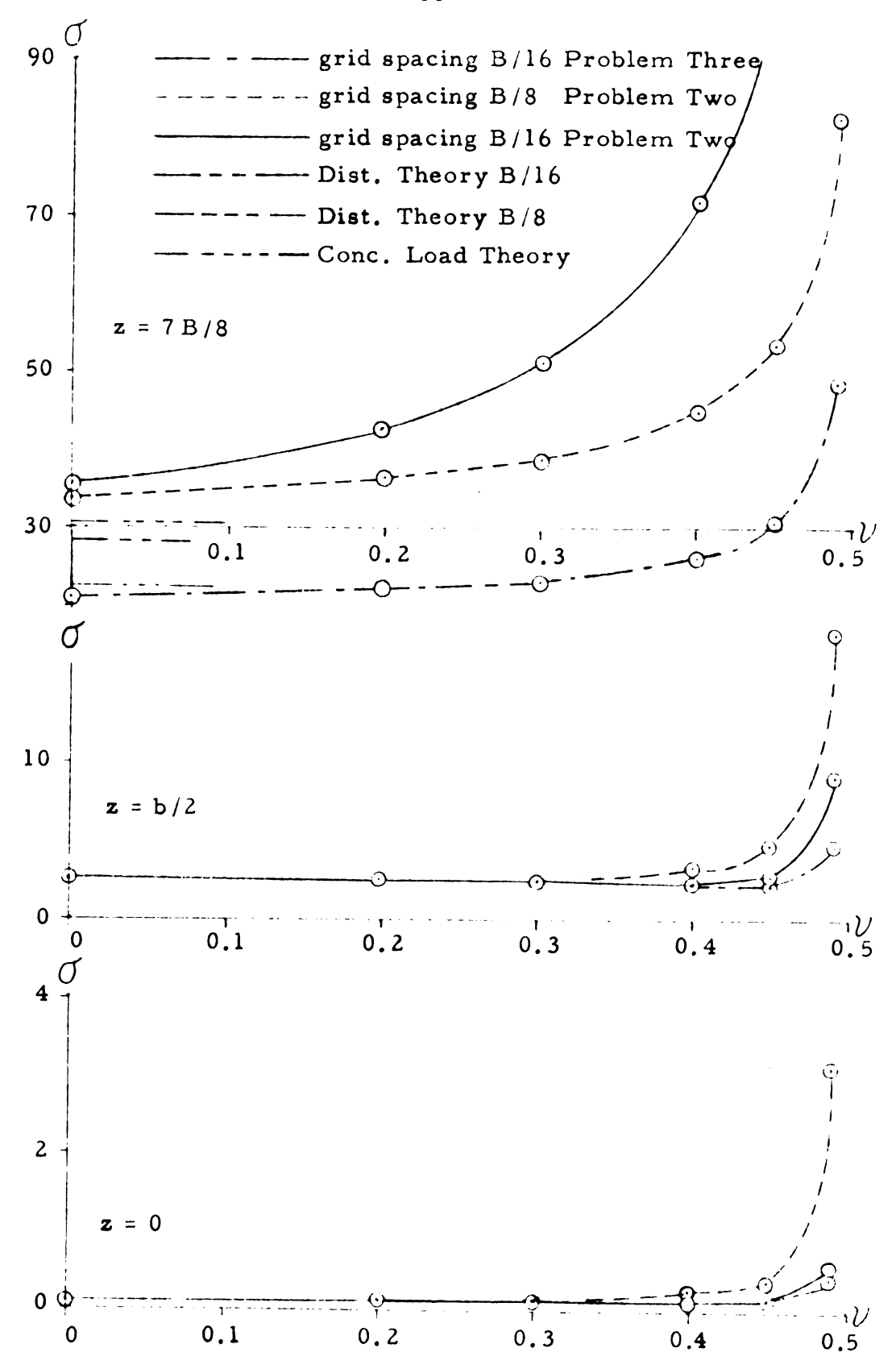


Figure 19. Values of σ_z on the centroidal Z-Axis for various values of z plotted with respect to Poisson's ratio.

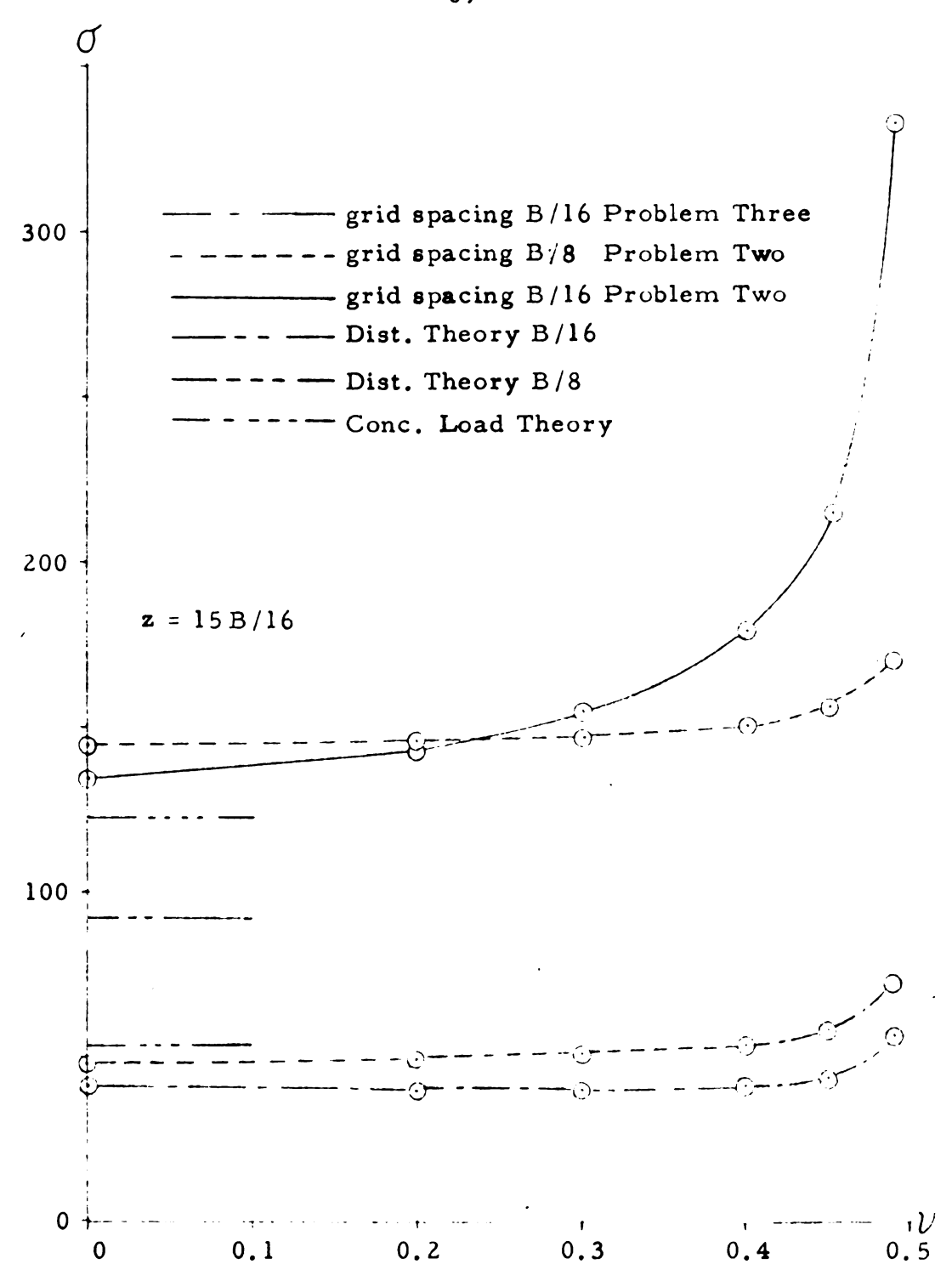


Figure 20. Values of σ_z on the centroidal Z-Axis for z = 15 B/16 plotted with respect to Poisson's ratio.

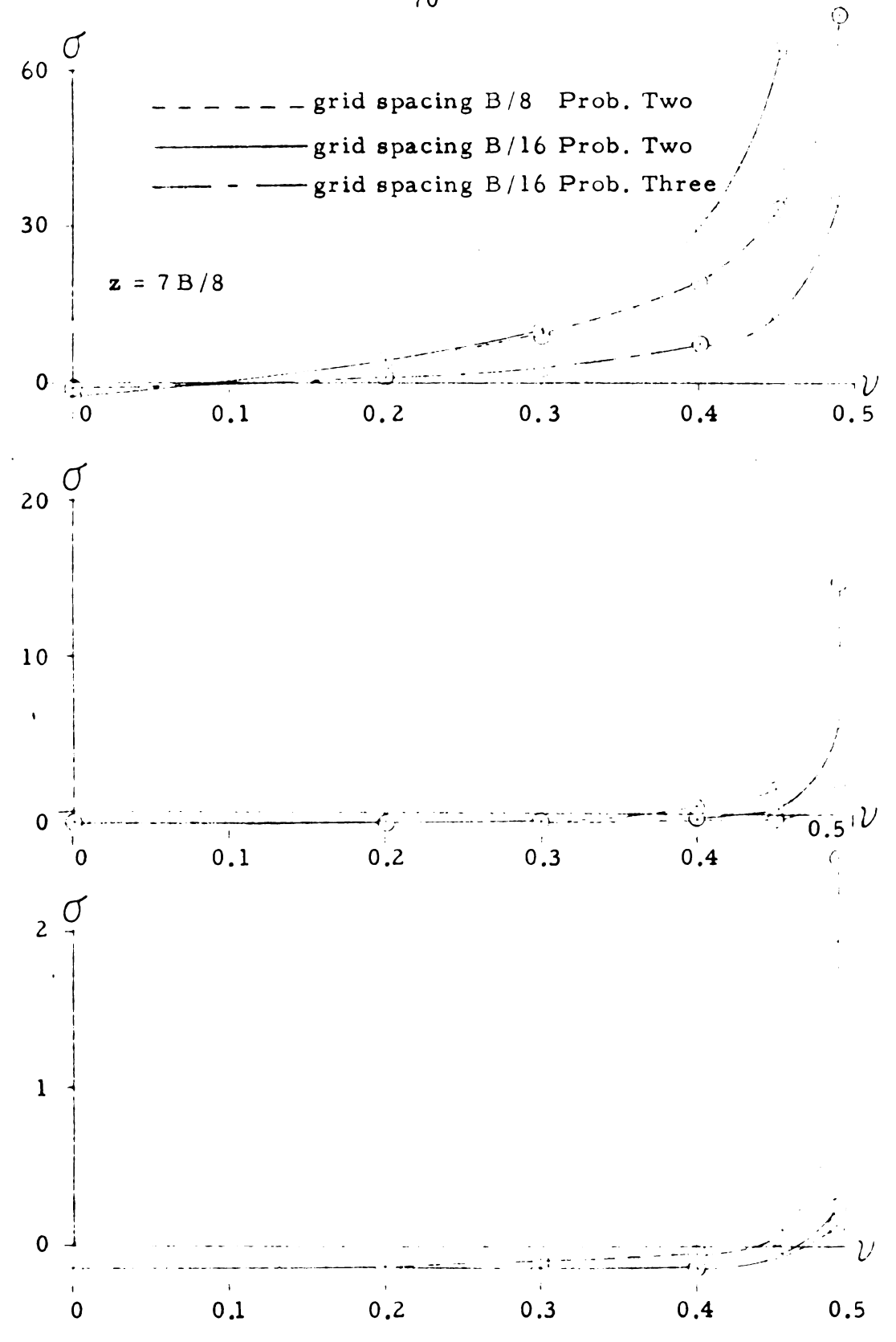


Figure 21. Values of σ_x and σ_y on the centroidal Z-Axis for various values of z plotted with respect to Poisson's ratio.

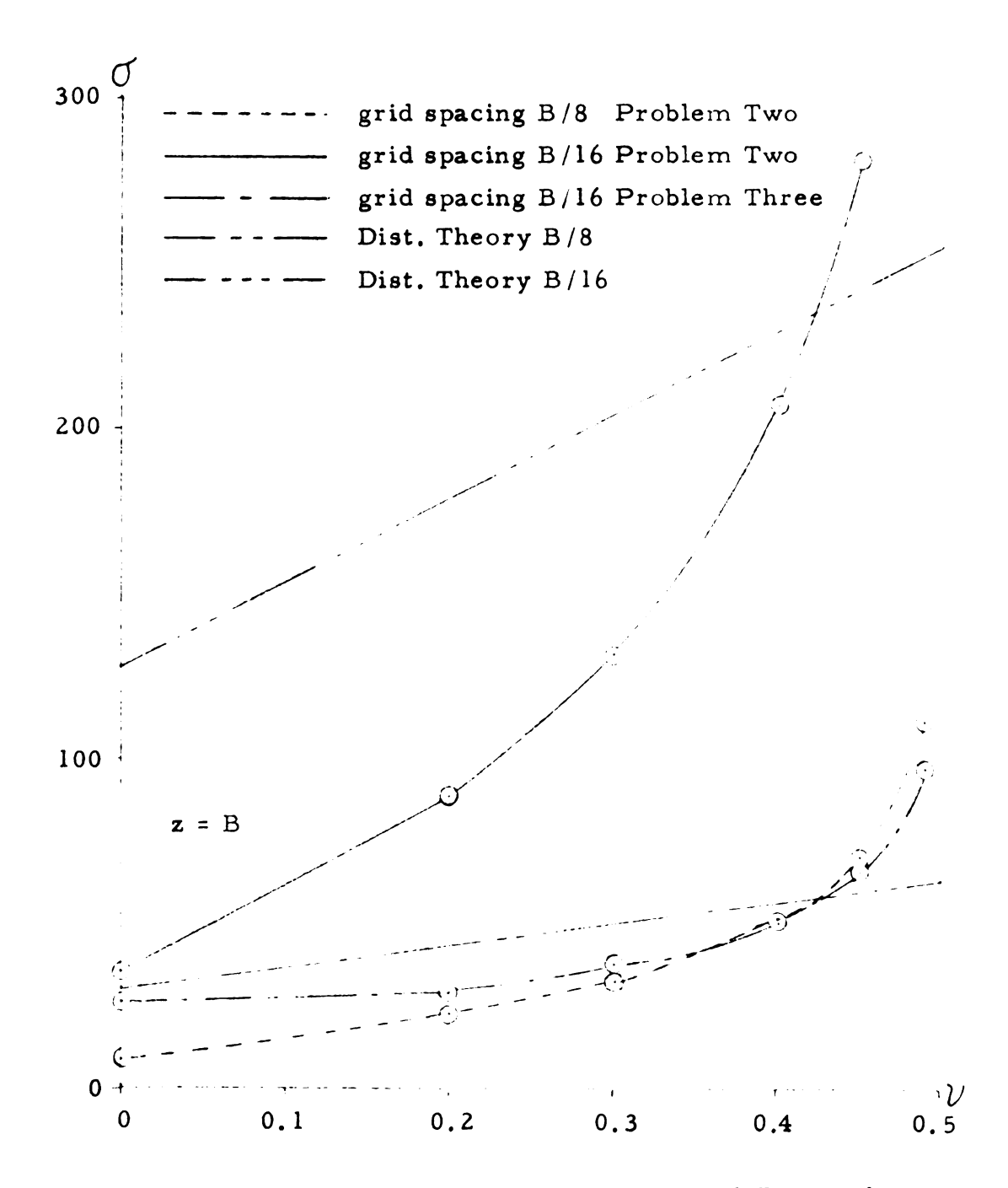


Figure 22. Values of σ_x and σ_y on the centroidal Z-Axis for z = B plotted with respect to Poisson's ratio.

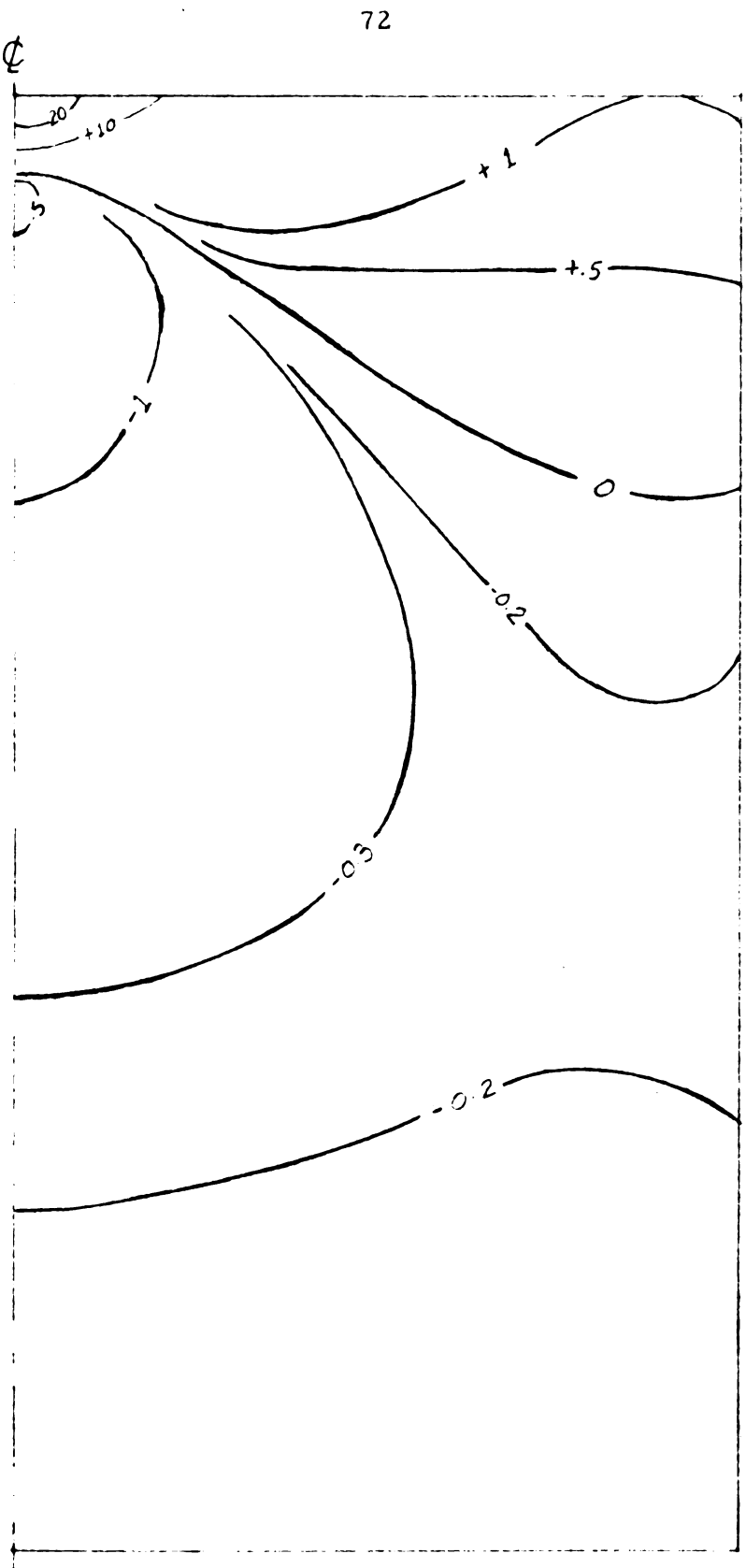


Figure 23. Lines of constant $\sigma_{\bf x}$ on the Y-Z plane with ${\bf x}=0$ for Poisson's ratio of 0 (+ = comp.). Problem Two.

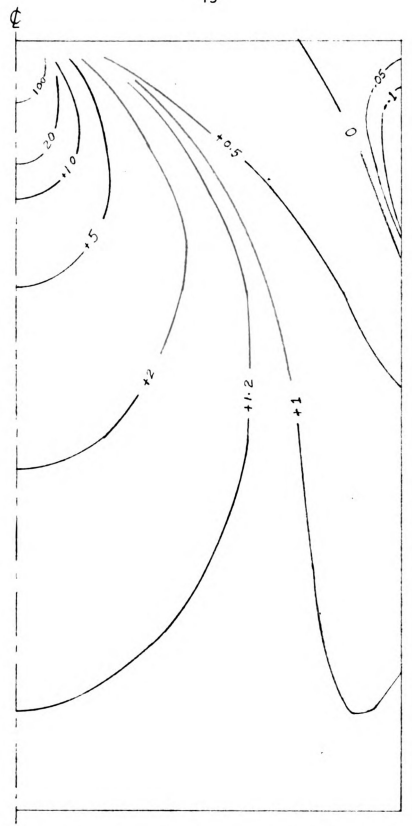


Figure 24. Lines of constant $\sigma_{\bf Z}$ on the Y-Z plane with x=0 for Poisson's ratio of 0 (+ = comp.). Problem Two.

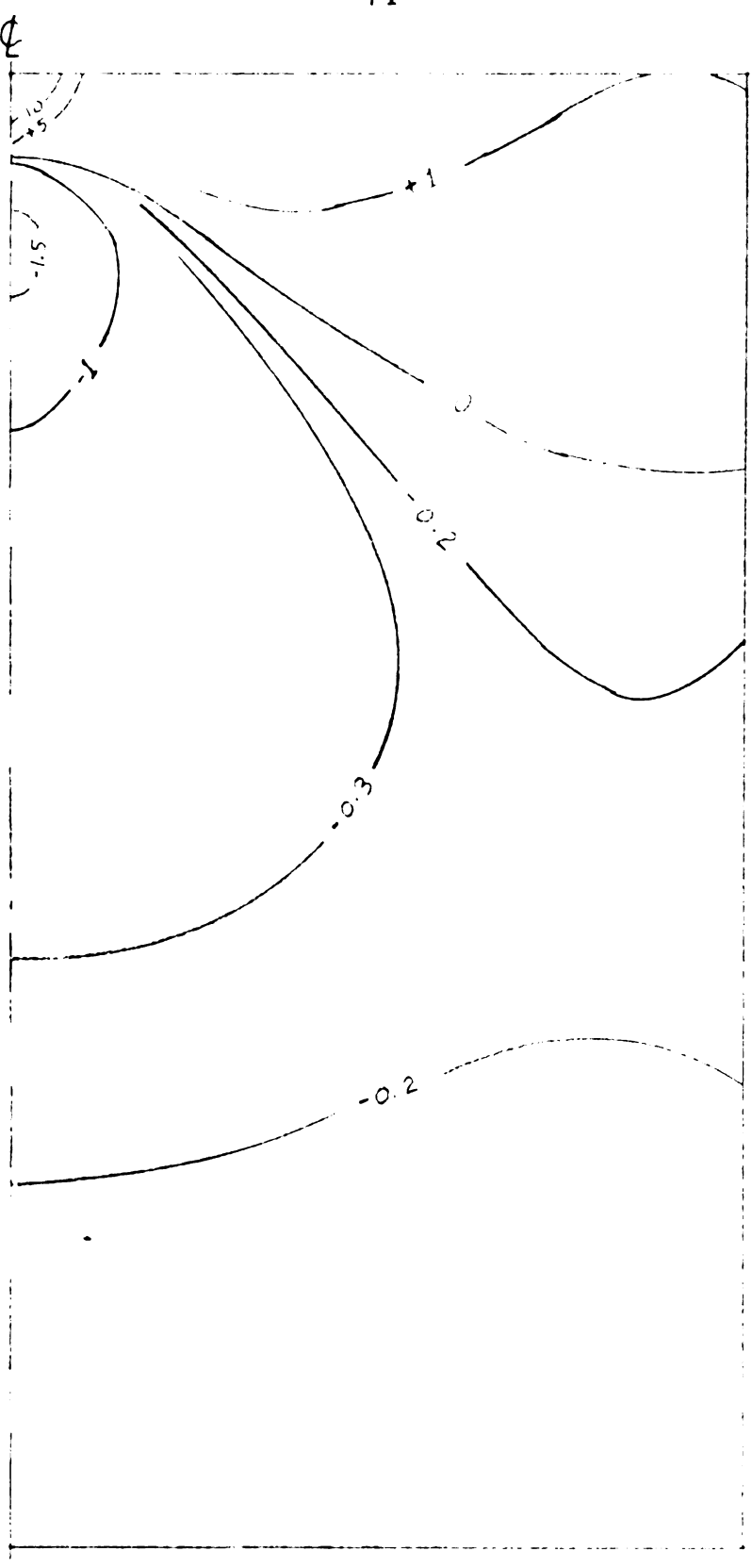


Figure 25. Lines of constant $\sigma_{\mathbf{x}}$ on the Y-Z plane with $\mathbf{x}=0$ for Poisson's ratio of 0 (+ = comp.). Problem Three.

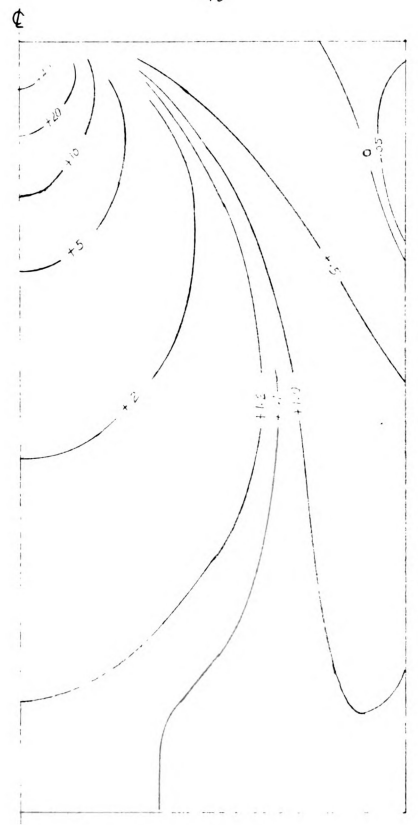


Figure 26. Lines of constant $\sigma_{\bf z}$ on the Y-Z plane with x = 0 for Poisson's ratio of 0 (+ = comp.). Problem Three.

EXAMPLE PROBLEM FOUR

In this problem (Figure 7), the stress distribution will be investigated in a beam column which is acted upon by an eccentric concentrated load. The problem will be divided into two parts. In the first part, the load will be considered to be concentrated on a square area centered around the nodal point, whose dimensions will be equal to the grid spacing which for this first part will be B/4 (Figure 27a). In the second part, the load will be considered to be concentrated on a rectangular area centered around two consecutive nodal points along the upper surface X-Axis, whose dimensions will be one grid spacing in the Y-Axis direction, and two grid spacings in the X-Axis direction. The grid spacing for this second part will be B/8 (Figure 27b). The assumed eccentricity in the first part will be B/4 and in the second part 3 B/16.

Symmetry will be assumed to exist across the centroidal Z-X plane, therefore, eliminating one-half of the structure for solution. As in the previous problems, the w displacements on the plane z=0 will be set equal to zero. Displacements of nodal points lying on the plane of symmetry will also be assumed zero in the normal direction. The equations of equilibrium and method of solution will be handled in the same way as in problem one.

The solution will in each case be computed for Poisson's ratio of 0.0, 0.2, 0.3 and 0.4. The solutions for values of Poisson's ratio

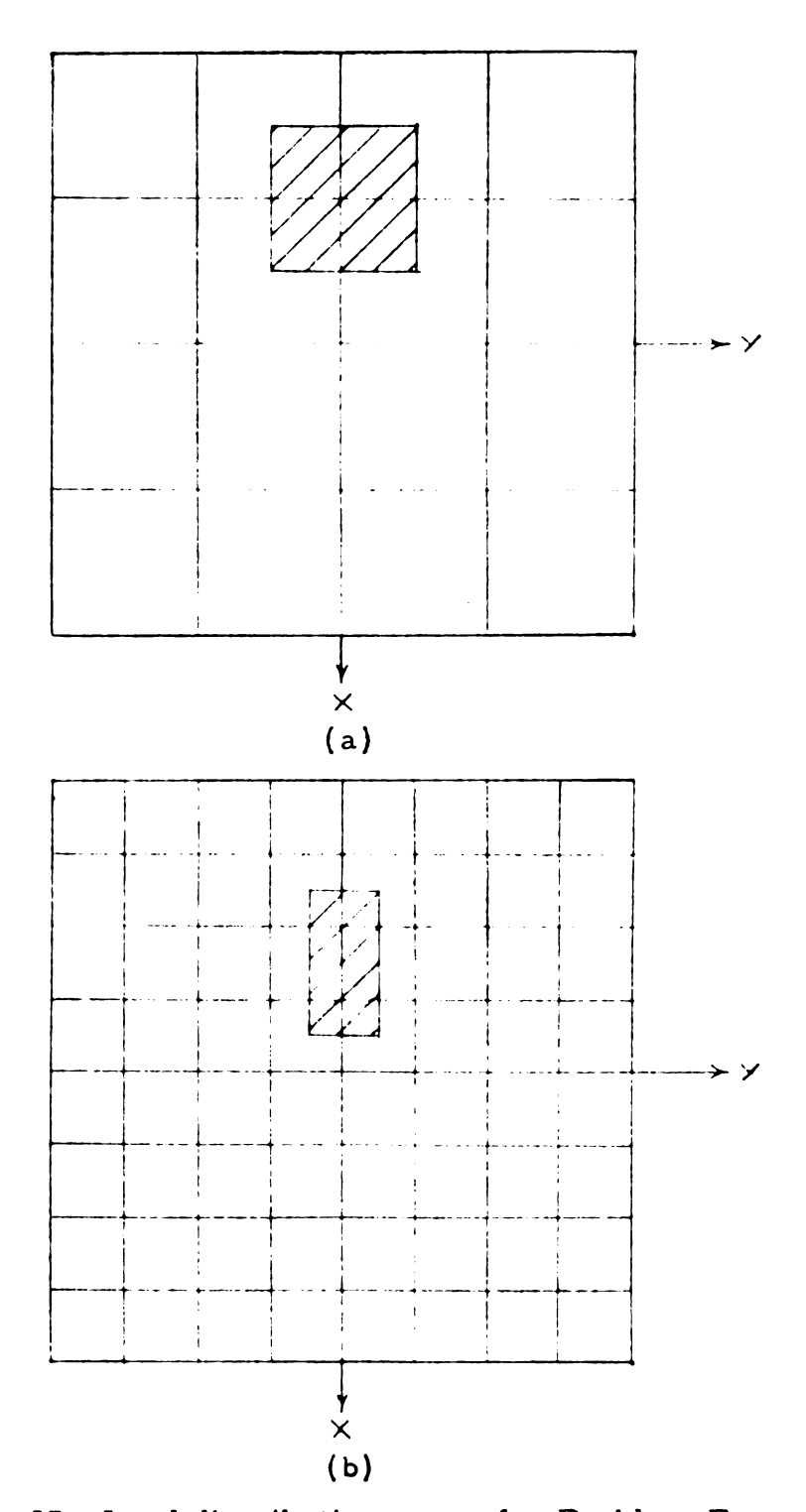


Figure 27. Load distribution areas for Problem Four.

nearer 1/2 will not be computed because of the instability of the equations as evidenced in the previous problems.

At a distance from the load, the stress distribution in the beam column will be governed by the equations:

$$\sigma_{z} = \frac{P}{A} + \frac{Pex}{I}$$

or,

$$\sigma_z = \frac{P}{A} \left(1 + \frac{12ex}{B^2}\right)$$

If we substitute into the equations above the value of the eccentricities for part one and two, the stress distribution across the beam
would be:

for part one:

$$\sigma_z = \frac{P}{A} \left(1 + \frac{3x}{B} \right)$$

for part two:

$$\sigma_z = \frac{P}{A} \left(1 + \frac{9x}{4B} \right)$$

In both parts, the average stress on the cross section of the beam column was set equal to 500. The stress distribution associated with this average stress would be the computed stress distribution from the above equations if the beam column was infinitely long, and if there was no error introduced because of the approximate nature of the equations.

Figure 28 shows the axial stress along the X-Axis in part one with z equal to zero and for Poisson's ratios between 0.0 and 0.4. The error in the extreme fiber stress with respect to a true straight line variation varies from -4% to +2%. Figure 29 shows the same stress distribution for part two. The error in the extreme fiber stress for this case varies from -2% to +2% which is a smaller range than in part one. The theoretical stress distributions for part one and two are indicated in Figures 28 and 29 by the broken lines. These stress distributions are based on the stress distribution in the infinite beam column. Figures 30 and 31 show the vertical stress distribution on the centroidal X-Axis for part one and two respectively with Poisson's ratio of 0.2. Only the distribution in proximity to the loaded surface is shown since the lines from the base to approximately B/2 are parallel. Figures 32 and 33 show the lines of constant vertical stress on the centroidal X-Z plane for part one and two respectively with Poisson's ratio of 0.2. In both cases, it can be seen that the trajectories are virtually vertical between the base of the column and the center of the column. Figure 34 shows the lines of constant stress $\sigma_{\mathbf{x}}$ on the centroidal X-Z plane with Poisson's ratio of 0.2 for part two. The maximum tension stress is approximately one-tenth of the maximum theoretical compression fiber stress or two-tenths of the average stress which would be of considerable interest in design practice if the material happened to be concrete.

It can be seen from these figures that the stress distribution agrees with the theoretical stress distribution when comparatively far from the loaded surface. The error varies with respect to Poisson's ratio and the range of the error decreases with decreasing grid spacing. Tension stresses that are small in comparison to the compression stress exist and may in some circumstances cause concern.

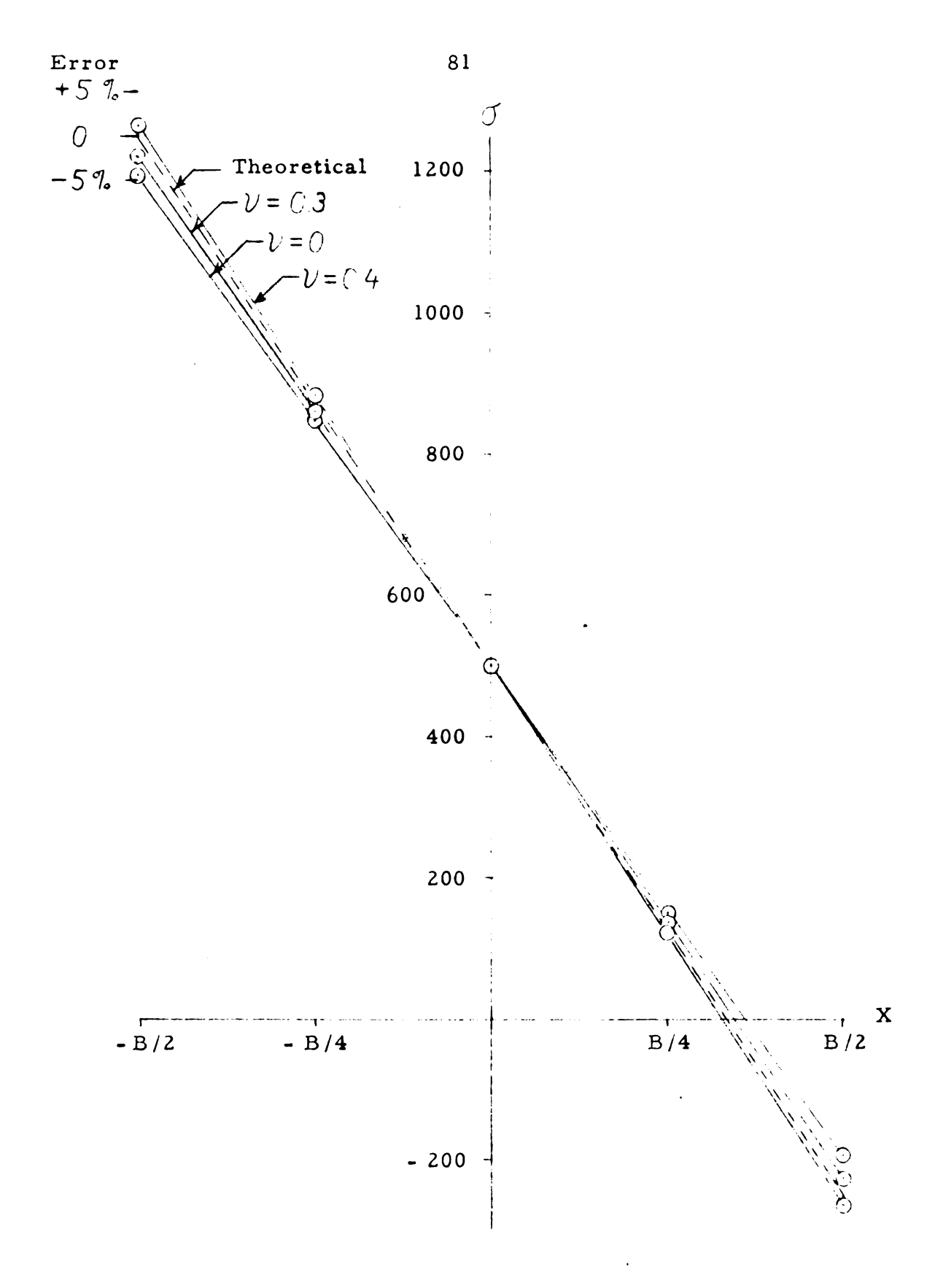


Figure 28. σ_z stress distribution on the centroidal X-Axis with z = 0 for various values of Poisson's ratio. Part One.

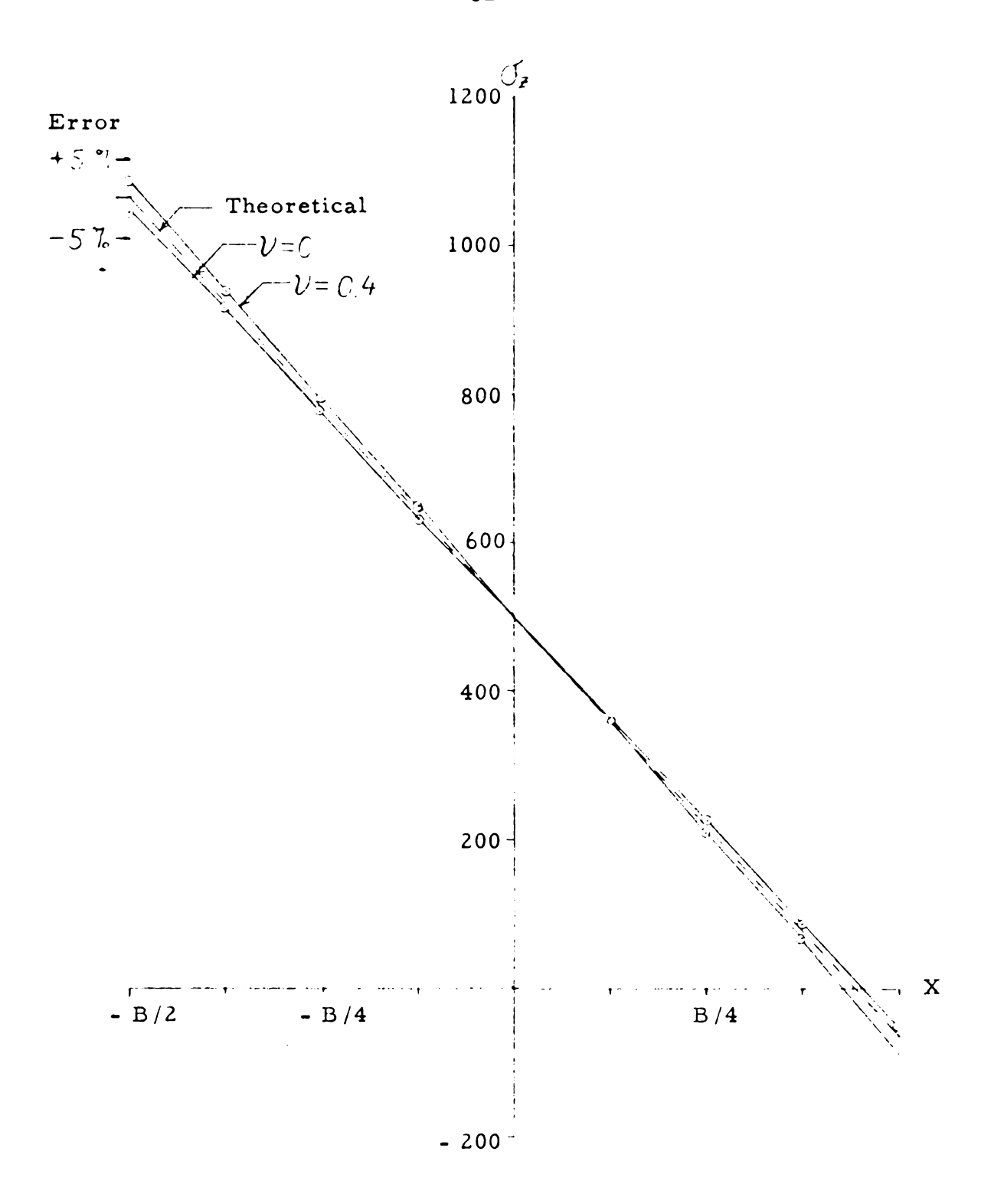


Figure 29. σ_z stress distribution on the centroidal X-Axis with z = 0 for various values of Poisson's ratio. Part Two.

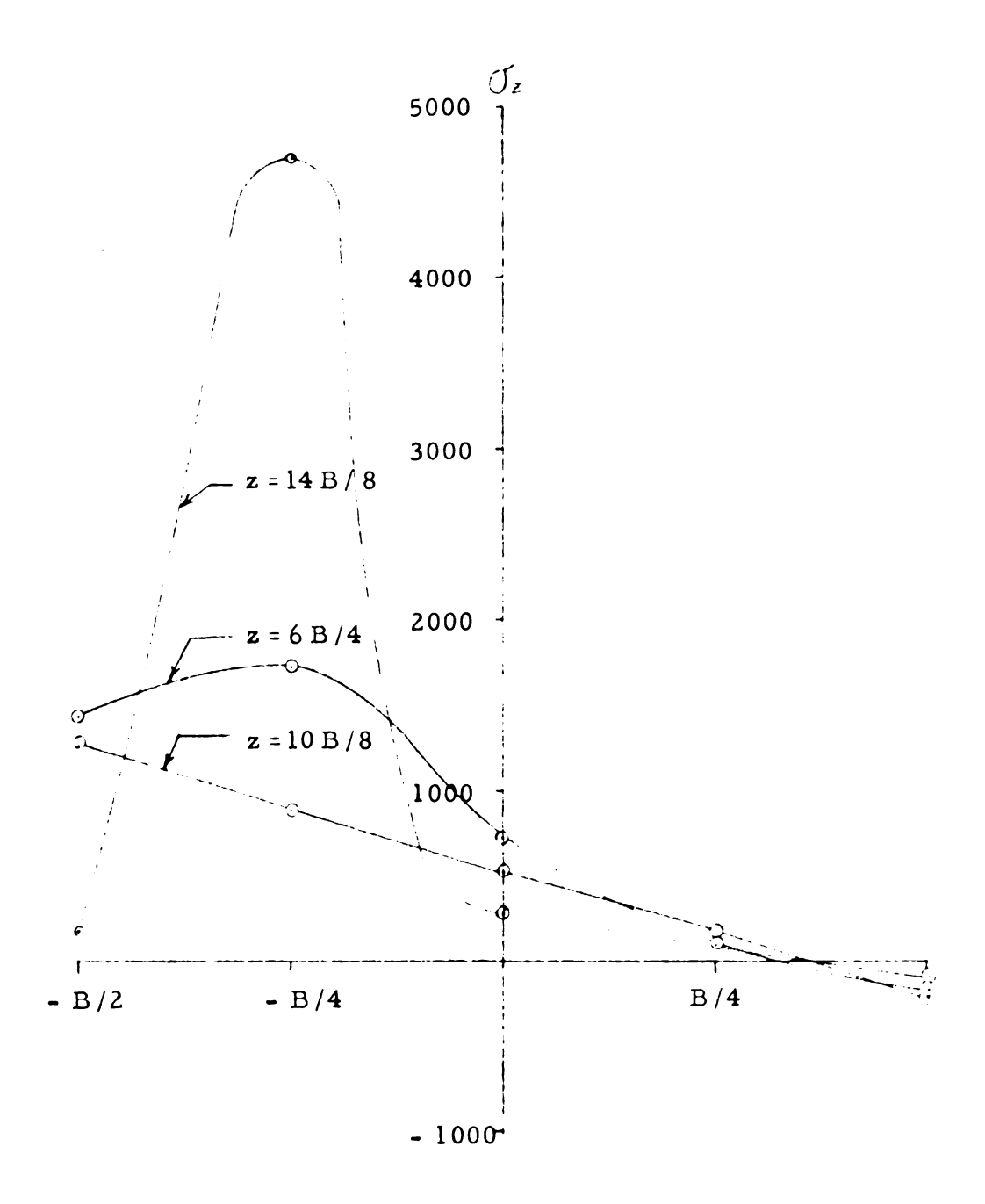


Figure 30. σ_z stress distribution parallel to the X-Axis with y = 0 and for various values of z and with Poisson's ratio of 0.2. Part One.



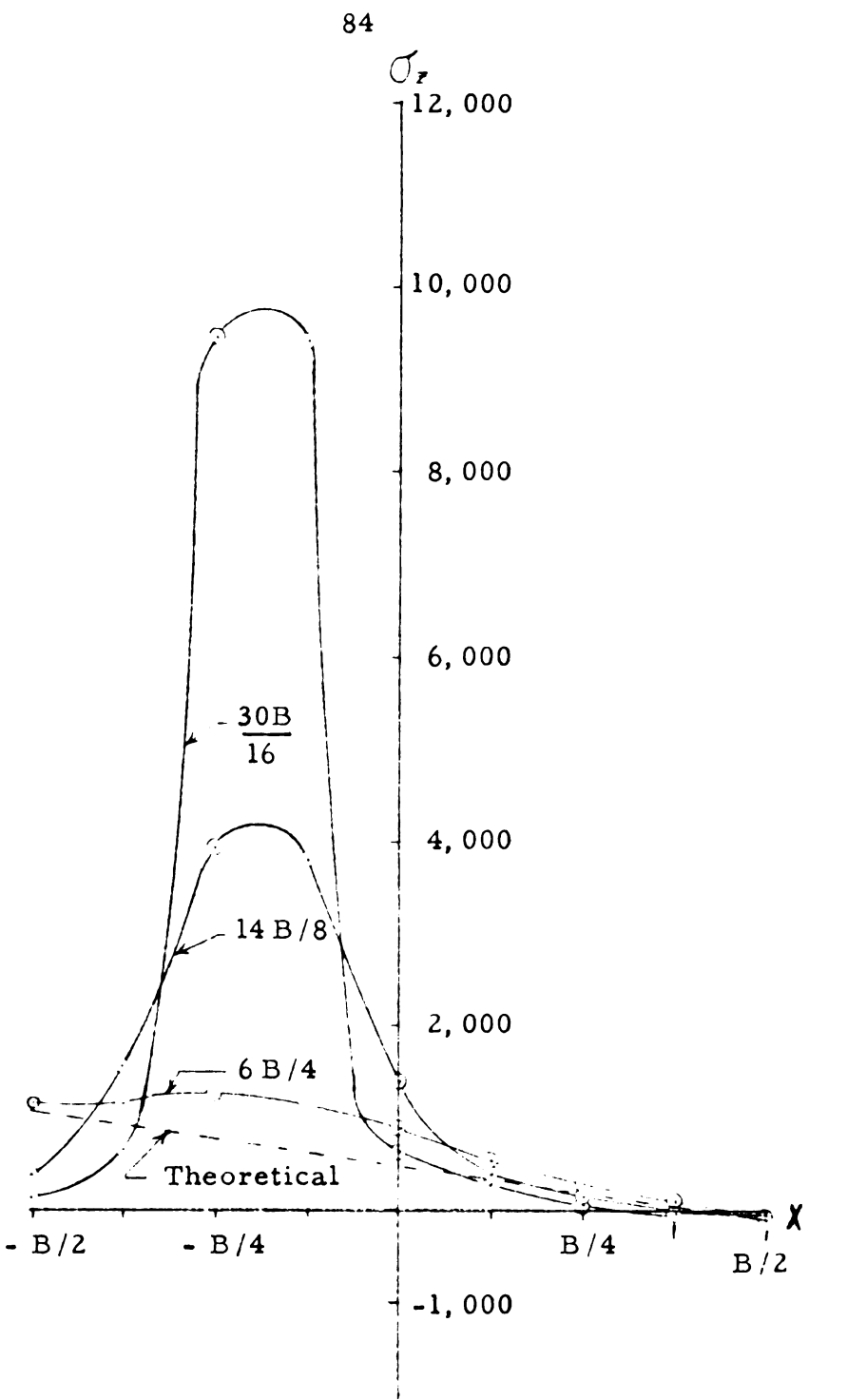


Figure 31. $\sigma_{\mathbf{z}}$ stress distribution parallel to the X-Axis with y = 0 and for various values of z with Poisson's ratio of 0.2. Part Two.

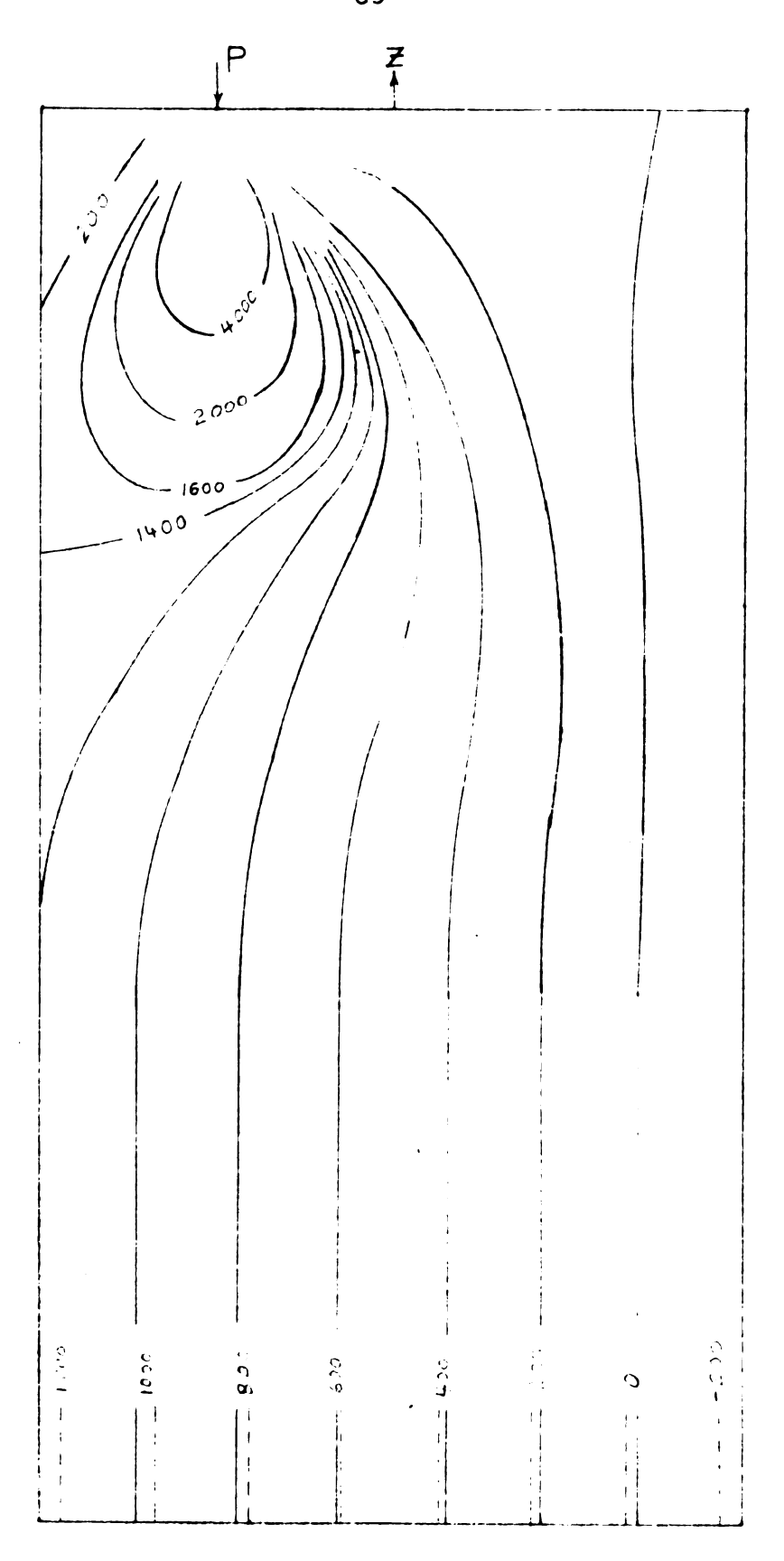


Figure 32. Lines of constant σ_z for the X-Z centroidal plane with Poisson's ratio of 0.2. Part One.

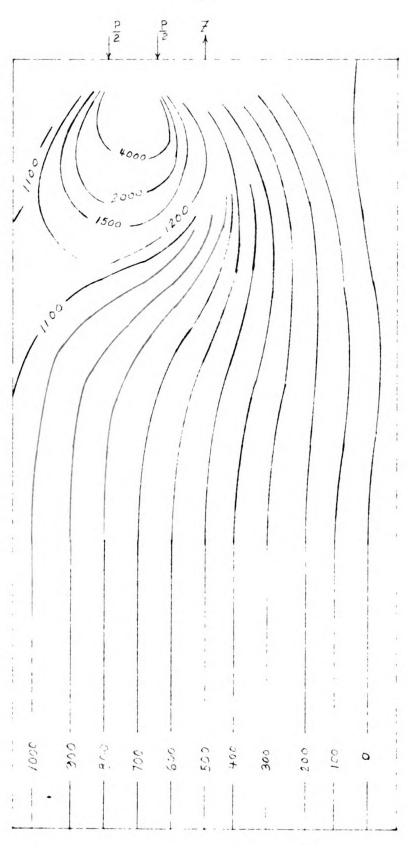


Figure 33. Lines of constant σ_z for the X-Z centroidal plane a with Poisson's ratio of 0.2. Part Two.

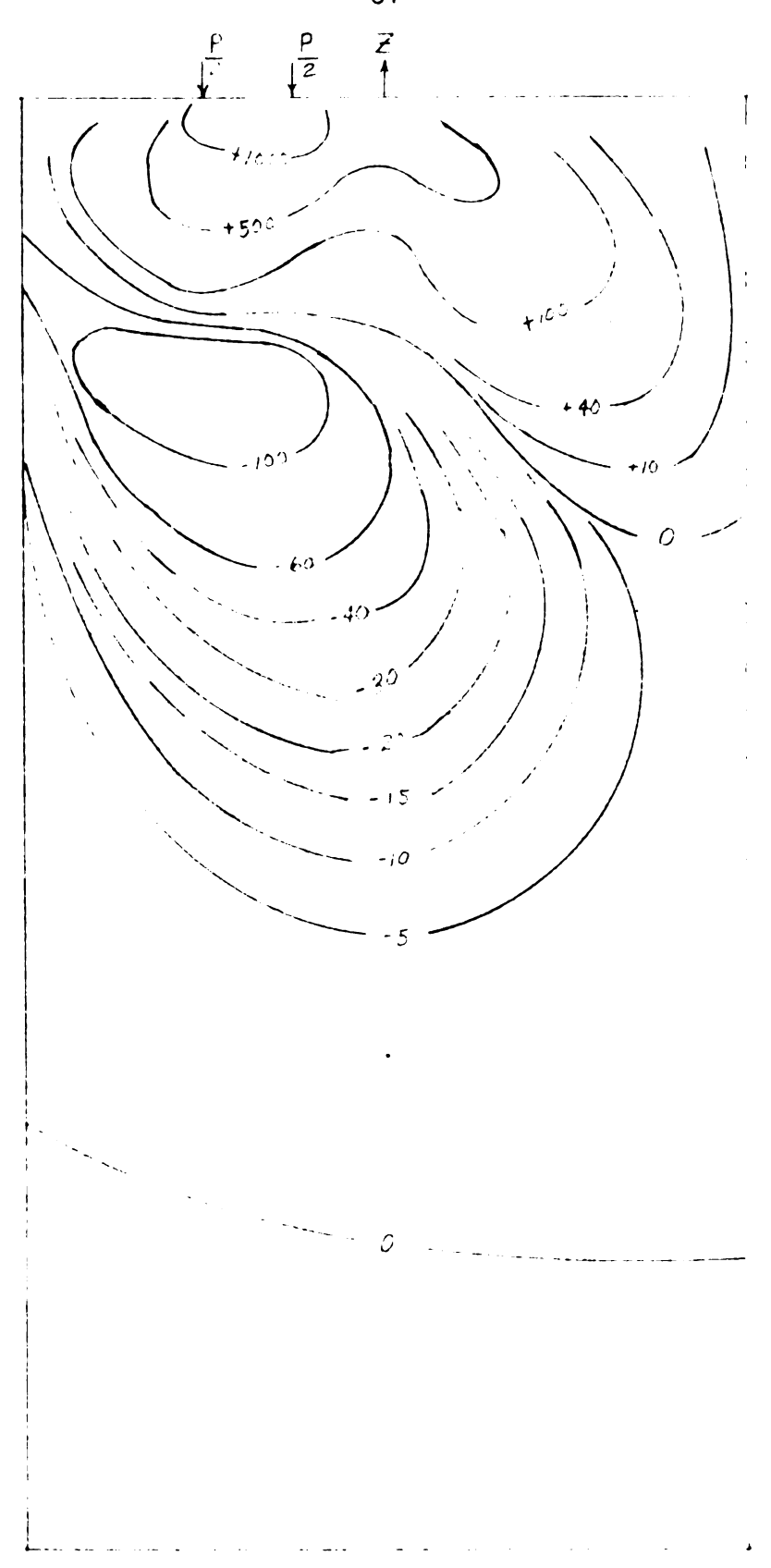


Figure 34. Lines of constant $\sigma_{\mathbf{x}}$ for the X-Z centroidal plane with Poisson's ratio of 0.2. Part Two.

EXAMPLE PROBLEM FIVE

In this problem (Figure 8), the accuracy of this proposed method will be studied by comparing the known stress distribution in a beam under constant moment and zero shear to the solution which results from the numerical method using the first order boundary equations. Figure 35a shows the assumed stress distribution on a line parallel to the X-Axis on the upper surface of the beam. Figure 35b and Figure 35c show the assumed boundary nodal stresses for grid spacings of B/4 and B/8 respectively. Symmetry was assumed to exist only with respect to the X-Z plane. The solution will be handled as in the previous problem. Figure 36 shows the outside fiber stress for solutions with various values of Poisson's ratio for the two grid spacings. In Figure 36, the error associated with a base stress of 500 is also shown. Within the usual range of Poisson's ratio (0.2 to 0.3), the error ranges from -2.761% to -0.782% for a grid spacing of B/4 and from -0.38% to +0.870%for a grid spacing of B/8. As in the previous problems, the accuracy of the solution is dependent on the value of Poisson's ratio, and instability of the equations becomes progressively worse as Poisson's ratio approaches 1/2.

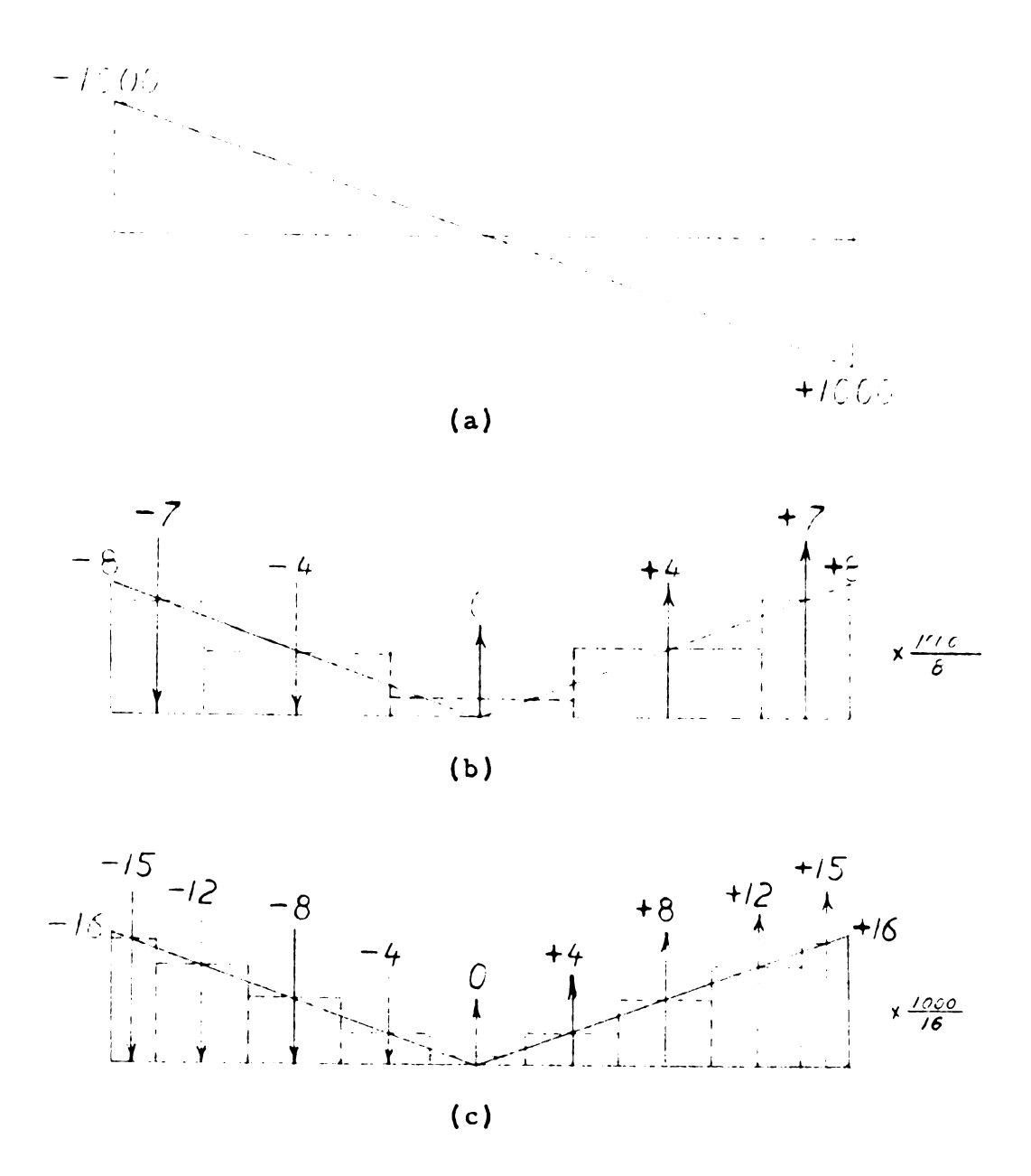


Figure 35. Assumed stress distribution acting on beam (a), nodal forces as determined by contributing areas, (b), for grid spacing of B/4, and nodal forces as determined by contributing areas (c) for grid spacing of B/8.



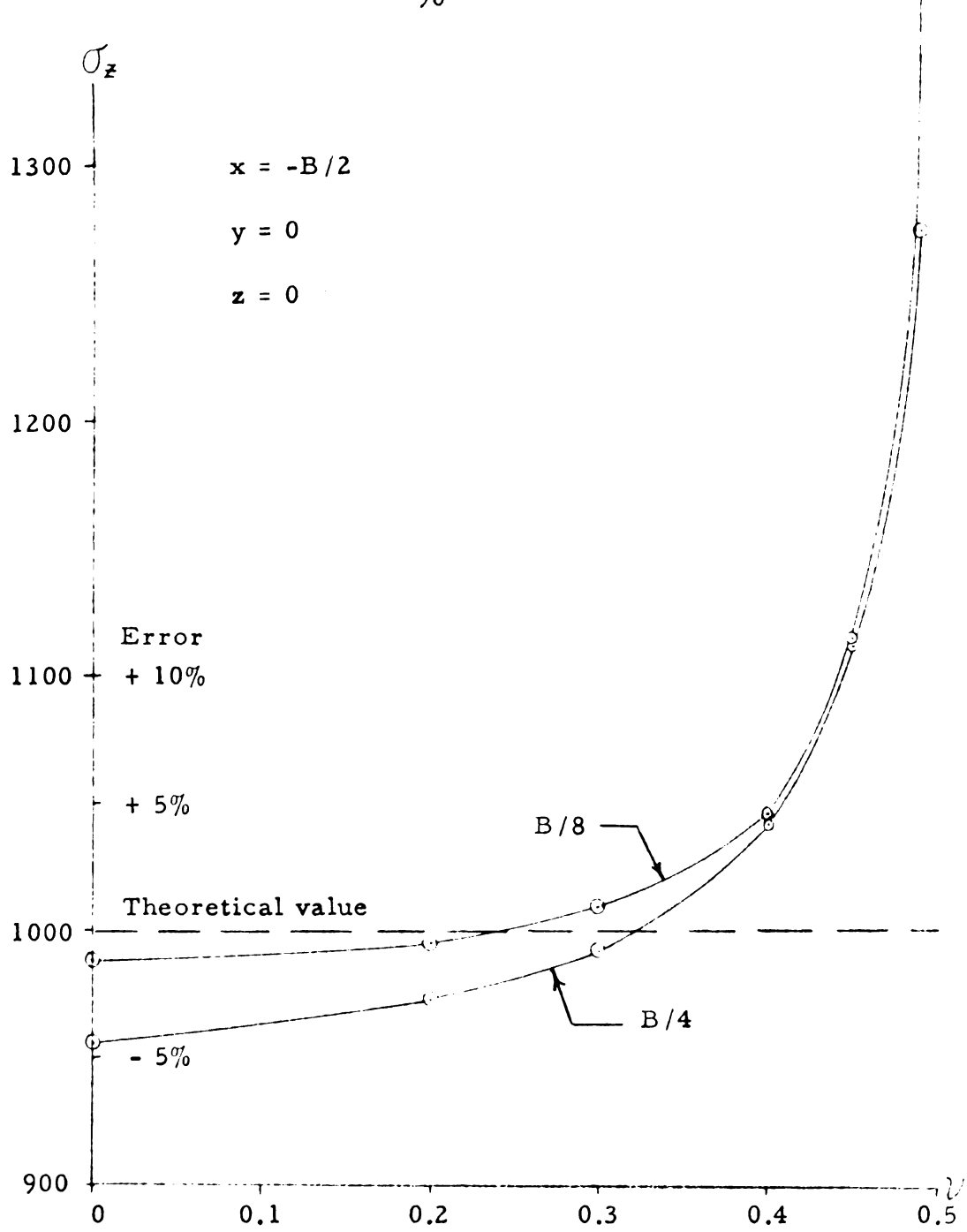


Figure 36. Extreme fiber stress at x = B/2, y = 0, and z = 0 for grid spacings of B/4 and B/8 for various values of Poisson's ratio.

CHAPTER V

SUMMARY AND CONCLUSIONS

A numerical method for the solution of the equilibrium equations for a three-dimensional body in terms of its displacements has been presented. The method is designed to satisfy the equilibrium equations for a region around a nodal point of the grid system employed to represent the body. The applicability of the equations was studied by applying them to various representative problems. The example problems for this study were chosen to show the disadvantages as well as the advantages of this method. The problems were also solved without any use of refinements that would tend to give better results. This objective was accomplished by first, not making use of fictitious nodal points to satisfy the boundary equations, which leads to first order equations with respect to the boundary, and second, by solving problems with concentrated loads on the boundaries which leads to singularities. Since, solutions of problems in three-dimensional elasticity which make use of the displacement functions are impossible when Poisson's ratio is one-half, because the dilatancy of the body is zero, the solutions were also studied with respect to this ratio approaching one-half.

In problem one, when ν = 0 it was found that the solution of the numerical method presented was better than the

classical solution with respect to grid size. It was also found that as Poisson's ratio approached one-half, the solutions became unstable.

In problems two and three, it was found that the instability of the equations was a function of the grid size. This is clearly evident because the solutions for the fine grid in problem one and problem three agree very well when not in close proximity to the load, but the coarse grid diverges sharply from this solution when Poisson's ratio approaches one-half.

In problem four, the solution of the concentrated eccentric load, when compared at a distance from the concentrated load, agreed with small error to the theoretical solution of the infinite beam column, which agrees with St. Venant's theorem. The maximum tension stress was approximately 20% of the average stress.

In problem five, it was found that in using the first order boundary conditions, the error within the usual ranges of Poisson's ratio was comparatively small.

In reviewing the results for these problems, a number of conclusions can be drawn:

1. A general method has been presented which can be used to solve problems in three dimensional elasticity. Up to this time very little literature has been available concerning the numerical solution of stress distribution problems in three dimensions. The method is applicable to all problems that can be described by a suitable mesh, and is limited only by the capability of the computer.

This method includes as a possible variable the use of Poisson's ratio. The primary influence of Poisson's ratio is in its effect upon the stress distribution in the region of a concentrated load. When the equilibrium equations on the boundary use the boundary forces rather than the boundary displacement derivatives, there is a secondary effect of Poisson's ratio that is introduced into the solution. If Poisson's ratio is limited to values less than 0.4, the accuracy of the solution is good.

3. The solutions appear to converge monotonically with respect to decreasing grid spacing. It has also been shown that when $\nu = 0$ the method presented in this thesis compares more favorably to the exact solution than the classical numerical solution with respect to grid spacing.

There are a number of refinements that can be included in the solution of a problem in three dimensional bodies that were not used in the presentation of the method. First, fictitious points once removed from the boundaries could be used to satisfy the boundary stress conditions. This would then lead to equilibrium equations on the boundary of the second order rather than that of the first order.

There are, however, a number of drawbacks in this approach. At the intersection of surfaces, there are more unknown nodal displacement values involved in the fictitious points than there are stress equations available. This leads to approximations as to the curvatures of the boundary surfaces at these points, and thus some error may be introduced.

Second, the well known subtractive process can be used to eliminate singularities from the numerical solution. This also would present some difficulties. The boundary conditions to be used in such a process would involve defining the displacements on some surfaces, and the stresses on other surfaces which would lead to some complications in writing the computer program necessary for the solution of the problem. It would, however, lead to a very accurate solution in the region of the singularity.

There are many avenues for the future development of this method. The application of the refinements to some problems should be attempted to evaluate their potential as useful inclusions in a general solution. The application of the use of these expanded differences should be attempted with plate problems to determine their applicability in this situation.

In conclusion, a numerical method for solution of three dimensional elasticity problems has been presented, and by all implications seems to be a method which is easy to use, and which gives good results for comparatively small grid spacings for the usual structural materials.

VI APPENDIX

FORTRAN COMPUTER PROGRAM FOR EXAMPLE PROBLEM FIVE

```
PROGRAM BEND
C
      FORMAT STATEMENTS
  500 FORMAT(5X.16HPOISSON'S RATIO=.F7.4)
  100 FORMAT(5X,19HNUMBER OF CYCLES = ,15,5X,7HRMAX = ,E14.8)
  101 FORMAT(315)
  102 FORMAT(2X+312+2X+9(E11+5+1X))
  103 FORMAT (3X.5HI J K.6X.2HU3.10X.2HV3.10X.2HW3.10X.3HSXX.9X.3HSYY.
     19X.3HSZZ.9X.3HTXY.9X.3HTXZ.9X.3HTYZ.14./1H0)
  104 FORMAT(1H1.5X.19HPROB FOR H A ELLEBY./1H0)
      DIMENSION U(1377) •V(1377) •W(1377) •RX(1377) •RY(1377) •RZ(1377) •IB(8)
     1.RX1(1377).RY1(1377).RZ1(1377)
      COMMON U.V.W.RX.RY.RZ.SXX.SYY.SZZ.TXY.TXZ.TYZ.R1.R2.R3,R4.R5.R6.
     1R7.R8
      GOVERN= . 0000001
      NUMBER=0
      RZ1(1)=0.07
      RZ1(2)=0.04
      RZ1(3)=0.0
      RZ1(4)=-0.04
      RZ1(5)=-0.07
      RX1(1)=0.0
      RX1(2)=0.2
      RX1(3)=0.3
     RX1(4)=0.4
      RX1(5)=0.45
      RX1(6)=0.49
      RX1(7)=3.0
      RX1(8)=3.0
      RX1(9)=5.0
      RX1(10)=5.
      RX1(11)=3.
      RX1(12)=9.
      RXI(13)=9.
      RX1(14)=5.
      RX1(15)=9.
      N4=1
       N5=2
 600 CONTINUE
      DO 11 L=1.1377
      U(L)=0.
      V(L)=0.
  11 W(L)=0.
      PAUSE 200
 601 IF(SENSE SWITCH 1) 130.602
 602 REWIND 5
      READ
            TAPE 5.U.V.W.NUMBER.N4.N5.RZ1(1).RZ1(2).RZ1(3).RZ1(4).
     1RZ1(5) •RZ1(6) •RZ1(7) •RZ1(8) •RZ1(9)
      REWIND 5
 130 N = RX1(3*N5+4)
      N2= RX1 (3#N5+5)
```

```
N3= RX1(3*N5+6)
      P1=RX1(N4)
      AL=1.-P1-P1
      RO=1.+AL+AL+AL
      R1=9. #R0
      R2=R0-4.
      R3=R0-2.+AL+AL
      R4=R0+8.
      R5=R3+4.
      R6=R0
      R7=-R0-R0+5.
      R8=-R0+AL+2.
      R18=8.*R1
      R24=4.#R2
      R32=2.#R3
      R44=4. #R4
      R52=2.*R5
      N1=N-1
      N12=N2-1
      N13=N3-1
      N132=N13+2
      IF(N-1) 504,504,115
  115 CONTINUE
      DO 123 MU=1.20
  118 IF (SENSE SWITCH 3) 603.10
  603 REWIND 5
      PAUSE 300
      WRITE TAPE 5.U.V.W.NUMBER.N4.N5.RZ1(1).RZ1(2).RZ1(3).RZ1(4).
     1RZ1(5) •RZ1(6) •RZ1(7) •RZ1(8) •RZ1(9)
      REWIND 5
      NU = 1
      GO TO 116
C
       Z AXIS AT THE SURFACE
   10 I=1
      NUMBER=NUMBER+1
      K=N3
      J=1
      L=LAKE(I.J.K)
      W(L)=W(L)-RZ1(I)
      CALL ZS(L,-71,0+0,0,0,0,0,0)
      W(L)=W(L)+RZI(I)
      CALL XS(L +-71+0+0+0+0+0+0+0)
C
      SYMETRICAL X AXIS ON THE PLUS Z SURFACE
   20 DO 204 I=2.N1
      L=LAKE(I.J.K)
      W(L)=W(L)-RZI(I)
      CALLZS(L+-71+-73+0+0+0+0+0+0)
      W(L)=W(L)+RZ1(I)
      CALLXS(L.-71.-73.0.0.0.0.0.0)
  204 CONTINUE
```

```
C
      OUTSIDE Y EDGE AT SYM INTERSECTION
   27 I=N
      L=LAKE(I.J.K)
      W(L)=W(L)-RZ1(I)
      CALLZS(L,-73.0.0.0.0.0.0.0)
      W(L)=W(L)+RZI(I)
      CALLXS(L,-73.0.0.0.0.0.0.0.0)
   21 DO 214 J=2.N12
C
       SYM Y AXIS ON Z SURFACE
      I = 1
      L=LAKE(I.J.K)
      W(L)=W(L)-RZ1(I)
      CALLZS(L,-71,-89,0,0,0,0,0,0)
      W(L)=W(L)+RZ1(I)
      CALLXS(L.-71.-89.0.0.0.0.0.0)
      CALLYS(L,-71,-89,0,0,0,0,0,0)
С
       SURFACE PLUS Z AXIS
   13 DO 134 I=2.N1
      L=LAKE(I,J,K)
      W(L)=W(L)-RZI(I)
      CALLZS(L --71 -- 89 -- 73 -- 91 -0 -0 -0 -0 )
      W(L)=W(L)+RZI(I)
      CALLYS(L,-71,-89,-73,-91,0,0,0,0)
      CALLXS(L.-71.-89.-73.-91.0.0.0.0)
  134 CONTINUE
C
         OUTSIDE EDGE Y AXIS
      I=N
      L=LAKE(I.J.K)
      W(L)=W(L)-RZI(I)
      CALLZS(L,-73,-91,0,0,0,0,0,0)
      W(L)=W(L)+RZ1(I)
      CALLYS(L,-73,-91,0,0,0,0,0,0)
      CALLXS(L--73--91-0-0-0-0-0-0)
  214 CONTINUE
      J=N2
C
      OUTSIDE EDGE X AT SYM INTERSECTION
   26 I=1
      L=LAKE(I,J,K)
      W(L)=W(L)-RZ1(I)
      CALLZS(L,-89.0.0.0.0.0.0.0)
      W(L)=W(L)+RZ1(I)
      CALLXS(L,-89,0,0,0,0,0,0,0)
      CALLYS(L,-89.0.0.0.0.0.0.0)
C
      OUTSIDE EDGE X AXIS
   16 DO 164 I=2.N1
      L=LAKE(I,J,K)
      W(L)=W(L)-RZ1(I)
      CALLZS(L,-89,-91,0,0,0,0,0,0)
      \(\(\) = \(\(\) + RZ1 (\(\))
      CALLYS(L,-89,-91,0,0,0,0,0,0)
```

```
CALLXS(L,-89,-91,0,0,0,0,0,0)
    164 CONTINUE
C
                 CORNER
       19 I=N
               L=LAKE(I+J+K)
               W(L)=W(L)-RZ1(I)
               CALLZS(L,-91.0,0.0,0.0,0.0)
               W(L)=W(L)+RZ1(1)
               CALLYS(L,-91.0.0.0.0.0.0.0.0)
               CALLXS(L,-91.0.0.0.0.0.0.0)
        18 DO 184 K1=2.N13
               K=N132-K1
               J=1
C
                  INSIDE Z AXIS
               I = 1
               L=LAKE(I,J,K)
               CALLZS(L,91,-71,0,0,0,0,0,0,0)
               CALLXS(L,91,-71,0,0,0,0,0,0,0)
С
                  INSIDE Y SURFACE
       31 DO 314 I=2.N1
               L=LAKE(I.J.K)
               CALLZS(L,89,91,-71,-73,0,0,0,0)
               CALLXS(L,89,91,-71,-73,0,0,0,0)
     314 CONTINUE
C
               SYM Z AXIS ON X SURFACE
               I=N
               L=LAKE(I.J.K)
               CALLZS(L+89+-73+0+0+0+0+0+0)
               CALLXS(L,89,-73,0,0,0,0,0,0)
       14 DO 144 J=2.N12
C
                 INSIDE X SURFACE
               1 = 1
              L=LAKE(I.J.K)
               CALLZS(L,73,91,-89,-71,0,0,0,0)
               CALLXS(L,73,91,-89,-71,0,0,0,0)
               CALLYS(L,73,91,-89,-71,0,0,0,0)
C
                 CENTRAL INTERIOR POINT
       29 DO 294 1=2.N1
              L=LAKE(I.J.K)
              RZ(L) = (-R18#W(L)+R24*(W(L+1)+W(L-1)+W(L+9)+W(L-9))+R32*(W(L+10)+R24*(W(L+10)+R24*(W(L+10)+R24*(W(L+10)+R24*(W(L+10)+R24*(W(L+10)+R24*(W(L+10)+R24*(W(L+10)+R24*(W(L+10)+R24*(W(L+10)+R24*(W(L+10)+R24*(W(L+10)+R24*(W(L+10)+R24*(W(L+10)+R24*(W(L+10)+R24*(W(L+10)+R24*(W(L+10)+R24*(W(L+10)+R24*(W(L+10)+R24*(W(L+10)+R24*(W(L+10)+R24*(W(L+10)+R24*(W(L+10)+R24*(W(L+10)+R24*(W(L+10)+R24*(W(L+10)+R24*(W(L+10)+R24*(W(L+10)+R24*(W(L+10)+R24*(W(L+10)+R24*(W(L+10)+R24*(W(L+10)+R24*(W(L+10)+R24*(W(L+10)+R24*(W(L+10)+R24*(W(L+10)+R24*(W(L+10)+R24*(W(L+10)+R24*(W(L+10)+R24*(W(L+10)+R24*(W(L+10)+R24*(W(L+10)+R24*(W(L+10)+R24*(W(L+10)+R24*(W(L+10)+R24*(W(L+10)+R24*(W(L+10)+R24*(W(L+10)+R24*(W(L+10)+R24*(W(L+10)+R24*(W(L+10)+R24*(W(L+10)+R24*(W(L+10)+R24*(W(L+10)+R24*(W(L+10)+R24*(W(L+10)+R24*(W(L+10)+R24*(W(L+10)+R24*(W(L+10)+R24*(W(L+10)+R24*(W(L+10)+R24*(W(L+10)+R24*(W(L+10)+R24*(W(L+10)+R24*(W(L+10)+R24*(W(L+10)+R24*(W(L+10)+R24*(W(L+10)+R24*(W(L+10)+R24*(W(L+10)+R24*(W(L+10)+R24*(W(L+10)+R24*(W(L+10)+R24*(W(L+10)+R24*(W(L+10)+R24*(W(L+10)+R24*(W(L+10)+R24*(W(L+10)+R24*(W(L+10)+R24*(W(L+10)+R24*(W(L+10)+R24*(W(L+10)+R24*(W(L+10)+R24*(W(L+10)+R24*(W(L+10)+R24*(W(L+10)+R24*(W(L+10)+R24*(W(L+10)+R24*(W(L+10)+R24*(W(L+10)+R24*(W(L+10)+R24*(W(L+10)+R24*(W(L+10)+R24*(W(L+10)+R24*(W(L+10)+R24*(W(L+10)+R24*(W(L+10)+R24*(W(L+10)+R24*(W(L+10)+R24*(W(L+10)+R24*(W(L+10)+R24*(W(L+10)+R24*(W(L+10)+R24*(W(L+10)+R24*(W(L+10)+R24*(W(L+10)+R24*(W(L+10)+R24*(W(L+10)+R24*(W(L+10)+R24*(W(L+10)+R24*(W(L+10)+R24*(W(L+10)+R24*(W(L+10)+R24*(W(L+10)+R24*(W(L+10)+R24*(W(L+10)+R24*(W(L+10)+R24*(W(L+10)+R24*(W(L+10)+R24*(W(L+10)+R24*(W(L+10)+R24*(W(L+10)+R24*(W(L+10)+R24*(W(L+10)+R24*(W(L+10)+R24*(W(L+10)+R24*(W(L+10)+R24*(W(L+10)+R24*(W(L+10)+R24*(W(L+10)+R24*(W(L+10)+R24*(W(L+10)+R24*(W(L+10)+R24*(W(L+10)+R24*(W(L+10)+R24*(W(L+10)+R24*(W(L+10)+R24*(W(L+10)+R24*(W(L+10)+R24*(W(L+10)+R24*(W(L+10)+R24*(W(L+10)+R24*(W(L+10)+R24*(W(L+10)+R24*(W(L+10)+R24*(W(L+10)+R24*(W(L+10)+R24*(W(L+10)+R24*(W(L+10)+R24*(W(L+10)+R24*(W(L+10)+R24*(W(L+10)+R24*(W(L+10)+R2
            1W(L-10)+W(L+8)+W(L-8))+R44+(W(L+81)+W(L-81))+R52+(W(L+72)+W(L-72)
            2+W(L+90)+W(L-90)+W(L+80)+W(L-80)+W(L+82)+W(L-82))+R6*(W(L+71)+W(L-
            371)+W(L+73)+W(L-73)+W(L+89)+W(L-89)+W(L+91)+W(L-91))+12•*(V(L+90)
            4+V(L-90)-V(L+72)-V(L-72)+U(L+82)+U(L-82)-U(L+80)-U(L-80))+2•*(V(L
            5+91)+V(L-91)+V(L+89)+V(L-89)-V(L+71)-V(L-71)-V(L+73)-V(L-73)+U(L+
            691)+U(L-91)+U(L+73)+U(L-73)-U(L+71)-U(L-71)-U(L+89)-U(L-89)))/R18
              W(L) = W(L) + 1.25 + RZ(L)
              RY(L) = (-R18*V(L)+R24*(V(L+81)+V(L-81)+V(L+1)+V(L-1))+R32*(V(L+80))
            1+V(L-80)+V(L+82)+V(L-82))+R44*(V(L+9)+V(L-9))+R52*(V(L+10)+V(L-10)
            2+V(L+8)+V(L-8)+V(L+72)+V(L-72)+V(L+90)+V(L-90)}+R6*(V(L+71)+V(L-71
```

```
3)+V(L+73)+V(L-73)+V(L+89)+V(L-89)+V(L+91)+V(L-91))+12.*(U(L+10)
     4+U(L-10)-U(L+8)-U(L-8)+W(L+90)+W(L-90)-W(L+72)-W(L-72)}+2•*(U(L+91
     5)+U(L-91)+U(L+71)+U(L-71)-U(L+73)-U(L-73)-U(L+89)-U(L-89}+W(L+91)
     6+W(L-91)+W(L+89)+W(L-89)-W(L+71)-W(L-71)-W(L+73)-W(L+73)))/R18
      V(L) = V(L) + 1.25 + RY(L)
      RX(L) = (-R18 + U(L) + R24 + (U(L + 81) + U(L - 81) + U(L + 9) + U(L - 9)) + R32 + (U(L + 90))
     1+U(L-90)+U(L+72)+U(L-72))+R44*(U(L+1)+U(L-1))+R52*(U(L+10)+U(L-10)
     2+U(L+8)+U(L-8)+U(L+82)+U(L-82)+U(L+80}+U(L-80))+R6#(U(L+71)+U(L-71
     3)+U(L+73)+U(L-73)+U(L+89)+U(L-89)+U(L+91)+U{L-91))+12•*(V(L+10)
     4+V(L-10)-V(L+8)-V(L-8)+W(L+82)+W(L-82)-W(L+80)-W(L+80)}+2•*(V(L+91
     5)+V(L-91)+V(L+71)+V(L-71)-V(L+73)-V(L-73)-V(L+89)-V(L-89)+W(L+91)
     6+W(L-91)+W(L+73)+W(L-73)-W(L+71)-W(L-71)-W(L+89)-W(L-89)))/R18
      U(L)=U(L)+1.25*RX(L)
  294 CONTINUE
C
      SURFACE PLUS X AXIS
      I=N
      L=LAKE(I.J.K)
      CALLZS(L,71,89,-91,-73,0,0,0,0)
      CALLYS(L,71,89,-91,-73,0,0,0,0)
      CALLXS(L+71+89+-91+-73+0+0+0+0)
  144 CONTINUE
      J=N2
C
       SYM Z AXIS ON Y SURFACE
      L=LAKE(I.J.K)
      CALLZS(L.73,-89,0,0,0,0,0,0)
      CALLXS(L,73,-89,0,0,0,0,0,0,0)
      CALLYS(L.73,-89.0.0.0.0.0.0)
  254 CONTINUE
C
       SURFACE PLUS Y AXIS
   15 DO 154 I=2.NI
      L=LAKE(I+J+K)
      CALLZS(L.71.73.-89.-91.0.0.0.0)
      CALLYS(L.71.73,-89,-91.0.0.0.0)
      CALLXS(L,71,73,-89,-91,0,0,0,0)
  154 CONTINUE
C
       OUTSIDE EDGE Z AXIS
      I=N
      L=LAKE(I.J.K)
      CALLZS(L.71.-91.0.0.0.0.0.0.0)
      CALLYS(L,71,-91,0,0,0,0,0,0)
      CALLXS(L+71+-91+0+0+0+0+0+0)
  184 CONTINUE
      K=1
      J=1
C
       INSIDE X AXIS
   33 DO 334 I=2,N1
      L=LAKE(I,J,K)
      CALLXS(L,91,89,0,0,0,0,0,0)
  334 CONTINUE
```

```
C
        X AXIS AT THE SURFACE
      I=N
      L=LAKE(I.J.K)
      CALLXS(L.89.0.0.0.0.0.0.0)
   23 DO 234 J=2.N12
C
        INSIDE Y AXIS
      I = 1
      L=LAKE(I.J.K)
      CALLYS(L.91.73.0.0.0.0.0.0)
      CALLXS(L.91.73.0.0.0.0.0.0)
C
       INSIDE Z SURFACE
   32 DO 324 I=2.N1
      L=LAKE(I.J.K)
      CALLYS(L,71,73,89,91,0,0,0,0)
      CALLXS(L,71,73,89,91,0,0,0,0)
  324 CONTINUE
С
      SYM Y AXIS ON X SURFACE
      I=N
      L=LAKE(I.J.K)
      CALLYS (L . 71 . 89 . 0 . 0 . 0 . 0 . 0 . 0)
      CALLXS(L,71,89,0,0,0,0,0,0)
  234 CONTINUE
      J=N2
C
      Y AXIS AT THE SURFACE
      I = 1
      L=LAKE(I.J.K)
      CALLYS(L,73,0,0,0,0,0,0,0)
      CALLXS(L.73.0.0.0.0.0.0.0)
C
      SYM X AXIS ON Y SURFACE
   24 DO 244 I=2.N1
      L=LAKE(I.J.K)
      CALLYS(L,71,73,0,0,0,0,0,0,0)
      CALLXS(L.71.73.0.0.0.0.0.0)
  244 CONTINUE
C
       OUTSIDE Z EDGE AT SYM INTERSECTION
   28 I=N
      L=LAKE(I.J.K)
      CALLYS(L+71+0+0+0+0+0+0+0)
      CALLXS(L.71.0.0.0.0.0.0.0.0)
  123 CONTINUE
  400 CONTINUE
      RMAX=0.
      DO 110 I=1.N
      DO 110 J=1.N2
      DO 110 K=1.N3
      L=LAKE(I.J.K)
      IF(ABSF(RMAX)-ABSF(RX(L)))
                                         106.121.121
  106 RMAX=RX(L)
  121 IF(ABSF(RMAX)-ABSF(RY(L)))
                                         107.122.122
  107 RMAX=RY(L)
```

```
122 IF(ABSF(RMAX)-ABSF(RZ(L))) 108.110.110
108 RMAX=RZ(L)
110 CONTINUE
    IF (ABSF (RMAX)-GOVERN) 125,125,401
125 N4=N4+1
    NUMBER=0
    NU=2
    IF(N4-6) 700,700,701
700 GO TO 116
701 N5=N5+1
    N4=1
    RZ1(1)=0.15
    RZ1(2)=0.12
    RZ1(3)=0.08
    RZ1(4)=0.04
    RZ1(5)=0.0
    RZ1(6) = -0.04
    RZ1(7) = -0.08
    RZ1(8) = -0.12
    RZ1(9) = -0.15
    IF(N5-3)702,702,703
703 NU=1
702 GO TO 116
401 GO TO 115
116 PRINT 104
    REWIND 5
    WRITE TAPE 5.U.V.W.NUMBER.N4.N5.RZ1(1).RZ1(2).RZ1(3).RZ1(4).
   1RZ1(5) •RZ1(6) •RZ1(7) •RZ1(8) •RZ1(9)
    REWIND 5
    PRINT 100 . NUMBER . RMAX
    PRINT 103, N
    PRINT 101.N.N2.N3
    PRINT 500 .P1
    DO 120 K=1.N3
    DO 120 I=1.N
    DO 120 J=1.N2
    L=LAKE(I.J.K)
    CALL STRESS (I,J,K,N,N2,N3)
120 PRINT 102 I.J.K.U(L).V(L).W(L).SXX.SYY.SZZ.TXY.TXZ.TYZ
    PAUSE 100
    GO TO (504,130), NU
504 CONTINUE
    STOP
    END
    SUBROUTINE STRESS(1.J.K.N.N2.N3)
    DIMENSION U(1377) .V(1377) .W(1377) .RX(1377) .RY(1377) .RZ(1377) .IB(8)
    COMMON U.V.W.RX.RY.RZ.SXX.SYY.SZZ.TXY.TXZ.TYZ.R1.R2.R3.R4.R5.R6.
   1R7.R8
    AL=R8+R6-2.
    AL1=AL+1.
```

```
ALM1=1.-AL
   L=LAKE(I.J.K)
45 N1=N-1
   AN1 = N1
   N12=N2-1
   AN12=N12
   AN=N
   AN11=AN-1.5
   C1=400000 • / (AN1 *R1)
   CA=C1*AL1
   CB=C1 *AL
   CC=C1*ALM1
   L1=L+1
   L2=L-1
   L3=L+9
   L4=L-9
   L5=L+81
   L6=L-81
   LX=L1
   LXX=L2
   LY=L3
   LYY=L4
   LZ=L5
  LZZ=L6
   UC=1.
  VC=1.
   WC=1.
 1 IF(I-1)2.2.3
 2 LXX=L
   UC=2.
 3 IF(N-1)4,4,5
 4 LX=L
   UC=2.
 5 IF(J-1)6,6,7
 6 LYY=L
   VC=2.
 7 IF(N2-J)8,8,9
 8 LY=L
   VC=2.
 9 IF(K-1)10.10.11
10 LZZ=L
   WC=2.
11 IF(N3-K) 12,12,13
12 LZ=L
   WC=2.
13 CONTINUE
    UXX=UC*(U(LX)-U(LXX))
   UYY=VC*(U(LY)-U(LYY))
   UZZ=WC*(U(LZ)-U(LZZ))
   VXX=UC*(V(LX)~V(LXX))
```

```
VYY=VC*(V(LY)-V(LYY))
   VZZ=WC*(V(LZ)-V(LZZ))
   WXX=UC*(W(LX)-W(LXX))
   WYY=VC*(W(LY)-W(LYY))
   WZZ=WC*(W(LZ)-W(LZZ))
   SXX=CA*UXX+CC*(VYY+WZZ)
   SYY=CA*VYY+CC*(UXX+WZZ)
   SZZ=CA*WZZ+CC*(UXX+VYY)
   TXY=CB*(UYY+VXX)
   TXZ=CB*(UZZ+WXX)
   TYZ=CB*(VZZ+WYY)
60 RETURN
   END
   FUNCTION LAKE (I.J.K)
   LAKE = I + J*9 + K*81 - 90
   SUBROUTINE XS (L. IB1 . IB2 . IB3 . IB4 . IB5 . IB6 . IB7 . IB8)
   DIMENSION U(1377) •V(1377) •W(1377) •RX(1377) •RY(1377) •RZ(1377) •IB(8)
   COMMON U.V.W.RX.RY.RZ.SXX.SYY.SZZ.TXY.TXZ.TYZ.R1.R2.R3.R4.R5.R6.
  1R7.R8
   IB(1) = IB1
   IB(2) = IB2
   IB(3) = IB3
   1B(4) = 1B4
   IB(5)=185
   1B(6) = 1B6
   1B(7) = 1B7
   1B(8) = 188
   XSUM=0.
   DO 9 M=1.8
   AM=M-1
   IA=1
   JA=9
   KA=81
   A1=1
   A2=1.
   A3=1.
   IF(IB(M))2.7.3
 2 KA=-81
   A3=-1.
 3 IF(IB(M)-KA)4.7.5
 4 JA=-9
   A2 = -1.
 5 IF(IB(M)-KA-JA)6,7,8
 6 IA=-1
   A1 = -1
 8 CONTINUE
   XSUM=(-R1*U(L)+R2*(U(L+KA)+U(L+JA))+R3*U(L+JA+KA)+R4*U(L+1A)+R5*(
  1U(L+IA+JA)+U(L+KA+IA))+R6*U(L+IA+JA+KA)+2.*A1*A2*(-3.*V(L)+R7*V(L
  2+JA)-V(L+KA)+R8*V(L+JA+KA)-R7*V(L+IA)+3.*V(L+IA+JA)-R8*V(L+IA+KA)
```

```
3+V(L+IA+JA+KA))+2。*A1*A3*(-3。*W(L)+R7*W(L+KA)-W(L+JA)+R8*W(L+JA+
 4KA)~R7*W(L+IA)+3.*W(L+IA+KA)-R8*W(L+IA+JA)+W(L+IA+JA+KA)))/R1
 5+XSUM
9 CONTINUE
  .B=MA
7 RX(L)=XSUM/AM
  U(L)=U(L)+1.25*RX(L)
  RETURN
  END
  SUBROUTINE YS (L, IB1, IB2, IB3, IB4, IB5, IB6, IB7, IB8)
  DIMENSION U(1377) . W(1377) . W(1377) . RX(1377) . RY(1377) . RZ(1377) . IB(8)
  COMMON U.V.W.RX.RY.RZ.SXX.SYY.SZZ.TXY.TXZ.TYZ.R1.R2.R3.R4.R5.R6.
 1R7,R8
  18(1) = 181
  IB(2) = IB2
  IB(3) = IB3
  1B(4) = 1B4
  18(5) = 185
  IB(6) = IB6
  18(8) = 188
  IB(7)=187
  YSUM=0.
  DO 9 M=1.8
  AM=M-1
  IA=1
  JA=9
  KA=81
  A1=1
  A2=1.
  A3=1.
  IF(IB(M))2,7,3
2 KA=-81
  A3=-1.
3 IF(IB(M)-KA)4.7.5
4 JA=-9
  A2=-1.
5 IF(IB(M)-KA-JA)6,7,8
6IA=-1
  A1=-1.
8 CONTINUE
  YSUM=(-R1*V(L)+R2*(V(L+KA)+V(L+IA))+R3*V(L+IA+KA)+R4*V(L+JA)+R5*(
 1V(L+IA+JA)+V(L+JA+KA))+R6*V(L+IA+JA+KA)+2.*A1*A2*(-3.*U(L)+R7*U(L
 2+IA)-U(L+KA)+R8*U(L+IA+KA)-R7*U(L+JA)+3。*U(L+IA+JA)-R8*U(L+JA+KA)
 3+U(L+IA+JA+KA))+2。*A2*A3*(-3.*W(L)+R7*W(L+KA)-W(L+IA)+R8#W(L+IA
 4+KA)-R7*W(L+JA)+3.*W(L+JA+KA)-R8*W(L+IA+JA)+W(L+IA+JA+KA)))/R1
 5+YSUM
9 CONTINUE
  .8=MA
7 RY(L)=YSUM/AM
  V(L)=V(L)+1.25#RY(L)
```

```
RETURN
  END
  SUBROUTINE ZS (L. IB1 . IB2 . IB3 . IB4 . IB5 . IB6 . IB7 . IB8)
  DIMENSION U(1377) . V(1377) . W(1377) . RX(1377) . RY(1377) . RZ(1377) . IB(8)
  COMMON U.V.W.RX.RY.RZ.SXX.SYY.SZZ.TXY.TXZ.TYZ.R1.R2.R3.R4.R5.R6.
 1R7.R8
  IB(1) = IB1
  IB(2) = IB2
  1B(3) = 1B3
  IB(4) = IB4
  IB(5)=185
  IB(6)=IB6
  IB(7)=IB7
  IB(8) = IB8
  ZSUM=0.
  DO 9 M=1.8
  AM=M-1
  IA=1
  JA=9
  KA=81
  A1=1.
  A2=1.
  A3=1.
  IF(IB(M))2.7.3
2 KA=-81
  A3=-1.
3 IF(IB(M)-KA)4.7.5
4 JA=-9
  A2=-1.
5 IF(IB(M)-KA-JA)6.7.8
6 IA=-1
  A1 = -1
8 CONTINUE
  ZSUM=(-R1*W(L)+R2*(W(L+1A)+W(L+JA))+R3*W(L+IA+JA)+R4*W(L+K&)+R5*
 1(W(L+JA+KA)+W(L+IA+KA))+R6+W(L+IA+JA+KA)+2。*A2*A3*(-3。*V(L)+R7*V(
2L+JA)-V(L+IA)+R8*V(L+IA+JA)-R7*V(L+KA)+3.*V(L+JA+KA)-R8*V(L+IA+KA)
 3+V(L+IA+JA+KA))+2.*A1*A3*(-3.*U(L)+R7*U(L+IA)-U(L+JA}+R8*U(L+IA+
 4JA)-R7#U(L+KA)+3•#U(L+IA+KA)-R8#U(L+JA+KA)+U(L+IA+JA+KA)))/R1
5+ZSUM
9 CONTINUE
  AM=8.
7 RZ(L)=ZSUM/AM
  W(L)=W(L)+1.25*RZ(L)
  RETURN
  END
  END
```

VII BIBLIOGRAPHY

- D'APPOLONIA, E. and NEWMARK, N. W., A method for the solution of the restrained cylinder under compression. 1st
 U.S. National Congress of Applied Mechanics, 1952, pp. 217-226.
- 2. HRENNIKOFF, A., Solution of problems in elasticity by the frame work method. Journal of Applied Mechanics, vol. 8, no. 4, Dec. 1941, pp. A-169 A-175.
- 3. KORN, A., Mathematical Annalen, vol. 75, 1914, pp. 497-544.
- 4. KUNZ, K. S., Numerical Analysis, McGraw-Hill Book Company, Inc., New York, 1957.
- 5. LICHTENSTEIN, L., Mathematisch Zeitschrift, vol. 20, 1924, pp. 21-28.
- 6. LOVE, A. E. H., A treatise on the Mathematical Theory of

 Elasticity, 4th ed., Cambridge University Press, London, 1927.
- 7. McHENRY, D., A lattice analogy for the solution of stress problems, Journal of the Institution of Civil Engineers, No. 2, Dec. 1943.
- 8. MELOSH, R. J., Structural analysis of solids, Journal of the Structural Division of the American Society of Civil Engineers, vol. 89, no. ST4, pt. 1, Aug. 1963.
- 9. NEUBER, H., Z. Angew. Math. Mech., vol. 14, p. 203, 1934.

- 10. NOVOZHILOV, V. V., Theory of Elasticity, Israel program for scientific translations, Jerusalem, 1961.
- PAPKOVITCH, P. F., Compt. Rend., vol. 195, 513, p. 754,
 1932.
- 12. SALVADORI, M. G. and BARON, M. L., Numerical Methods in Engineering, 2nd ed., Prentice Hall, 1961.
- 13. SOKOLNIKOFF, I. S., Mathematical Theory of Elasticity,

 McGraw-Hill Book Company, Inc., New York, 1956.
- 14. SOUTHWELL, R. V., Theory of Elasticity for Engineers and Physicists, 2nd ed., Oxford University Press, London, 1941.
- 15. TIMOSHENKO, S. P. and GOODIER, J. N., Theory of Elasticity, 2nd ed., McGraw-Hill Book Company, Inc., New York, 1951.

ROOM USE ONLY

